DESIGN AND PERFORMANCE EVALUATIONS OF THE PROPELLER OF A UAV

A THESIS SUBMITTED TO
THE GRADUATE SCHOOL OF NATURAL AND APPLIED SCIENCES
OF
MIDDLE EAST TECHNICAL UNIVERSITY

BY

MURAT BAĞÇE

IN PARTIAL FULFILLMENT OF THE REQUIREMENTS
FOR
THE DEGREE OF MASTER OF SCIENCE
IN
MECHANICAL ENGINEERING

FEBRUARY 2015

Approval of the thesis:

DESIGN AND PERFORMANCE EVALUATIONS OF THE PROPELLER OF A UAV

submitted by **MURAT BAĞÇE** in partial fulfillment of the requirements for the degree of **Master of Science in Mechanical Engineering Department, Middle East Technical University** by,

Prof. Dr. Gülbin Dural Ünver _____
Dean, Graduate School of **Natural and Applied Sciences**

Prof. Dr. Tuna Balkan _____
Head of Department, **Mechanical Engineering**

Prof. Dr. M.Haluk Aksel _____
Supervisor, **Mechanical Engineering Dept., METU**

Assist. Prof. Dr. Ali Ruhşen Çete _____
Co-Supervisor, **Aircraft and Space Eng. Dept., Gaziantep Uni.**

Examining Committee Members:

Prof. Dr. Kahraman Albayrak _____
Mechanical Engineering Dept., METU

Prof. Dr. M.Haluk Aksel _____
Mechanical Engineering Dept., METU

Assist. Prof. Dr. Ali Ruhşen Çete _____
Aircraft and Space Eng. Dept., Gaziantep Uni.

Assoc. Prof. M.Metin Yavuz _____
Mechanical Engineering Dept., METU

Instructor Dr. Tahsin Çetinkaya _____
Mechanical Engineering Dept., METU

Date: 06.02.2015

I hereby declare that all information in this document has been obtained and presented in accordance with academic rules and ethical conduct. I also declare that, as required by these rules and conduct, I have fully cited and referenced all material and results that are not original to this work.

Name, Last Name : Murat Bağçe

Signature :

ABSTRACT

DESIGN AND PERFORMANCE EVALUATIONS OF
THE PROPELLER OF A UAV

Bağçe, Murat
M.S., Department of Mechanical Engineering
Supervisor : Prof. Dr. M.Haluk Aksel
Co-Supervisor: Assist. Prof. Dr. Ali Ruhşen Çete

February 2015, 118 pages

In this study, the performances of mini aircraft propellers which are designed and prototyped by Turbotek Ltd Inc. are determined by static and dynamic tests. A propeller test apparatus is designed and assembled to evaluate the performance of propellers statically. For dynamic tests, the same apparatus is placed in the wind tunnel of Fluid Mechanics Laboratory of Mechanical Engineering Department in METU. In static tests, thrust, power and efficiencies of four different Turbotek propellers are obtained as a function of the rotational speed of the propellers. These obtained data are compared with the results of the calculated, Computational Fluid Dynamics (CFD) analysis and static tests results of Turbotek. In dynamic tests, the variation of the thrust coefficient, power coefficient and efficiency of these four Turbotek propellers are obtained as a function of the advance ratio. These experimental results are compared to the analytical and CFD results of Turbotek and experimental results are found to be satisfactory.

Keywords: Mini Aircraft Propellers, Propeller Design, Propeller Performance Evaluation, Static Propeller Tests, Dynamic Propeller Tests

ÖZ

İNSANSIZ HAVA ARACI PERVANESİNİN TASARIM VE PERFORMANS DEĞERLENDİRMELERİ

Bağçe, Murat
Yüksek Lisans, Makine Mühendisliği Bölümü
Tez Yöneticisi : Prof. Dr. M.Haluk Aksel
Ortak Tez Yöneticisi :Yrd. Doç. Dr. Ali Ruhşen Çete

Şubat 2015, 118 sayfa

Bu çalışmada, dizaynı ve prototipleri Turbotek Turbomakina Teknolojileri Ltd Şti tarafından yapılan mini uçak pervanelerinin performansları statik ve dinamik testlerle belirlenmiştir. Pervanelerin statik olarak performanslarını değerlendirmek için bir pervane test düzeneği tasarlanmış ve bunun montajı yapılmıştır. Aynı test düzeneği, dinamik testler için ODTÜ Makine Mühendisliği Akışkanlar Mekaniği Laboratuvarında bulunan rüzgar tüneli içine yerleştirilmiştir. Statik testlerde, dört farklı Turbotek pervanesine ait itki, güç ve verim değerleri, pervane dönme hızının bir fonksiyonu olarak elde edilmiştir. Elde edilen bu veriler, Turbotek firmasının hesap sonuçları, Hesaplamalı Akışkanlar Dinamiği (HAD) analizi ve statik test sonuçları ile karşılaştırılmıştır. Dinamik testlerde, bu dört Turbotek pervanesinin itki katsayısı, güç katsayısı ve verim değerlerinin ilerleme oranının bir fonksiyonu olarak değişimi elde edilmiştir. Bu deneysel sonuçlar, Turbotek firmasının yaptığı analitik ve HAD sonuçları ile karşılaştırılmış ve deneysel sonuçlar başarılı bulunmuştur.

Anahtar Kelimeler: Mini Uçak Pervaneleri, Pervane Tasarımı, Pervane Performans Değerlendirme, Statik Pervane Testleri, Dinamik Pervane Testleri

To my wife & son

ACKNOWLEDGMENTS

I would like to thank first to my wife Nihan and son Kaan for their great patience they had to endure during my study since I have stolen their time that should be shared with me in this period.

Secondly, I would like to offer a special thank to my dear friend M.Ersan Taner for his positively influencing me to finish my thesis throughout my Master of Science period.

I have got great supports from my supervisor and co-supervisor during my thesis period. They behaved me very helpfully. Thus, I would also like to thank to my supervisor Prof. Dr. M.Haluk Aksel and co-supervisor Assist. Prof. Dr. A.Ruhşen Çete for their great supports, guidance, advices, criticisms, encouragements and insights throughout my research.

As a part of my thesis, I have done some laboratory tests in the wind tunnel of Fluid Mechanics Laboratory of Mechanical Engineering Department in METU, by the help of my instructor and the laboratory technicians. The technical assistance of Assoc. Prof. Dr. M.Metin Yavuz, and the laboratory technicians, Mr. Rahmi Ercan and Mr. Mehmet Özçiftçi, are gratefully acknowledged.

TABLE OF CONTENTS

LIST OF TABLES

TABLES

LIST OF FIGURES

FIGURES

LIST OF SYMBOLS

SYMBOLS

a	axial induction factor
b	radial induction factor
A	propeller disk area, πR^2
B	number of blade
c	chord
C_D	coefficient of drag
C_L	coefficient of lift
$C_{L\alpha}$	slope of the lift-curve at an angle of attack
C_T	thrust coefficient
C_P	power coefficient
C_p	pressure coefficient
d_p	propeller diameter
D	drag force
F	thrust
F_Q	radial force for the torque
G	read out value from the portable electronic scale
h	geometric pitch
i	current
I	current
I_{in}	input voltage
J	advance ratio, $J = V_\infty / n d_p$
k	ratio of specific heats of gas / coefficient of C_D formula

K_v	constant for electric motor, rpm/Volt
L	lift force
M	Mach number
M_{cr}	critical Mach number
$\dot{m}$	mass flowrate
n	revolutions per second, $\omega/2\pi$
N	rpm in electric motor
P	power
P_S	propeller shaft power
P_{shaft}	propeller shaft power
P_{use}	useful power
P_{ind}	induced power
P_{ideal}	ideal power
P_∞	free stream pressure
P_0	atmospheric pressure at inlet
P_1	pressure in front of the actuator disk
P_2	pressure behind the actuator disk
P_3	atmospheric pressure at outlet
Q	torque
r	radial coordinate
r_h	propeller hub radius
R	propeller radius / tip radius
$R_{0.75}$	propeller radius at 75% radius location ($r_{0.75}$)
R	specific gas constant J/(kg K)
R_m	internal resistance
Re	Reynolds number
Re_p	propeller Reynolds Number
T	temperature

V_{in}	input voltage
V_∞	free stream velocity / forward speed of airplane
V_1	velocity in front of the actuator disk
V_2	velocity behind the actuator disk
V_3	velocity at outlet
V_0	free stream velocity
V_T	tip velocity
V_R	resultant velocity
V_E	resultant velocity
$V_{R,max}$	maximum resultant velocity
w	induced velocity
w_a	induced velocity parallel to the thrust vector
x	nondimensional radial location, $x = r/R$,

Greek symbols

α	angle of attack
a_0	lift-curve slope
α_i	induced angle of attack
β	geometric pitch angle
$\beta_{0.75}$	geometric pitch angle at 75% radius location
γ	angle between the lift force and the resultant force $\text{atan}(\gamma) = C_d/C_l$
ε	drag to lift ratio
η_{pr}	propeller efficiency
λ	tip velocity ratio, $\lambda = J/\pi = V/n\pi\, d_p = V/\omega R$
μ	dynamic (absolute) gas viscosity (Ns/m^2)
v	kinematic gas viscosity (m^2/s)

ρ	density of fluid (Air)
σ	local solidity
σ_{ref}	reference solidity
ϕ	flow angle /effective pitch angle / blade pitch angle
Ω	induced angular speed
ω	angular frequency, rad/s

Abbreviations

AC	Alternative current
BEM	Blade Element Momentum Theory
BET	Blade Element Theory
CAD	Computer Aided Design
CFD	Computational Fluid Dynamics
DC	Direct current
ESC	Electronic Speed Control
METU	Middle East Technical University (ODTU)
NACA	National Advisory Committee for Aeronautics
SUAS	Small Unmanned Aircraft Systems
UAV	Unmanned Aerial Vehicle
UDF	Unducted Fan
Prop6	Turbotek Inc.'s propeller (10x7) having airfoil section of NACA 4409
Prop1	Turbotek Inc.'s propeller (10x6) having airfoil section of GO 797
eProp2	Turbotek Inc.'s propeller (12x7) having different NACA 4 series airfoils
eProp1	Turbotek Inc.'s propeller (10x7) having different NACA 4 series airfoils

CHAPTER 1

INTRODUCTION

The propeller is a system that produces thrust by accelerating a large amount of fluid such as air or water in front to the back of it thus providing the vehicle move forward while impelling the fluid in opposite direction by the help of mechanical energy obtained from a turbo-propeller engine or an internal combustion engine [1].

Actually, the propeller can be thought as a screw. Screw propellers advance as it turns like a screw and move an aircraft or a ship which is directly connected to itself and have been used for aircraft or ship propulsion. In this study, the attention is focused to aircraft propulsion.

More than 2000 years ago, a Chinese toy illustrated in Figure 1.1 (a) was constructed. This simple toy consists of a propeller and a stick and the propeller spins by moving the propeller upward by hand. Nowadays, it is a common toy [2]. But, Leonardo da Vinci (1452-1519) may be accepted as the first inventor of a screw propeller. Figure 1.1 shows a sketch of a model of a helicopter and Figure 1.2 shows a construction made from this sketch [2], [3].

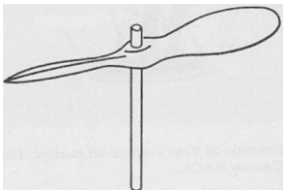

Figure 1.1 Chinese toy [2]

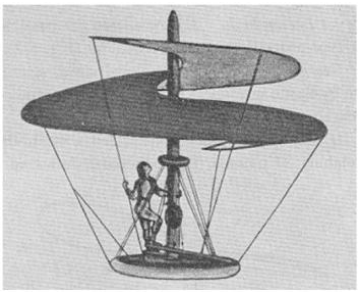

Figure 1.2 Leonardo da Vinci's "Helicopter"[3]

In 1865, Rankine developed his momentum theory and this was adapted to the actuator disk theory for the propeller design. In 1878, William Froude used blade element theory that provides a dimensional aspect for the propeller design. After Wright Brothers succeeded a piloted and first powered flight in history in 1903, the propeller (Figure 1.3) that they have used gained a great importance. So far, efficiencies, and thrust capabilities have been developed since the Wright Brothers.

Figure 1.3 Reproduction of Wright Brothers' propeller [4]

Propeller is specified by using its two properties: the first one is the diameter and the second one is the pitch. Pitch is defined as the distance that the propeller advances in one revolution [4]. For example, 10x6 propeller represents a propeller which is 10 inches in diameter and 6 inches in pitch as seen Figure 1.4).

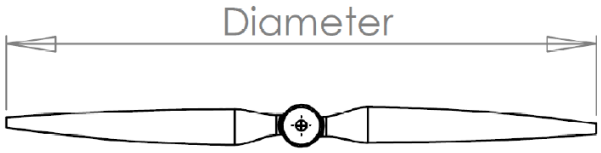

Figure 1.4 Propeller diameter [4]

Propeller consists of a central hub and blades connected to the hub at equal intervals of angle. Today's aircraft propellers are still used commonly in turboprop engines and internal combustion engines. There are several different propeller types for aircraft propulsion as seen in Figure 1.5. [5]

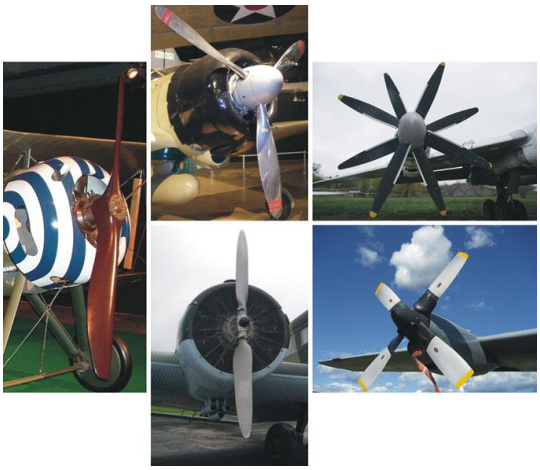

Figure 1.5 Propellers through the years [5]

In 1980s, NASA and industry developed high speed propellers (propfans and unducted fans) for transportation aircrafts as seen in Figure 1.6 [6].

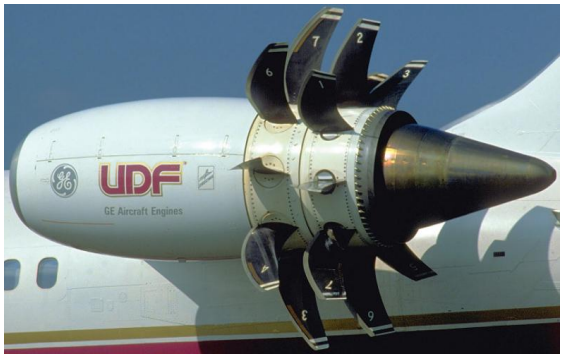

Figure 1.6 General Electric GE-36 Unducted Fan (UDF) with two eight-bladed sets of contra-rotating blades [6]

1.1 Literature Survey

In reference [4], the effects of the Reynolds number on the performance of propellers were investigated. It is found that the geometrical properties of the propeller such as shape, twist and chord are strongly dependent on the Reynolds number. In the wind tunnel tests propellers manufactured by Advanced Precision Composites (APC) (see Figure 1.7) with glass filled epoxy for high torsion strength are used.

Figure 1.7 APC Propeller [4]

APC 18x12 and APC 18x8 propellers were tested at 7 different rotational speeds for different Reynolds number ranging from 400,000 to 502,000 and from 1,080,000 to 1,213,000 respectively.

It is found that the efficiency, thrust coefficient, power coefficient as well as pitch, increase when the Reynolds number is increased. It is found that the efficiency of the APC 18x12 propeller is increased by 5% as the Reynolds number is increased from 400,000 (1.700 rpm) to 1,155,000 (4850 rpm). It is observed that the same thrust is produced at lower velocities as the pitch is decreased while the diameter is kept constant. In other words, as the pitch or pitch to diameter ratio increases, the efficiency increases and the propeller produces thrust at higher advance ratios.

Consequently, experimental results show that Reynolds number has a strong effect on small propellers. Therefore, a designer should take the Reynolds number into account when selecting airfoil profile because twist distribution and the chord length of the blade strongly depend on the Reynolds number.

In another study [7], a passive propeller system having 15 total degrees of pitch travel for self-adjustment to incoming flows was developed. It is stated that this property was achieved by a system where the pitch angles of the blades of the

propeller changes aerodynamically according to inflow conditions. This process was carried out by adjusting the axis of rotation of a propeller blade to a point ahead of the blade's aerodynamic center so that the blades will come to a foreseen lift "trim" condition automatically or naturally. First, a computational analysis was performed using a code named QPROP developed at Massachusetts Institute of Technology (MIT) and a second code developed at the Air Force Research Labs (AFRL). It has been explained that the performances of these codes were compared to data collected by AFRL at the NASA Basic Aerodynamic Research Tunnel (BART) and AFRL Vertical Wind Tunnel. It is concluded that the results obtained from these codes were matching quite well with the experimental data. In this study, a test setup including a load cell, data acquisition system, speed control system, brushless motor and power analyzer was constructed in North Carolina State University (NCSU). Moreover, initial test blades (see Figure 1.8) prototyped using a stereo lithography technique were used as a fixed pitch propeller in the wind tunnel. The data obtained for this propeller showed more scatter than the off-shelf propellers (APC 18x8) tested in the same test cell for validation.

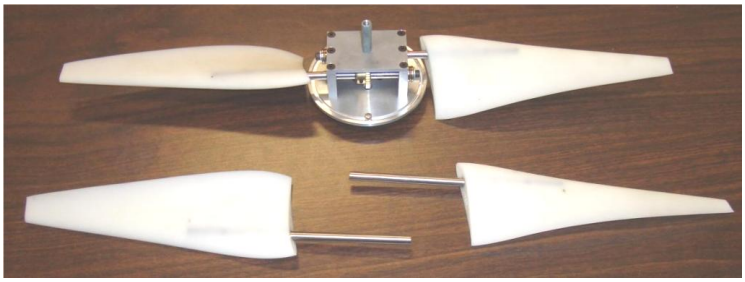

Figure 1.8 Stereo lithography blades with stainless shafts installed

It is stated that after the initial tests, the blade that was tested, was as not of fixed pitch, and it showed a bad performance due to plastic deformation and brittle failure of two sets of prototyped blades. New rapid prototypes as seen in Figure 1.9 were produced using wet lay-up technique from fiberglass and uni-directional carbon fiber.

Figure 1.9 Propeller blade molds with test lay-up

In latter case, it is found that the test results were consistent. As a final proof, a flight test in NCSU Flight Research Laboratory Converse was conducted. It is assessed that the data from the flight test was compared to data from the same aircraft with an off-the shelf fixed pitch propeller and the power obtained from the variable pitch propeller had a much tighter band when the electrical power drawn was plotted against the rotational speed. Consequently, computational, wind tunnel, and flight test results of the variable pitch propellers demonstrated that the range of the efficient propeller operation could be extended with respect to fixed pitch propellers.

In reference [8], a propeller is designed and analyzed for an Unmanned Aerial Vehicle (UAV) by using the subsonic airfoil analysis program XFOIL and numerical optimization programs QMIL and QPROP. After theoretical verification of thrust and efficiency, a model of this propeller was manufactured. It was then tested in a 1 foot- by- 1 foot wind tunnel to obtain power consumption. Four different propeller designs were compared in two different configurations. In the first configuration, the propeller was operating behind a fuselage while in the other configuration involved; the propeller was operating in the free air stream without a fuselage as seen in Figure 1.10. The propeller in test results revealed that the blanketed propeller had higher power consumption than the free air stream. In

addition, experimental and simulation results were found to be consistent with each other.

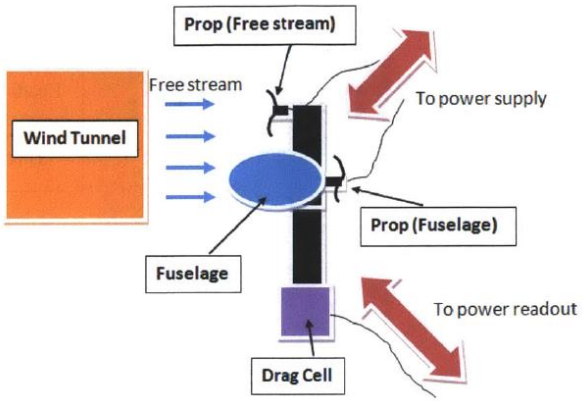

Figure 1.10 Power consumption testing apparatus set-up with fuselage and with free stream

In Reference [9] for the analysis, manufacturing and experimental testing of propellers for Small Unmanned Aircraft Systems (SUAS) has been performed (see Figure 1.11). A multi-bladed propeller for a SUAS was optimized with respect to the thrust requirements of the vehicle at a reduced cruising rotational velocity. Wet lay-up technique was used to produce solid carbon fiber composite propellers.

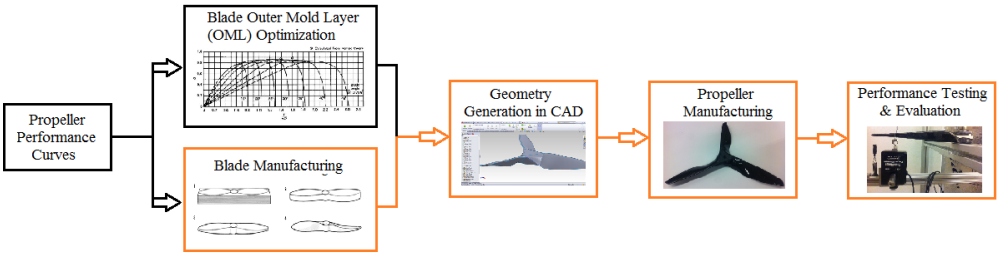

Figure 1.11 Propeller design and construction process [9]

A test setup shown in Figure 1.12 was constructed to verify the theoretical analysis of the propeller blade and the deflections and corresponding loads at various

locations on the propeller blade were measured and the stiffnesses of the propeller blades were obtained.

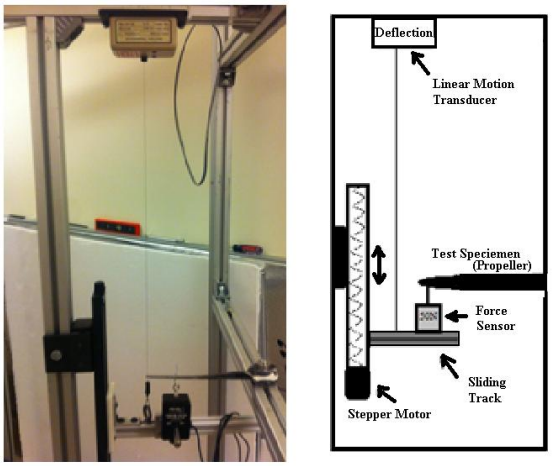

Figure 1.12 Load deflection test apparatus [9]

It is stated that another validation of stiffness of the propeller blade was performed by using stain gages attached on the top and bottom surfaces of the propeller blades. For the performance validation of the propellers, the propellers were also tested in Oklahoma State University (OSU)'s wind tunnel as seen in Figure 1.13. The dynamometer, which was used in this wind tunnel, is shown in Figure 1.14.

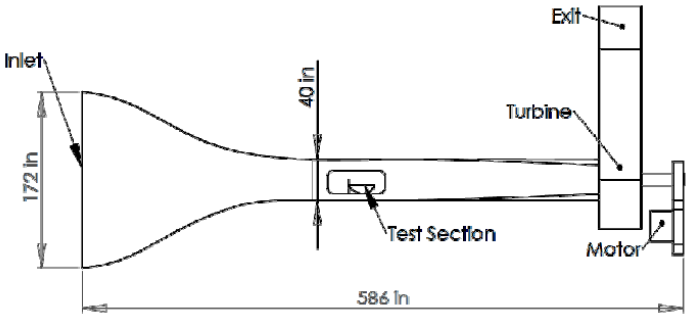

Figure 1.13 OSU wind tunnel

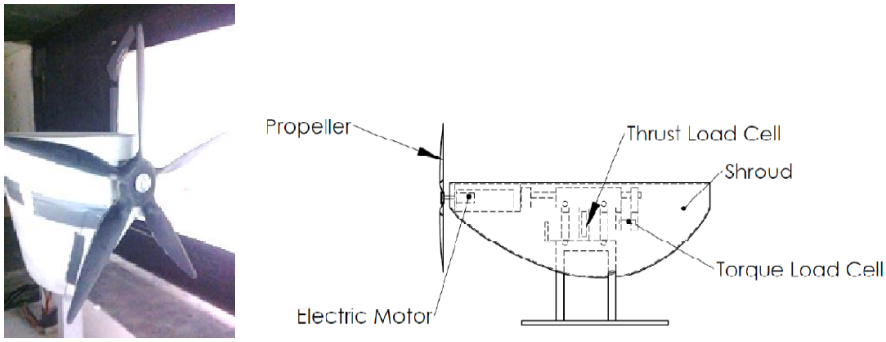

Figure 1.14 OSU dynamometer

In addition, another test setup with a dynamometer shown in Figure 1.15 installed on the bed of a pick-up truck was used for determining both the static and dynamic conditions experienced by the propeller during flight. In the set a gas engine shown in Figure 1.15 (c) was used to measure the propeller tip deflection for a range of rotational speeds by using a high-speed digital camera under static conditions. It was observed that the deflection at the tip also increases as the rotational speed increases.

(a) (b) (c)

Figure 1.15 (a, b) Propeller test module with a 5-bladed propeller (c) Gas engine with a 5-bladed propeller [9]

Finally it is assessed that the manufacturing of propellers was successfully achieved and the test analysis of the propeller blades was found to be comparable

in both strength and performance. The results of tests have been compared with the theoretical prediction of deflection and a factor or error between the theoretical and the experimental data ranging from 1.1 to 1.5 exists. This deviation might be as a result of several different reasons including defective incompatibility of the material, human error during the manufacturing of test specimens, not perfectly modeled propeller blades due to air pockets in the core material.

An Integrated Propulsion Test System (IPTS) shown in Figure 1.16 was constructed in order to obtain the performance of small off-the self-propellers at Reynolds numbers between 30,000 to 300,000 [10]. These propellers that are generally used in Unmanned Aerial Vehicle (UAV) and Micro Aerial Vehicles (MAV), whose propellers have diameters less than two feet (from 6-inches to 22-inches) and which are generally radio controlled. The tests are carried out in the 3 ft x 3 ft low speed open return wind tunnel (Figure 1.17) at Wichita State University (WSU).

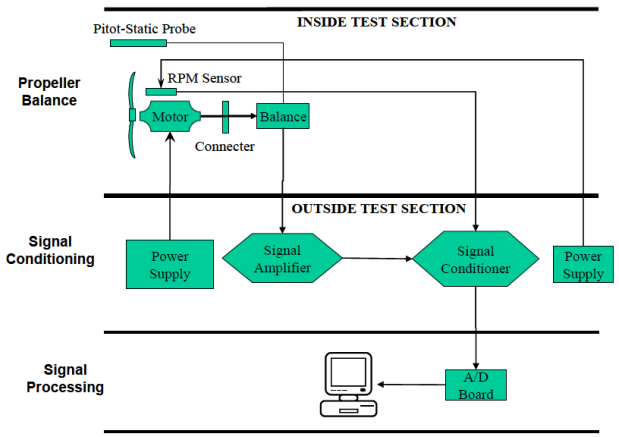

Figure 1.16 IPTS Schematic overview [10]

Figure 1.17 The 3’x4’ low speed wind tunnel, WSU

It is assessed that the system and the test apparatus were highly repeatable with minimal scatter. Two propellers having the same geometry and manufactured by the same manufacturer showed a distinct variation in propeller performance especially in efficiency and thrust coefficient.

A thrust measurement apparatus for a variable pitch propeller was designed and manufactured in the Aerospace Laboratory in Southern Polytechnic University [11]. The conceptual design is shown in Figure 1.18.

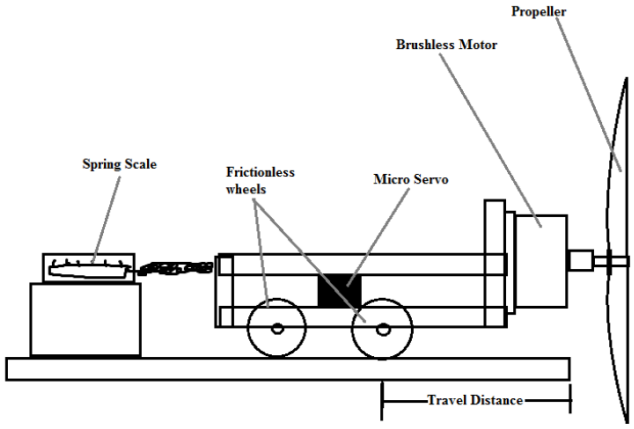

Figure 1.18 Conceptual design of the thrust measurement apparatus

The pitch control mechanism is shown in Figure 1.19 where the operator controls the pitch by a control knob that is connected to a control arm on the shaft of the

propeller. The thrust measurements are affected by the speed, span, chord, twist, pitch and taper ratio of the propeller.

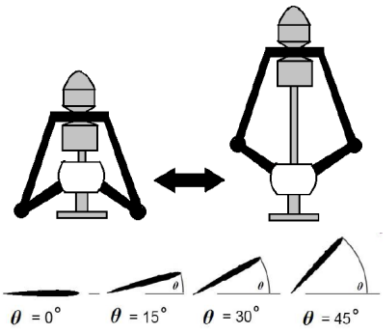

Figure 1.19 The pitch control mechanism

Most of the UAV's use propeller that operates at low Reynolds numbers ranging between 50,000 and 100,000. Although sufficient data was not available for these propellers, performance of propellers for the larger airplanes has been well documented. For this reason, the tests of this type of propellers were performed at the University of Illinois at Urbana-Champaign (UIUC) and performance of 79 propellers ranging from 9- to 11-in diameter were determined and their static thrust was measured [12]. It was reported that the UIUC subsonic wind tunnel (see Figure 1.20) having a rectangular cross-section of 2.8 x 4.0 ft (0.853 x 1.219 m) and reaching a maximum flow speed of 160 mph (71.53 m/s) was used.

Figure 1.20 Wind tunnel with the experimental rig installed

Thrust on the propeller is obtained by a T-shaped pendulum using a load cell. In order to prevent the drag on the beam inside the wind tunnel, a fairing structure was used as seen in Figure 1.20. For these propellers, thrust and power coefficients were obtained as a function of the advance ratio. Tests have been performed at four different rotational speeds from 1,500 to 7,500. It was found that the performance of the propeller improves as the propeller speed is increased with increased efficiency. It was reported that a higher thrust coefficient is obtained as the propeller speed is increased. This is most easily seen in static thrust. Similarly, increasing the propeller speed increases the Reynolds number which plays a key role on aircraft performance.

Today, for the numerical solution of rotating propellers and turbine blades are still quite difficult to achieve, even with the fastest, parallel computers by using Computational Fluid Dynamics (CFD). Thus, engineering design methods are still preferred. Nowadays, three engineering design methods have been used to calculate the steady-state flow through rotating turbine blades and propellers. These are Goldstein's vortex theory, propeller momentum theory and blade element theory. Blade element and momentum theories are combined to produce the Blade Element Momentum (BEM) theory. The BEM theory which uses the momentum theory to calculate the induced velocity was used as a single prediction design tool since the blade element theory alone lacks the prediction of induced velocity. However, BEM theory also gives inaccurate results at high advance ratios and along the inner half-span of the blade. To avoid these, a nonlinear solution method for the BEM equations is introduced. In reference [13], mathematical formulae for blade element theory, momentum theory, for small angle BEM theory and finally for nonlinear large angle solution to the BEM theory are derived. It is stated that as an analytical comparison, thrust and power coefficient solutions have been compared for the assumptions of the chord profiles of APC 8x4, 8x6, 8x8 thin electric propellers. It is evaluated that the McCormick [13]'s small angle BEM (analytical) solution produced higher thrust and power

than the nonlinear BEM solution especially at the larger advance ratios. In addition, this difference was larger at lower pitch propellers.

An APC 8x8 thin electric remote control model airplane propeller was tested in a wind tunnel having a test section dimension of 40.6 x40.6 x 121.9 cm and allowing air speed approximately from 10 to 30 m/s by using the test setup shown in Figure 1.21.

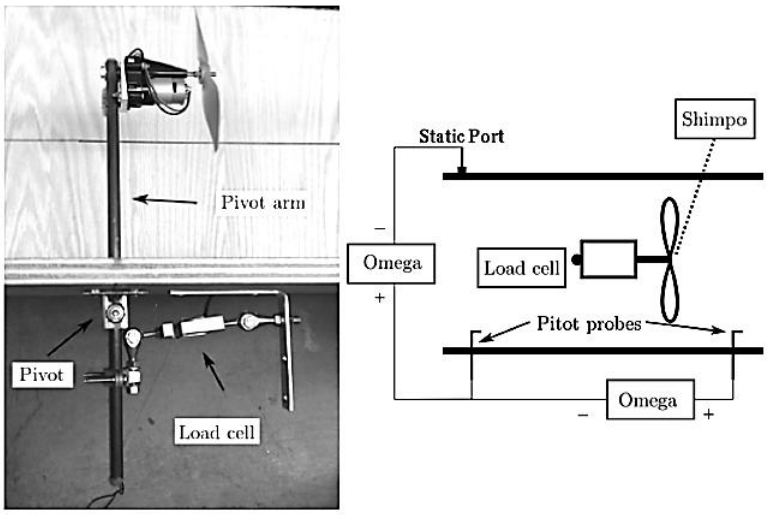

(a) (b)

Figure 1.21 (a) Mechanical layout of test apparatus, (b) Functional block diagram of instrumentation system

The experimental thrust data matched quite well with the nonlinear BEM for advance ratios over 0.4 while the analytical BEM over predicted the thrust for advance ratios over 0.4. The power data showed good agreement with the nonlinear BEM at an advance ratio of 0.5. For low advance ratios less than 0.4 analytical BEM and nonlinear BEM over predicted thrust and under predicted power with respect to the test results.

In reference [14], the aerodynamic design of a propeller blade based on the cruise data for a low speed aircraft has been carried out by using the blade element

theory. The critical Mach number for a selected NACA 4412 airfoil and corresponding local Mach numbers, local lift coefficient and local drag coefficient at each station of the propeller blade for an angle of attack of 5 degrees are obtained by using a commercial CFD program FLUENT/ANSYS. Then after geometry of the propeller blade has been obtained after some iterations for axial and radial induction factors and optimization processes. Then, the total thrust, total moment, total power and efficiency of the propeller blade are calculated analytically and the performance of the propeller before and after optimization is compared. Consequently, it is found that the performance values of thrust and torque are increased as the efficiency is decreased could be due the fact that the propeller is designed for ideal conditions.

In reference [15], propellers with a NACA 4412 airfoil profile are modelled at four different angles of attack (21^o, 53^o, twisted from 53^o to 21^o, twisted from 53^o to 13^o by using the commercial CFD program FLUENT/ANSYS. These propellers are then manufactured from aluminum with a scale ratio of 1/5. These prototypes have been tested in a wind tunnel at 70 m/s and 20 m/s. It is found that as angle of attack is increased, the pressure difference between upstream and downstream of the propeller blade is decreased.

1.2 The Purpose and Scope of the Study

The purpose of the study is to determine the performances of mini aircraft propellers which are designed and prototyped by Turbotek Turbomakina Teknolojileri Ltd Inc. Tests of these propellers have been carried out at various air velocities and rotational speeds in the wind tunnel of Fluid Mechanics Laboratory of Mechanical Engineering Department in METU. In order to achieve this, a basic and inexpensive propeller test apparatus has been designed and manufactured for the wind tunnel. By the wind tunnel tests, thrust, power and efficiencies of these propellers have been determined. Consequently, performances of the tested propellers have been evaluated by comparison techniques.

The chapters of this thesis are organized as starting from the propeller theories, continuing with test apparatus through the propeller testing. Briefly, in Chapter 2, propeller theories and related formulae used are presented. In Chapter 3, information regarding the propeller test apparatus and its design are introduced. In Chapter 4, propellers are tested both statically and dynamically in the wind tunnel. These test results are compared with the previous test data. Finally, in Chapter 5, test results are discussed and evaluated with some conclusions. The shortcomings are summarized and future work is proposed.

CHAPTER 2

PROPELLER THEORIES

There are mainly two theories regarding the propeller design. The first one is the momentum theory or the actuator disk theory; and the second one is the blade element theory. There is a third one, combining the first two theories, called Blade-Element Momentum Theory (BEM). None of these first two theories is sufficient alone while BEM is more useful nowadays since it considers both momentum theory and blade element theory.

2.1 Actuator Disk Theory (*Momentum Theory*)

By considering the propeller as a thin actuator disk, the **conservation of momentum** principle was applied to this actuator disk by Froude [5].

Through the disk, there will be a static pressure increase of flow as seen in Figure 2.1. If the momentum equation is applied between sections 0 and 1, sections 0 and 3 sections are applied,

Applying the continuity equation to the stream tube between sections 1 and 3 yields:

$$A_3V_3 = A_1V_1, \quad \dot{m} = \rho A_1V_1 = \rho A_3V_3 \tag{2.1}$$

where $\dot{m}$ is the mass flow rate, ρ is the density of the fluid, A is the cross-sectional area and V is the flow velocity.

$$F = \dot{m}(V_3 - V_0) = \rho A_1 V_1 (V_3 - V_0) = \rho A_3 V_3 (V_3 - V_0) \quad (2.2)$$

and

$$F = A_1 (p_2 - p_1) \quad (2.3)$$

are obtained respectively where F is the force acting on the stream tube.

Application of the Bernoulli's equation between sections 0 and 2 and sections 2 and 3 yields,

$$p_0 + \frac{1}{2}\rho V_0^2 = p_1 + \frac{1}{2}\rho V_1^2 \quad (2.4)$$

and

$$p_2 + \frac{1}{2}\rho V_2^2 = p_3 + \frac{1}{2}\rho V_3^2 \quad (2.5)$$

respectively. Subtracting Equation (2.4) from Equation (2.5) and using $V_1 = V_2$ and $p_0 = p_3$, it is possible to obtain

$$p_2 - p_1 = \frac{1}{2}\rho (V_3^2 - V_2^2) = \frac{1}{2}\rho (V_3 - V_0)(V_3 + V_0) \quad (2.6)$$

Combining Equations (2.2), (2.3) and (2.6), it is possible to obtain

$$V_1 = \frac{V_3 + V_0}{2} \quad (2.7)$$

This means that the airflow velocity at the entrance of the actuator disk is the average of the upstream velocity and the downstream velocity of the stream tube. The free stream velocity, V_0 , increases to V_1 at the upstream of the actuator disk as

$$V_1 = V_0 + w \tag{2.8}$$

where w is the induced velocity. Solving Equations (2.7) and (2.8) for V_3, one can obtain

$$V_3 = V_0 + 2w \tag{2.9}$$

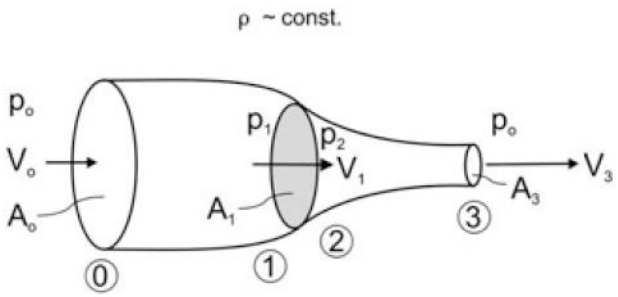

(a)

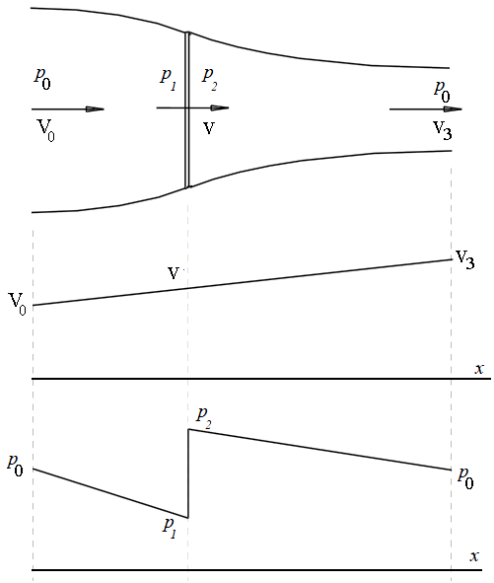

(b)

Figure 2.1 (a) Stream tube for the flow across the actuator disk (b) Velocity and pressure distribution in the stream tube

According to the momentum theory, as observed from equations (2.8) and (2.9), half of the velocity increase occurs in front of the actuator disk, while half of it occurs behind the actuator disk [23].

If the force acting on the stream tube given by Equation (2.2) is combined with Equations (2.8) and (2.9), it is possible to obtain

$$F = 2\rho A_1 (V_0 + w)\, w \tag{2.10}$$

So we have found the thrust from the actuator disk theory in Eq. (2.10). Let's find the ideal power similarly. The ideal power can be obtained by applying the energy equation to the stream tube of Figure 2.1 as

$$P = \dot{m}\left[\frac{V_3^2}{2} - \frac{V_0^2}{2}\right] = \frac{1}{2}\rho A_1 V_1 (V_3^2 - V_0^2) \tag{2.11}$$

Using Equation (2.8) and (2.9), the above equation can be expressed as

$$P = 2\rho A_1 w (V_0 + w)^2 \tag{2.12}$$

Now, if Equation (2.10) is substituted into Equation (2.12), then

$$P_{ideal} = F(V_0 + w) \tag{2.13}$$

Hence, the ideal power is the product of thrust and velocity through the actuator disk. In this equation, the first term FV_0 is called useful power, P_{use}, while the second term, Fw , is called induced power, P_{ind} .

Equation (2.10) yields a quadratic equation for the induced velocity, which can be solved for the positive root as

$$w = -\frac{V_0}{2} + \frac{1}{2}\sqrt{V_0^2 + \frac{2F}{\rho A_1}} \tag{2.14}$$

The ideal efficiency is then defined as the useful power divided by ideal power as

$$\eta_{ideal} = \frac{FV_0}{F(V_0 + w)} = \frac{1}{1 + \frac{w}{V_0}} = \frac{V_0}{V_1} \tag{2.15}$$

When there is no induced velocity ($w = 0$), the efficiency becomes 1.

The thrust coefficient can be defined as

$$C_T = \frac{F}{\frac{1}{2}\rho A V_0^2} \tag{2.16}$$

while the power coefficient is

$$C_P = \frac{P_{shaft}}{\frac{1}{2}\rho A V_0^3} = \frac{FV_0/\eta_{pr}}{\frac{1}{2}\rho A V_0^3} \tag{2.17}$$

where P_{shaft} is the engine shaft power and η_{pr} is the real efficiency of the propeller.

$$\eta_{pr} = \frac{FV_\infty}{P_{shaft}} \tag{2.18}$$

The actuator disk theory provides an estimate of induced velocity, amount of thrust (in the absence of losses) and amount of engine shaft power (in the absence of losses).

$$P_{ideal} = F(V_0 + w) = correction\ factor.P_{shaft} \tag{2.19}$$

where a correction factor of 75 to 80% is acceptable.

Briefly, momentum theory gives an initial idea relating the performance of a propeller but does not provide the detailed design of the propeller. Detailed design data is obtained in Blade Element Theory (BET) dividing up the blade into a

sufficient number of elements and calculating the forces acting on the blade elements with the help of the lift and drag coefficients of the airfoil used in each elements of blades and integrating these forces along the propeller radius gives the thrust, torque and power [18]. But, the blade element theory is not sufficient alone since it lacks calculating induced velocity. Thus, both momentum and blade element theories are required for a detailed analysis and design of a propeller so that it is common to use a combined blade element momentum theory (BEM) in propeller design.

2.2 Blade Element Momentum (BEM) Theory

Since the momentum theory does not provide sufficient information for the detailed design, the forces acting on a propeller blade can be determined via Blade Element Theory. In the blade element theory, the aerodynamics of the propeller blade is analyzed to obtain the information that the actuator disk theory cannot provide. In blade element theory, the blade is divided into sections or elements (usually between ten and twenty) as shown in Figure 2.2 and then aerodynamic properties (forces, torques, etc.) in a section are locally examined along the whole blade from hub ($r = r_h$) to tip ($r = R$). First the elementary forces acting over each section are determined and then integrated over the propeller radius in order to obtain the total thrust, torque and power values. [5][18]

The blade element momentum theory combines the actuator disk theory and blade element theory. Blade element Momentum theory does not include 3D effects such as tip vortex or radial components of the induced flow due to the angular acceleration of the rotating propeller. When compared to the actual results, blade element theory gives higher values for thrust, lower values for torque and 5% to 10% higher values for efficiencies. But, this theory is very useful for the initial prediction of thrust, torque and efficiency of the propellers. [19]

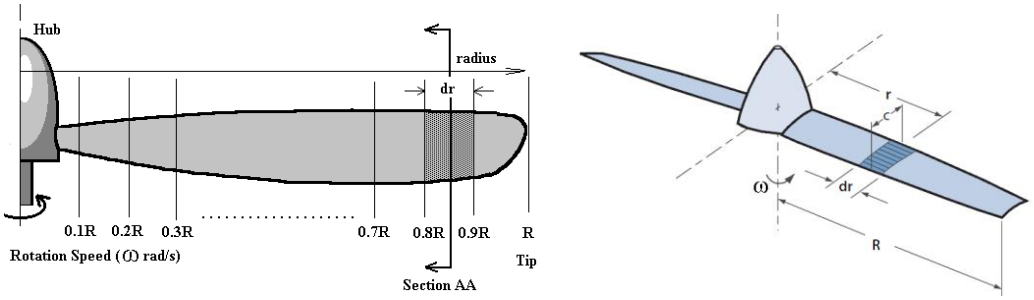

Figure 2.2 Sections on the propeller blade [19], [20]

The pitch of a screw is defined as advance of the screw per revolution. Propellers make a similar movement like a screw so they follow a helical path. The geometrical pitch angle β at a distance r from the axis of the propeller is the angle between the plane of rotation and zero lift line of a blade section as shown in Figure 2.3.

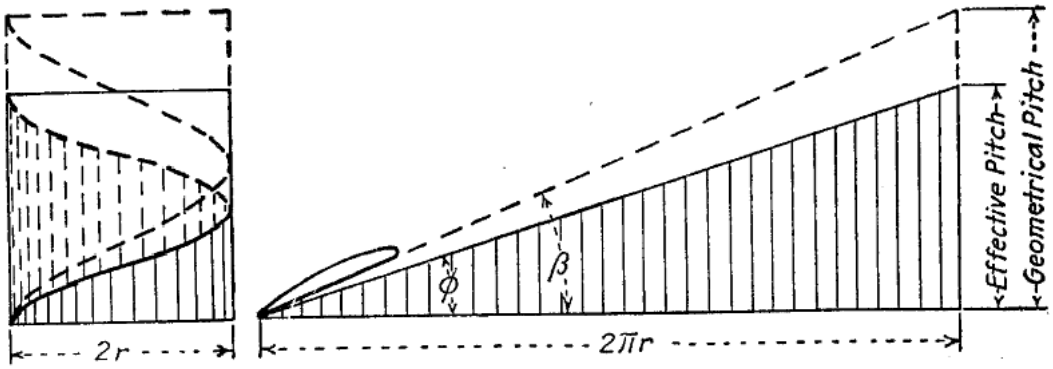

Figure 2.3 The difference between effective and geometrical pitches [23]

There are two different pitches. These are the effective pitch and geometrical pitch. The geometrical pitch, h is the distance that the propeller advances along the axis of the rotation in one revolution and is given by

$$h = 2\pi r \tan\beta \tag{2.20}$$

Instead of geometrical pitch angle β, if the flow angle, ϕ, is used the *effective pitch* which is the actual distance that the propeller advances in one revolution.

These two differences are shown in Figure 2.3. In general, the *nominal or standard geometrical pitch* of a propeller is calculated at its ¾ radius station [21] and calculated as

$$h = 2\pi(r_{0.75}) \tan(\beta_{0.75}) \tag{2.21}$$

In a constant flight speed V_∞ of a propeller, the rotational speed at the hub of the propeller is small in comparison to the speed at the tip of the propeller. As a result the rotational speed changes along the radius of the propeller. In order to prevent the change angle of attack at various sections due to the change in rotational speed along the radius of the propeller, the propeller blade is twisted so that the geometrical pitch and geometrical pitch angle becomes larger at the hub. This situation is illustrated in Figure 2.4. [1]

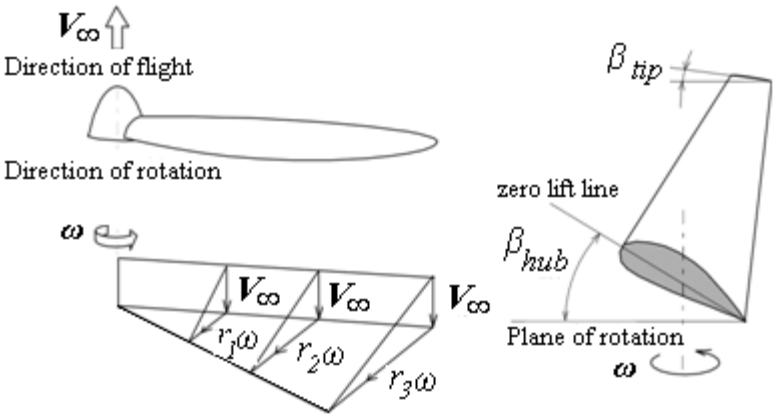

Figure 2.4 Change in geometrical pitch along the blade [1]

An example of twisting distribution from the root (hub) to the tip along the blade is shown in Figure 2.5. [21].

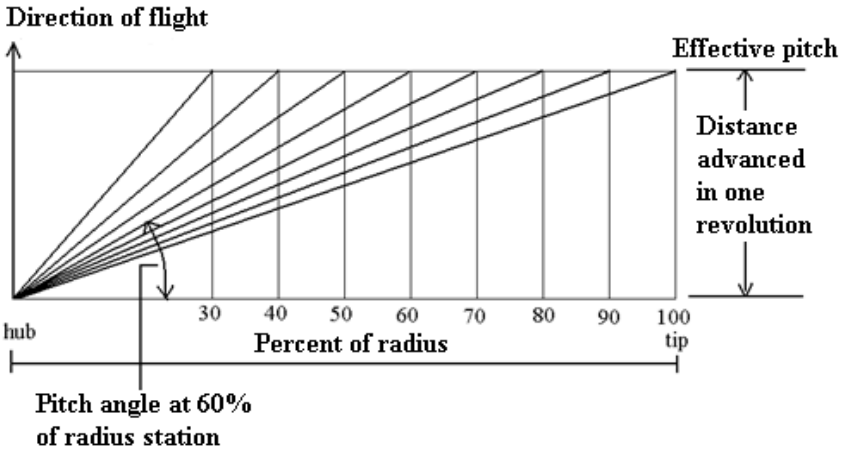

Figure 2.5 Blade pitch angles at different radius stations [21]

As may observed from Figure 2.6, there are three different velocities. These are the forward speed of aircraft of V_∞, the rotational speed of the propeller ωr, and the induced velocity of *w*. The section's local induced angle of attack is α_i. The normal angle of attack of the blade section is α, while the induced angle of attack of this section is α_i .

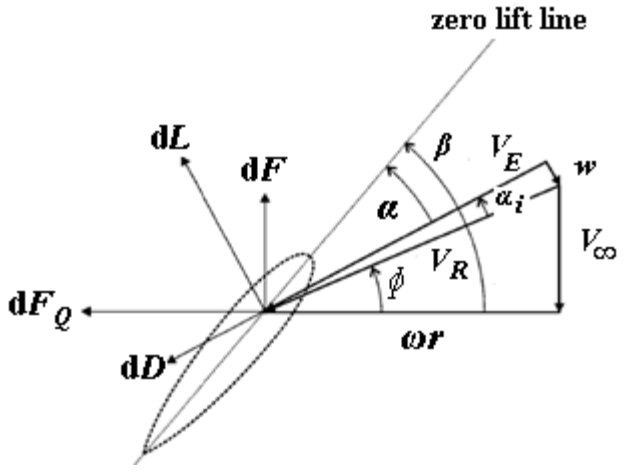

Figure 2.6 Forces acting on a propeller blade section

The forces acting on the section of a real propeller blade can be observed in a better way from Figure 2.7. [19]

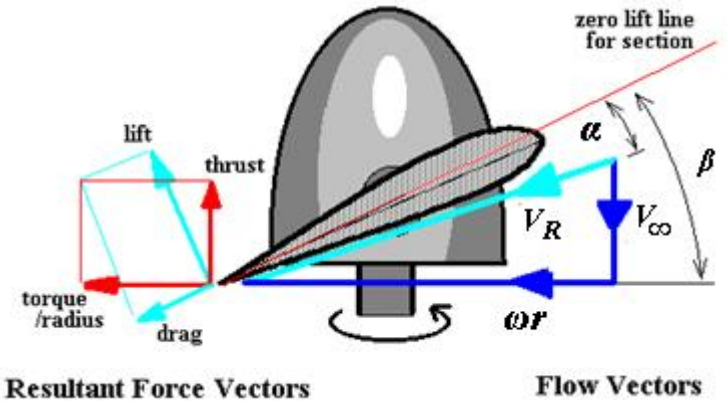

Figure 2.7 Forces acting on one section of a propeller blade [19]

The local infinitesimal thrust dF is,

$$\mathrm{d}F = \mathrm{d}L\cos(\phi + \alpha_i) - \mathrm{d}D\sin(\phi + \alpha_i) \tag{2.22}$$

where ϕ is the angle between the resultant velocity V_R and the angular flow velocity ωr. The resultant velocity is defined as,

$$V_R = \sqrt{(\omega r)^2 + V_\infty^2} \tag{2.23}$$

The local infinitesimal orque for one section is defined as,

$$\mathrm{d}Q = r\,\mathrm{d}F_Q = r[\mathrm{d}L\sin(\phi + \alpha_i) + \mathrm{d}D\cos(\phi + \alpha_i)] \tag{2.24}$$

The incremental lift of local chord- c is,

$$\mathrm{d}L = \frac{1}{2}\rho V_E^2 c C_L \mathrm{d}r \tag{2.25}$$

where C_L is the lift coefficient of the incremental section. Similarly, the incremental drag is,

$$\mathrm{d}D = \frac{1}{2}\rho V_E^2 c C_D \mathrm{d}r \tag{2.26}$$

where C_D is the drag coefficient of the incremental section.

The overall resultant velocity, V_E, can be expressed

$$V_E = \sqrt{[\omega r - w\sin(\phi + \alpha_i)]^2 + [w\cos(\phi + \alpha_i) + V_\infty]^2} \tag{2.27}$$

while induced angle of attack can be found as

$$\alpha_i = \sin^{-1}(\frac{w}{V_R}) \tag{2.28}$$

C_L can be estimated by the formula below by using the slope of the lift-curve $C_{L\alpha}$,

$$C_L = C_{L_\alpha}\alpha = C_{L_\alpha}(\beta - \alpha_i - \phi) \tag{2.29}$$

C_D can be estimated according to the below assumptions;

$$C_D = C_{D,min}, \quad \text{if } C_L < C_{L,min} \tag{2.30a}$$

$$C_D = C_{D,min} + k(C_L - C_{L,min})^2, \quad \text{if } C_{L,min} < C_L < C_{L,max} \tag{2. 30b}$$

$$C_D = C_{D,\alpha_{max}} + k_1(\alpha - \alpha_{max}), \quad \text{if } \alpha > \alpha_{max} \tag{2. 30c}$$

When the airfoil stalls, C_L becomes $C_{L,max}$ and α becomes α_{max}.

The theoretical value of lift-curve slope a_0 or C_{L_α} is 2π but it is determined as 5.7 per radian or 0.1 per degree experimentally [18].

If α_i is very small but ϕ is not small, then the drag force is small in comparison to lift forces. As a result w is small, $V_E \approx V_R$ and α_i is zero. In this case, $\mathrm{d}D$ is zero and combination of Equation (2.22), (2.25) and (2.28) yields,

$$\mathrm{d}F \approx \mathrm{d}L\cos\phi = \frac{1}{2}\rho V_R^2 c C_L \cos\phi\,\mathrm{d}r = \frac{B}{2}\rho V_R^2 c a_0(\beta - \alpha_i - \phi)\cos\phi\,\mathrm{d}r \tag{2.31}$$

where B is the number of blades in a propeller.

Using Equation (2.10) from the actuator disk theory, the infinitesimal thrust acting on an infinitesimal thickness of the propeller disk in Figure 2.8 is

$$\mathrm{d}F \approx 2\rho(2\pi r\mathrm{d}r)(V_0 + w_a)\,w_a \approx 2\rho(2\pi r\mathrm{d}r)(V_\infty + w\cos\phi)w\cos\phi \tag{2.32}$$

By using the component of w parallel to the thrust as shown in Figure 2.9 for small α_i , sin α_i = α_i and Equation (2.28) becomes

$$w = \alpha_i V_R \tag{2.33}$$

and by assuming the area dA of circular element of thichness dr as $2\pi r\mathrm{d}r$ as seen in Figure 2.8, we find the incremental thrust

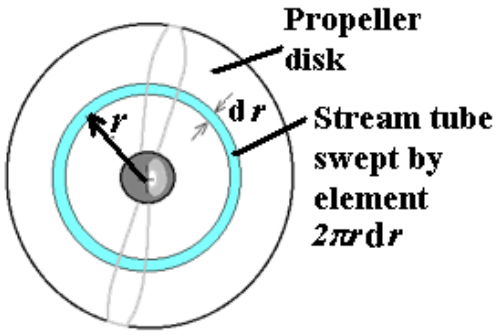

Figure 2.8 Circular element of the propeller disk [19]

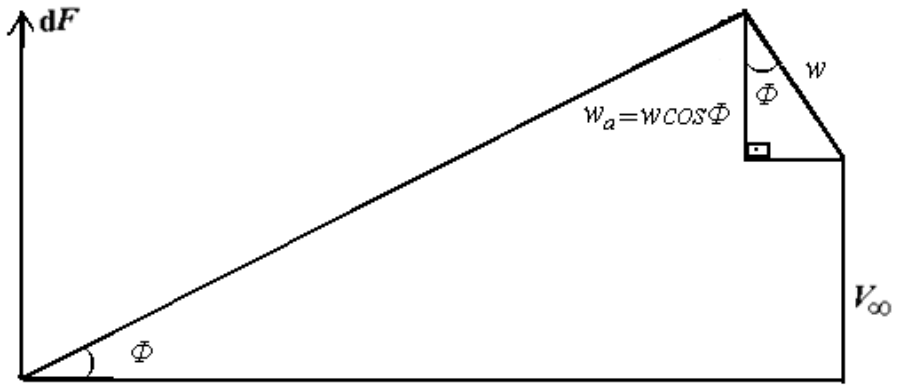

Figure 2.9 Component of w parallel to thrust dF

Combining Equations (2.31), (2.32) and (2.33), one can obtain a quadratic equation for α_i.

$$\alpha_i^2 + \left(\frac{V_\infty}{V_R \cos\phi} + \frac{ca_0 B}{8\pi r \cos\phi}\right)\alpha_i - \frac{ca_0 B}{8\pi r \cos\phi}(\beta - \phi) = 0 \qquad (2.34)$$

The above equation can be simplified by defining solidity, advance ratio and tip velocity.

The overall solidity is defined as the blade area divided by the disk area as,

$$\sigma_{ref} = \frac{blade\ area}{disk\ area} = \frac{Bc_{ref}R}{\pi R^2} = \frac{Bc_{ref}}{\pi R} \qquad (2.35)$$

while the local solidity becomes in terms of nondimensional form,

$$\sigma = \frac{Bc}{\pi R} = x\frac{Bc}{\pi R} \qquad (2.36)$$

with $x = r/R$.

A nondimensional air speed parameter known as advance ratio is defined as

$$J = \frac{V_\infty}{nd_p} = \frac{\pi V_\infty}{\omega R} \tag{2.37}$$

where n, is the rotational speed of the propeller shaft in revolution per second. Another nondimensional parameter called tip velocity ratio which is the ratio of flight speed to the propeller rotational tip speed can be defined as

$$\lambda = \frac{V_\infty}{\omega R} = \frac{J}{\pi} \tag{2.38}$$

Using blade tip speed $V_T = \omega r$, Equation (2.34) becomes,

$$\alpha_i^2 + \left(\frac{\lambda}{x} + \frac{\sigma a_0 V_R}{8x^2 V_T}\right)\alpha_i - \frac{\sigma a_0 V_R}{8x^2 V_T}\,(\beta - \phi) = 0 \tag{2.39}$$

which can be solved for

$$\alpha_i = \frac{1}{2}\{-\left(\frac{\lambda}{x} + \frac{\sigma a_0 V_R}{8x^2 V_T}\right) + \left[(\frac{\lambda}{x} + \frac{\sigma a_0 V_R}{8x^2 V_T})^2 + \frac{\sigma a_0 V_R}{2x^2 V_T}\,(\beta - \phi)\right]^{1/2}\} \tag{2.40}$$

After determining the induced angle of attack, the incremental thrust and torque which are expressed by Equations (2.22) and (2.24) respectively. The whole blade can be integrated to obtain the thrust and torque for the propeller shaft. The thrust coefficient C_T and the power coefficient C_P can now be defined as

$$C_T = \frac{F}{\rho n^2 d^4} \tag{2.41}$$

and

$$C_P = \frac{P_S}{\rho n^3 d^5} \tag{2.42}$$

respectively.

Now, integrating Equation (2.31) over the propeller blade

$$F = \frac{B}{2}\rho \int_0^R V_R^2 c C_L \cos\phi \, \mathrm{d}r$$
$$= \frac{B}{2}\rho \int_0^R V_R^2 c a_0 (\beta - \alpha_i - \phi) \cos\phi \, \mathrm{d}r \tag{2.43}$$

Recalling that α_i is very small, but ϕ is not small, then the drag force is negligible when compared to the lift force. As a result, w is small so that $V_E \approx V_R$ and α_i is zero and Equation (2.24) becomes

$$\mathrm{d}Q = r\mathrm{d}F_Q \approx \mathrm{d}L \sin\phi = \tfrac{B}{2}\rho V_R^2 c C_L \sin\phi \, r\mathrm{d}r \tag{2.44}$$

which can be integrated over the blade to obtain

$$Q = \frac{B}{2}\,\rho \int_0^R r V_R^2 c C_L \sin\phi \, \mathrm{d}r = \frac{B}{2}\,\rho \int_0^R r V_R^2 c a_0 (\beta - \alpha_i - \phi) \sin\phi \, \mathrm{d}r \tag{2.45}$$

The shaft power P_S can be obtained as

$$P_S = \int_0^R \omega \mathrm{d}Q = \frac{B}{2}\,\rho \int_0^R \omega r V_R^2 c C_L \sin\phi \, \mathrm{d}r$$
$$= \frac{B}{2}\,\rho \int_0^R \omega r V_R^2 c a_0 \,(\beta - \alpha_i - \phi)\sin\phi \, \mathrm{d}r \tag{2.46}$$

Noting that

$$V_E^2 \approx V_R^2 = V_\infty^2 + \omega^2 r^2 = \frac{\omega^2 r^2}{\pi^2}(J^2 + \pi^2 x^2) \tag{2.47}$$

the thrust coefficient can be obtained as

$$C_T = \frac{\pi^2}{4\rho\omega^2 R^4}\int dF$$
$$= \frac{\pi}{8}\int_{x_h}^{1} \sigma(J^2 + \pi^2 x^2)\,[C_L \cos(\phi + \alpha_i) - C_D \sin(\phi + \alpha_i)]dx \tag{2.48}$$

while the power coefficient becomes

$$C_P = \frac{\pi^3}{4\rho\omega^3 R^5}\int dP_S$$
$$= \frac{\pi^2}{8}\int_{x_h}^{1} \sigma x(J^2 + \pi^2 x^2)\,[C_l \sin(\phi + \alpha_i) + C_d \cos(\phi + \alpha_i)]dx \tag{2.49}$$

The propeller efficiency given by Equation (2.18) takes the following form by using Equations (2.41) and (2.42).

$$\eta_{pr} = \frac{C_T \rho n^2 d^4 V_\infty}{C_P \rho n^3 d^5} = \frac{C_T}{C_P} J \tag{2.50}$$

If geometric pitch angle, blade chord, c, ratio of flight speed to the propeller rotational tip speed, λ, are given, one can calculate the induced angle of attack, α_i from Equation (2.40) and then find angle of attack α from the formulae, $\alpha = \beta - \alpha_i - \phi$. Having this, lift coefficient C_L can be calculated from the assumptions in

Equation (2.29) or from the value of a_0 or C_{L_α} as 5.7 per radian that is found experimentally. Drag coefficient C_D can then be estimated from again Equation (2.30). The thrust, torque and power can be found as approximate predictions using the above formulas. Thus momentum blade element theory gives a good prediction for the initial calculations, but it is not well enough yet to have an exact solution. In order to achieve this, vortex analysis at the blade tips must be studied in detail [17] [18].

2.3 Blade Element-Momentum Theory with induction factors

Briefly, the Blade Element Momentum Theory was the combination of two methods. One is to use momentum balance and the other is to analyze the forces formed by the lift and drag coefficients of the aerofoil at different sections on the blade. Equations obtained from these methods have to be solved in an iterative method and the blade is divided into sufficient number of elements (generally between ten and twenty) as shown in Figure 2.10. Overall result is obtained by numerical integration along the blade of the propeller. [22]

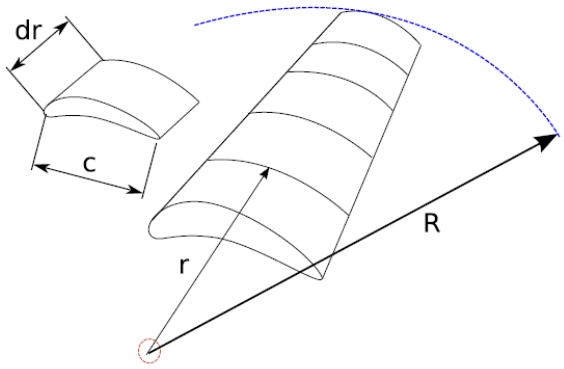

Figure 2.10 The Blade Element Model

Instead of using induced velocity w, here axial induction factor a, and radial induction factor b .

Axial induction factor a is defined as,

$$a = \frac{V_1 - V_0}{V_0} \tag{2.51}$$

With this definition, it can be obtained that

$$V_1 = V_0(1 + a) \tag{2.52}$$

$$V_3 = V_0(1 + 2a) \tag{2.53}$$

In this case the new figure showing the forces acting on a blade section is depicted in Figure 2.11.

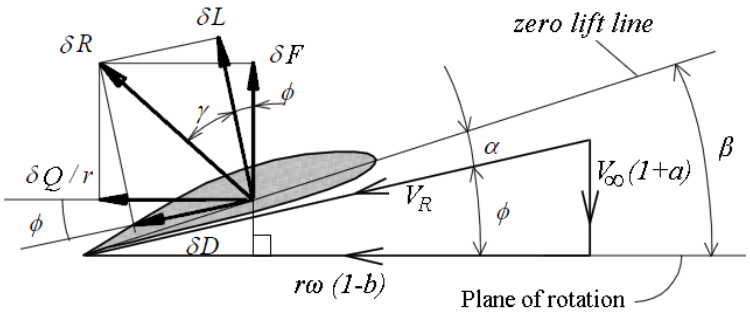

Figure 2.11 Forces acting on propeller blade [1]

The formulas being used a and b induction factors are indicated below [1]:

$$tan\gamma = \frac{\delta D}{\delta L} = \frac{C_D}{C_L} \tag{2.54}$$

$$V_R = \frac{V_\infty(1 + a)}{Sin(\phi)} = \frac{\omega r\,(1 - b)}{cos\,(\phi)} \tag{2.55}$$

$$\frac{V_\infty}{\omega r} = \frac{1 - b}{1 + a} tan(\phi) \tag{2.56}$$

$$\delta F = \delta R.cos(\gamma + \phi) \tag{2.57}$$

$$\frac{\delta Q}{r} = \delta R.sin\,(\gamma + \phi) \tag{2.58}$$

Shaft power and the power given by the engine are respectively,

$$\delta P_s = V_\infty.\delta F \tag{2.59}$$

$$\delta P = \delta Q.\omega \tag{2.60}$$

and efficiency can be expressed by

$$\eta_{pr} = \frac{\delta P_s}{\delta P} = \frac{V_\infty.\delta F}{\delta Q.\omega} = \frac{V_\infty.\delta R.cos(\gamma + \phi)}{\omega r.\delta R.sin(\gamma + \phi)} \tag{2.61}$$

or

$$\eta_{pr} = \frac{V_\infty.cos(\gamma + \phi)}{\omega r.sin(\gamma + \phi)} \tag{2.62}$$

and by using

$$\frac{V_\infty}{\omega r} = \frac{1-b}{1+a} tan(\phi)$$

it is obtained that the propeller efficiency as,

$$\eta_{pr} = \frac{1-b}{1+a}\,\frac{tan(\phi)}{tan(\gamma + \phi)} \tag{2.63}$$

The total lift and total drag of local chord- c with number of blade B and the lift coefficient C_l is,

$$\delta L = \tfrac{1}{2}\rho V_R^2 C_L B c \delta r \tag{2.64}$$

$$\delta D = \tfrac{1}{2}\rho V_R^2 C_D B c \delta r \tag{2.65}$$

The thrust is,

$$\begin{aligned}\delta F &= \delta L\cos(\phi) - \delta D\sin(\phi) \\ &= \tfrac{1}{2}\rho V_R^2 B c \delta r (C_L\cos(\phi) - C_D\sin(\phi))\end{aligned} \tag{2.66}$$

$$\begin{aligned}\frac{\delta F}{\delta r} &= \frac{1}{2}\rho V_R^2 B c C_L\left(\cos(\phi) - \frac{C_D}{C_L}\sin(\phi)\right) \\ &= \frac{1}{2}\rho V_R^2 B c C_L(\cos(\phi) - \tan(\gamma)\sin(\phi))\end{aligned} \tag{2.67}$$

$$\begin{aligned}\frac{\delta F}{\delta r} &= \frac{1}{2}\rho V_R^2 B c C_L\left(\frac{(\cos(\gamma)\cos(\phi) - \sin(\gamma)\sin(\phi))}{\cos(\gamma)}\right) \\ &= \frac{1}{2}\rho V_R^2 B c C_L\left(\frac{cos\,(\phi+\gamma)}{cos\,(\gamma)}\right)\end{aligned} \tag{2.68}$$

Similarly the torque is,

$$\begin{aligned}\frac{\delta Q}{r} &= \delta L\sin(\phi) + \delta D\cos(\phi) \\ &= \frac{1}{2}\rho V_R^2 B c \delta r (C_L\sin(\phi) + C_D\cos(\phi))\end{aligned} \tag{2.69}$$

$$\frac{\delta Q}{\delta r} = \frac{1}{2}\rho V_R^2 B c r C_L \left(\sin(\phi) + \frac{C_D}{C_L}\cos(\phi)\right) \tag{2.70}$$

$$= \tfrac{1}{2}\rho V_R^2 B \mathrm{c} C_L (\sin(\phi) + \tan(\gamma)\cos(\phi))$$

$$\frac{\delta Q}{\delta r} = \frac{1}{2}\rho V_R^2 B c r C_L \left(\frac{(\cos(\gamma)\, si\, n(\phi) + \sin(\gamma)\cos(\phi))}{\cos(\gamma)}\right)$$

$$\frac{\delta Q}{\delta r} = \frac{1}{2}\rho V_R^2 B \mathrm{cr} C_L \left(\frac{sin\,(\phi+\gamma)}{cos\,(\gamma)}\right) \tag{2.71}$$

obtained.

Generally $tan\gamma \approx 0.02$ and L/D is around 50 thus if it is calculated it is found that $cos\gamma \approx 1$ and by using solidity and simplifying the thrust and torque as follows:

solidity σ, is

$$\sigma = \frac{blade\ area}{stream\ tube\ area} = \frac{B.c.\delta r}{2\pi r\ \delta r} = \frac{B.c}{2\pi r} \tag{2.72}$$

$$\frac{\delta F}{\delta r} = \pi r \sigma \rho V_R^2 C_L cos\,(\phi+\gamma) \tag{2.73}$$

$$\frac{\delta Q}{\delta r} = \pi r^2 \sigma \rho V_R^2 C_L sin\,(\phi+\gamma) \tag{2.74}$$

Separately, the thrust acting on a stream tube is equal to the change of momentum passing through that stream tube.

$$\delta F = \dot{m}.\Delta V \tag{2.75}$$

$$V_1 = (V_3 + V_\infty)/2 = V_\infty(1+a) \tag{2.76}$$

$$V_3 = V_\infty(1 + 2a) \tag{2.77}$$

$$\Delta V = V_3 - V_\infty = V_\infty(1 + 2a) - V_\infty = 2aV_\infty \tag{2.78}$$

$$\dot{m} = \rho V_1(2\pi r\delta r) = \rho V_\infty(1 + a)(2\pi r\delta r) \tag{2.79}$$

$$\delta F = \rho V_\infty(1 + a)(2\pi r\delta r)(2aV_\infty) = 4\pi r\rho V_\infty^2 a(1 + a)\delta r \tag{2.80}$$

or

$$\frac{\delta F}{\delta r} = 4\pi r\rho V_\infty^2 a(1 + a) \tag{2.81}$$

Similarly, the torque can be found by applying momentum equation to the same stream tube,

$$\delta Q = \dot{m}.\Delta(\Omega r^2) \tag{2.82}$$

Where Ω is the induced angular speed at the exit plane of the propeller which can be written as,

$$\Omega = 2b\omega \tag{2.83}$$

$$\dot{m} = \rho V_\infty(1 + a)(2\pi r\delta r) \tag{2.84}$$

$$\delta Q = \rho V_\infty(1 + a)(2\pi r\delta r).(2b\omega r^2) \tag{2.85}$$

$$\frac{\delta Q}{\delta r} = 4\pi r^3\rho V_\infty b(1 + a)\omega \tag{2.86}$$

$\delta F/\delta r$ and $\delta Q/\delta r$ expressions both in momentum equation and blade element equation are combined and equaled to each other in the following order.

$$\frac{\delta F}{\delta r} = 4\pi r\rho V_\infty^2 a(1 + a) = \pi r\sigma\rho V_R^2 C_L cos\,(\phi + \gamma) \tag{2.88}$$

$$\frac{\delta Q}{\delta r} = 4\pi r^3 \rho V_\infty b(1+a)\omega = \pi r^2 \sigma \rho V_R^2 C_L sin\,(\phi+\gamma)$$

Separately, instead of V_R , it can be written as

$$V_R = \frac{V_\infty(1+a)}{Sin(\phi)} = \frac{\omega r\,(1-b)}{cos\,(\phi)} \tag{2.89}$$

Finally, the following relations are found:

$$\frac{a}{1+a} = \frac{\sigma}{4} C_L \frac{cos\,(\phi+\gamma)}{\sin^2(\phi)} \tag{2.90}$$

$$\frac{b}{1-b} = \frac{\sigma}{2} C_L \frac{sin\,(\phi+\gamma)}{\sin(2\phi)} \tag{2.91}$$

Induction factors a and b can be initiated with a first estimation and then found by iteration method. After induction factors a and b converge, the corresponding flow angle ϕ, lift coefficient C_l, angle of attack $\alpha = \beta - \phi$ if β is given, $\phi + \gamma$, V_R, flight speed V_∞ , Mach number M, $(dC_L/d\alpha)_M$, thrust $\delta F/\delta r$, torque $\delta Q/\delta r$, efficiency η can be found by the help of the following formulas.

$$C_L = C_{L_\alpha}.\alpha = (\tfrac{dC_L}{d\alpha})_M.\alpha = a_M.\alpha \tag{2.92}$$

$$a_M = \frac{a_0}{\sqrt{1-M^2}} \tag{2.93}$$

(For M < 0.6 -0.7)

$$M = \frac{V_\infty}{\sqrt{kRT}} \tag{2.94}$$

For the iteration of a and b in order to be converged sooner, it is recommended that the arithmetical mean of the previous value and the next value should be taken by the following formulas [1]:

$$a_i = \frac{a_i + \bar{a}_{i-1}}{2}, \qquad b_i = \frac{b_i + \bar{b}_{i-1}}{2} \tag{2.95}$$

CHAPTER 3

PROPELLER TEST APPARATUS

3.1 Propeller Test Apparatus

The propeller test apparatus is mainly designed to measure the thrust and torque values of a propeller at different air flow speeds. In static tests, the air velocity is zero since there is just rotational speed of the propeller, while it is a combination of the rotational speed of the propeller and wind tunnel axial velocity in dynamic tests.

3.2 Design of the Propeller Test Apparatus for Static Tests

A schematic three-dimensional and two-dimensional front view of the test apparatus are shown in Figures 3.1 and 3.2, respectively. The test apparatus has mainly a lower and an upper section. The lower section is a box frame having dimensions of 290x300x190 (*w*x*h*x*d*) mm and the upper section is something like an excavator arm having a vertical part followed by a horizontal part carrying an electric motor and a propeller to be tested. The whole structure is constructed from aluminum profiles having a cross-section of 20 mm by 20 mm.

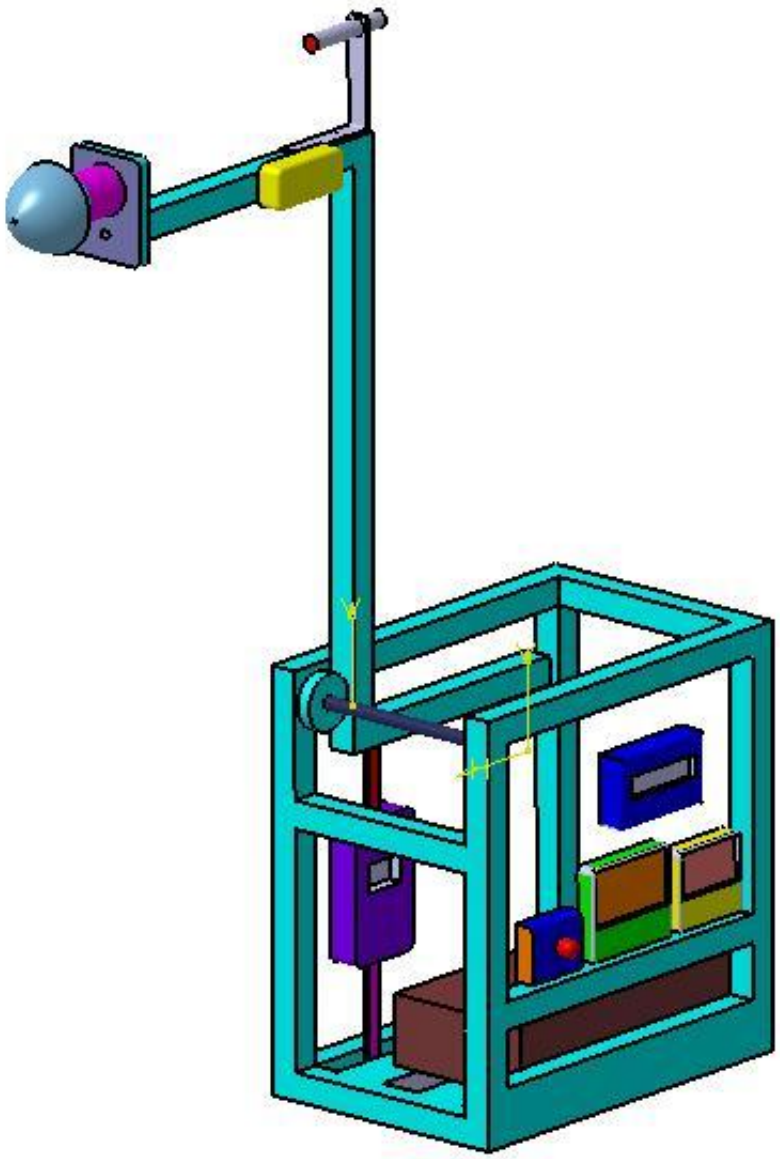

Figure 3.1 3D view of the propeller test apparatus

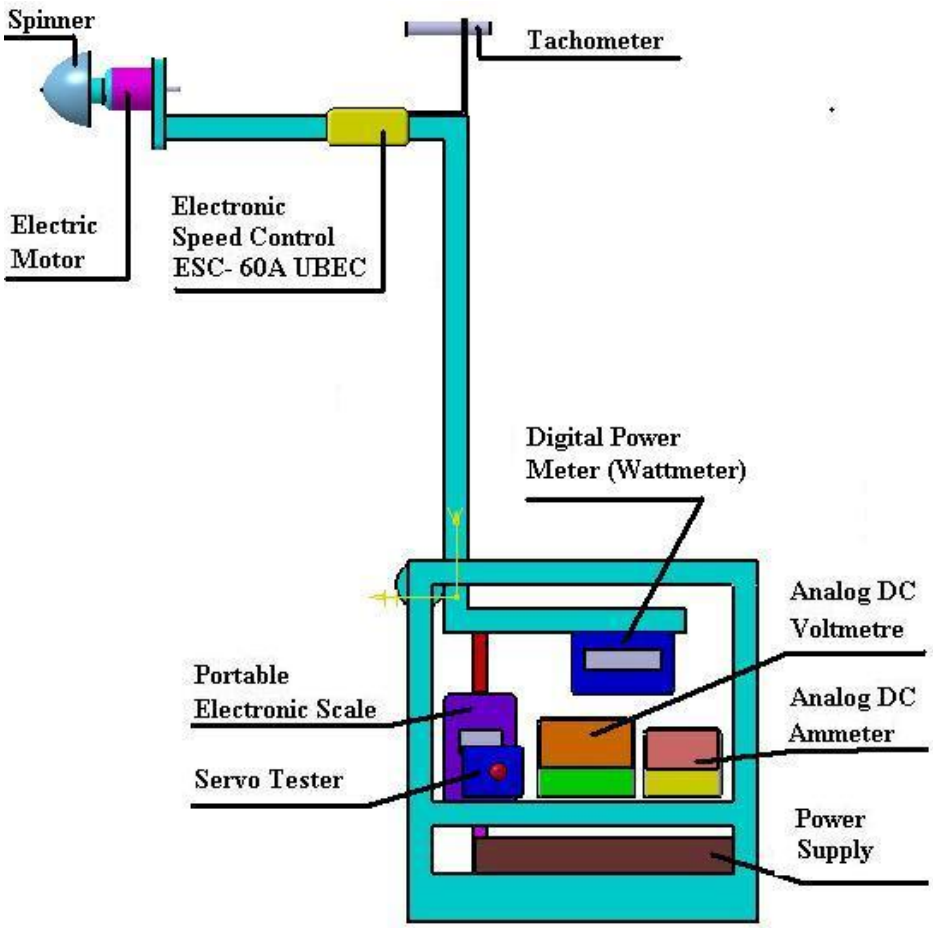

Figure 3.2 Schematic view of the propeller test apparatus

A Z-shaped simple cantilever beam at the upper section is connected to a portable electronic scale. The total length of this profile is 880 mm and it is constructed from aluminum profile having a cross-section of 20 mm by 20 mm. The dimensions and the general view of this cantilever beam are shown in Figure 3.3.

The thrust of the tested propeller has been calculated by applying the moment equation at a fixed point where there is a bearing allowing the free rotation of the cantilever system in the propeller test apparatus. The thrust of the propeller, *F*, can be related to the force, *G*, read out from the scale as follows:

$$F = \frac{b}{a}G = \frac{50\ mm}{425\ mm}G = \frac{G}{8.5} \tag{3.1}$$

It should be noted that the ratio of the force acting on the electronic scale to the propeller thrust has been taken as 8.5 in static tests, which is the ratio of the moment arms of having lengths of 425 mm and 50 mm.

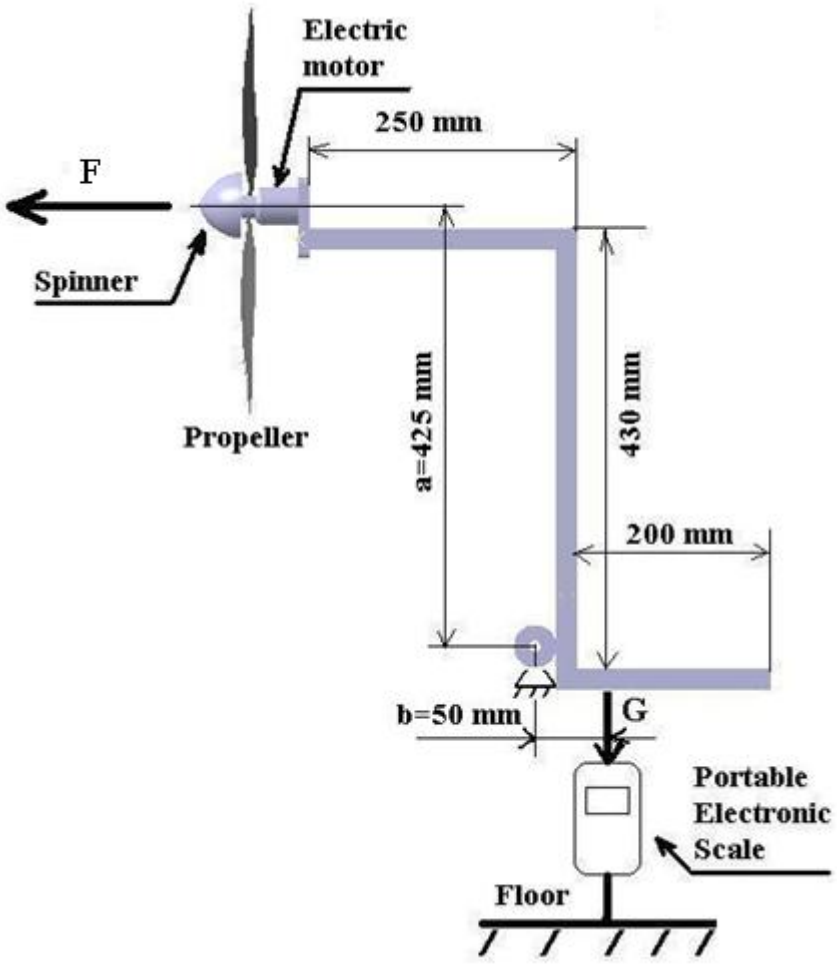

Figure 3.3 The structure and general view of cantilever beam

The complete view of the propeller test apparatus and the components installed are shown in Figure 3.4, while the upper and lower parts are shown separately in Figure 3.5, 3.6 respectively.

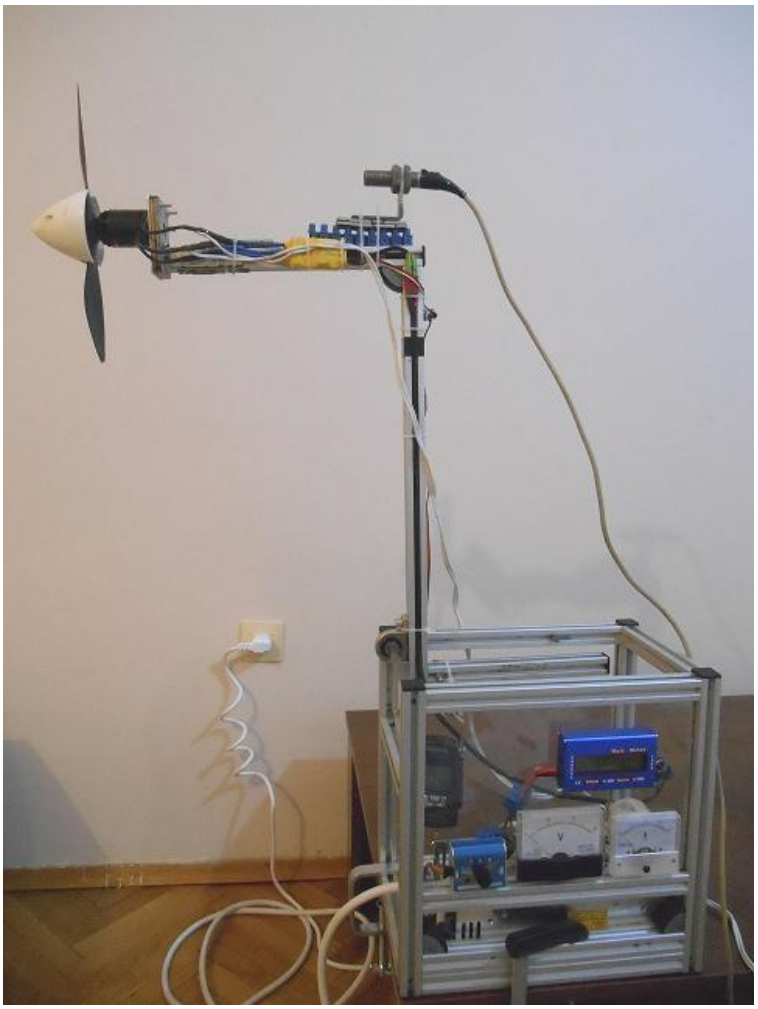

Figure 3.4 Whole view of the propeller test apparatus

The mechanical and electrical components installed to the test apparatus (see Figure 3.1) are the brushless electric motor (Emax Grand Turbo Electric Motor - GT 2826/04), electronic speed control (ESC- 60A UBEC), portable electronic scale, power supply, servo tester, digital power meter (Wattmeter), analog

Voltmeter, analog Ammeter, and propellers. A digital multimeter was used separately.

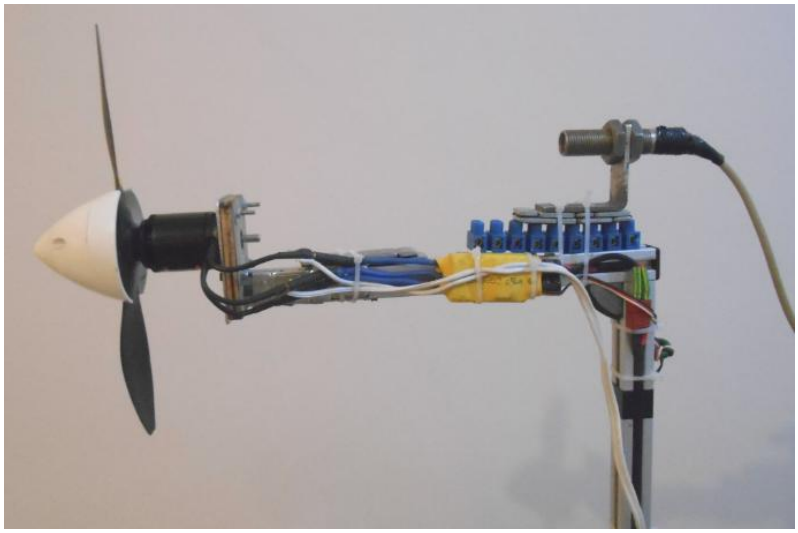

Figure 3.5 Upper section of the propeller test apparatus

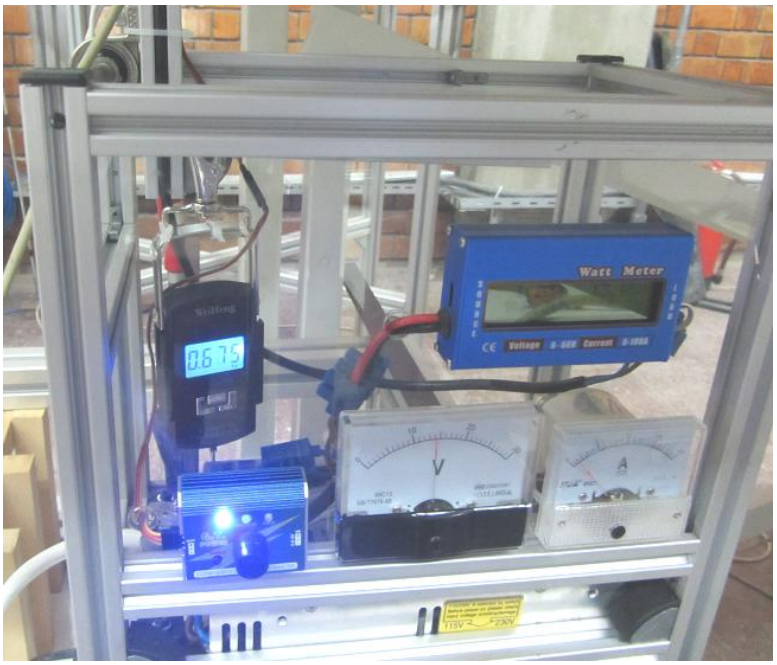

Figure 3.6 Lower section of the propeller test apparatus

Various types of propellers have been gathered for the tests. These propellers are designed and prototyped by Turbotek Turbomakina Teknolojileri Ltd Inc. The diameters and pitches in inch range as 10x6, 10x7, and 12x7. The set of propellers is shown in Figure 3.7.

Figure 3.7 Turbotek propellers

Electric Circuit Diagram of the Test Apparatus

In propeller test apparatus, power supply, voltmeter, ammeter, servo tester, electronic speed control (ESC), brushless electric motor, wattmeter, multimeter, tachometer and propeller have been installed according to the electric diagram shown in Figure 3.8.

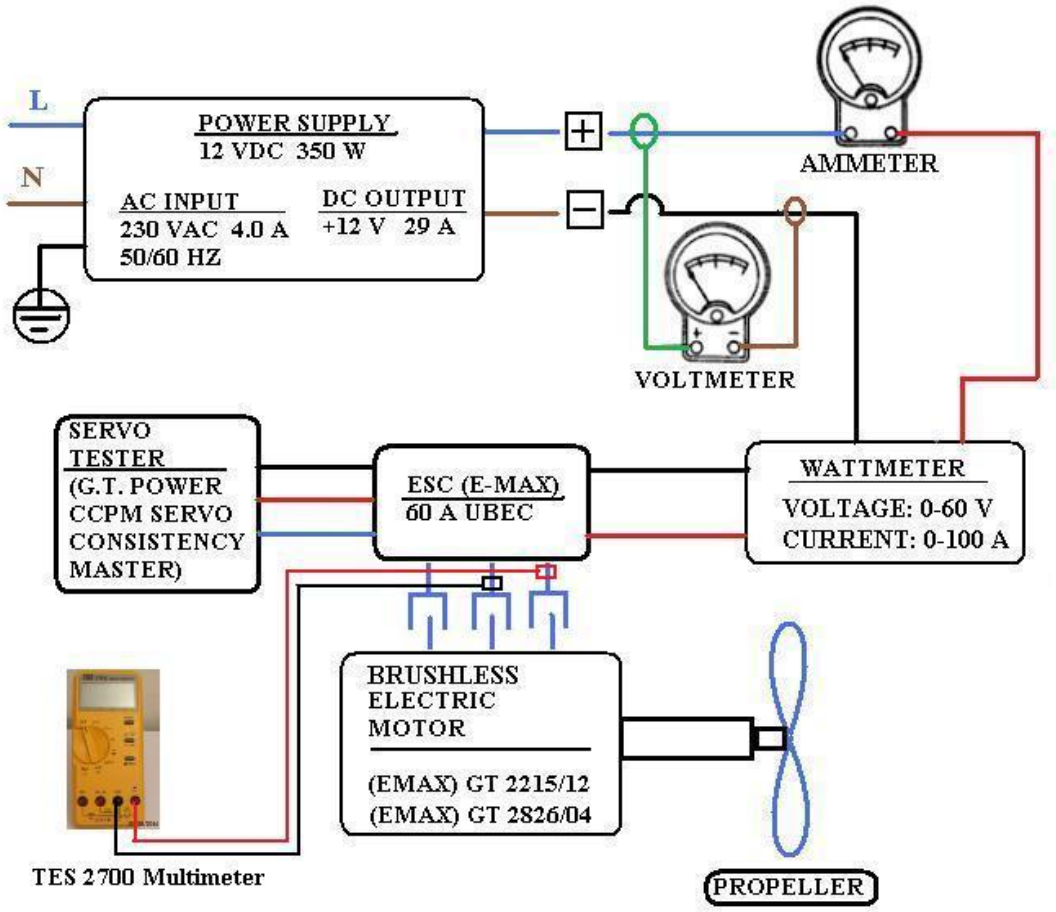

Figure 3.8 Electric diagram of the propeller test apparatus

RPM and Power Measurement

Besides the wattmeter, the voltage values at the electric motor's connection are measured via a multimeter for comparison in order to calculate rpm and power consumed.

There are two methods for measuring the speed of rotation. One of them is to use a standard tachometer for measuring revolutions per minute (rpm) value of the rotating propeller. The other is to use below formula shown in Equation (3.2) [26] [27].

$$N = K_v(V_{in} - I_{in}R_m) \tag{3.2}$$

where N is the rpm, K_v is the constant specific for themotor, that is rpm per volt, V_{in} is the input voltage, I_{in} is input current, R_m is the winding resistance of the motor, the product $I_{in}R_m$ is the voltage loss in the resistor. For this reason, the current and voltage values of the electric motor should be measured during the operation of the propeller.

At the same time, the shaft output power $P_{m,out}$ and the shaft input power $P_{m,in}$ can be calculated by using voltage and current values as follows [26][27]:

$$P_{m,out} = (V_{in} - I_{in}R_m)(I_{in} - I_0) \tag{3.3}$$

$$P_{m,in} = V_{in}I_{in} \tag{3.4}$$

where I_0 is the no load current of the electric motor.

Equation 3.2 has been used to determine the rpm values of the rotating propeller in the wind tunnel tests and is compared with the readout value at the tachometer. Equation 3.3 has been used to calculate the power consumed by the propeller. Because, a torque meter is not used for calculating the power consumed by the propeller.

The other method is to use a photo reflector laser beam device that senses each pass of the propeller blade with the help of a reflector tape placed on the blade surface facing the laser beam and a main processor device. This device is called tachometer and thus it consists of two main parts. One is the sensor and the other is the electronic processing device. The components of the tachometer are shown in Figures 3.9 and 3.10, respectively.

Figure 3.9 Laser sensor of the tachometer

Figure 3.10 Tachometer

The holder of the laser component has been fixed on an arm at the same axis with the propeller at a distance away from the back side of the propeller as shown in Figure 3.11. The laser beam is to be targeted to the propeller blade so that the propeller blade reflects the laser beam back to the sensor via a reflector sticked on the propeller blade. The sensor sends a signal of each reflected beam to the electronic processing unit by a connection cable where the laser signal is converted into a digital data that represents revolution per minute (rpm) value at its readout screen.

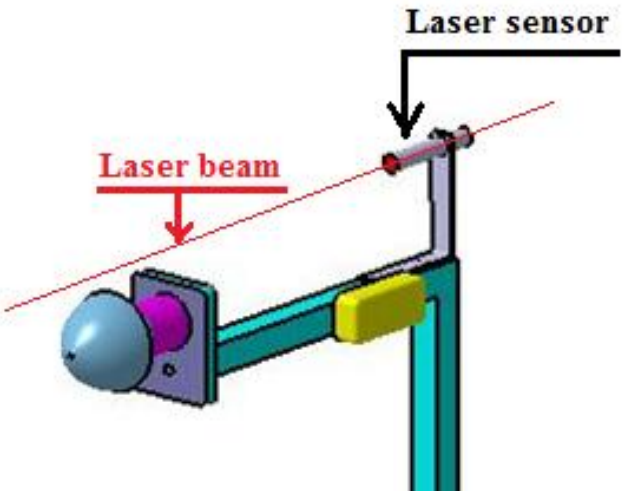

Figure 3.11 Laser beam sensor targeting the propeller blade

Since brushless electric motors are hobby market products depending on their quality and do not have a standard power formula and since AC motor formulas are also complex and do not show a linear characterization for the power calculation, a DC motor power formula has been used in determining the power. So, it may sometimes show larger deviations especially in lower voltage values. Therefore, the power of brushless electric motors may differ from the powers written on their labels. For this reason, there is no method for the power calibration. Thus, the power calibration could be carried out by RPM formulations which are dependent on each other. But, since higher voltage values are taken into account, power calculations are sufficient to evaluate the power. The efficiency of electric motor becomes approximately 95 % similar to the other motors. Thus, this study will give an approximate power value and the calibrated power value will be used as $P_{m,\,out}$.

3.3 Propeller Test Apparatus for Dynamic Tests

For dynamic tests, the propeller test apparatus is placed in a wind tunnel. The wind tunnel that is used in dynamic tests is an open-return wind tunnel of Mechanical Engineering Department at the Middle East Technical University (METU). The tunnel has a fully transparent test section having dimensions of 750 x 502 x 2400 mm. Although the tunnel can provide free stream velocities up to 30 m/s, the tunnel was operated in the range of 5 to 20 m/s. The average velocities corresponding to percentage fan powers and turbulence intensities measured at different velocities are tabulated in Tables 3.1 and 3.2, respectively. The air is sucked into the wind tunnel through the twin inlets and then accelerated in the contraction cone having a contraction ratio of 8.4:1. The tunnel has a 45 kW fan that can be operated at 1,000 rpm. The whole view of the wind tunnel is shown in Figure 3.12.

Table 3.1 Average velocities corresponding fan powers in METU wind tunnel

Fan Power (%)	4.5	10	15	20	25	30	35	40	45	50	55	60	65	70	75
Velocity in Test Section (m/s)	0.41	1.86	3.14	4.47	5.75	7.12	8.42	9.77	11.11	12.48	13.72	15.24	16.69	17.81	19.32

Table 3.2 Turbulence intensities measured at different velocities in METU wind tunnel

Velocity (m/s)	Turbulence Intensity
1.06	0.783
3.47	0.928
6.36	0.754
9.12	0.807
12.20	0.865
16.70	0.931
20.72	0.862

Figure 3.12 Wind tunnel of Mechanical Engineering Department in METU

The technical drawing of the wind tunnel can also be seen in Figure 3.13

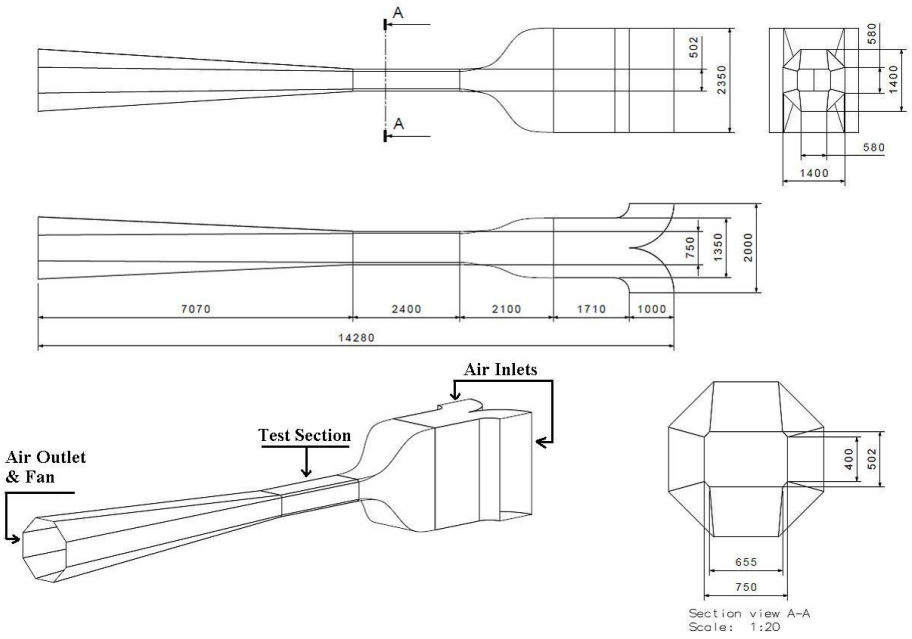

Figure 3.13 Technical drawing of the wind tunnel in the Mechanical Engineering

The technical specification of the METU wind tunnel is given in Table 3.3.

Table 3.3 Specification of METU Wind Tunnel

Wind Tunnel Sections	Specification Data
Type	Open return
Test Cross-Section	750 x 502 mm
Length of Test Section	2400 mm
Length of Entry Section	2710 mm
Length of Contraction Section	2100 mm
Length of Diffuser Section	7070 mm
Total Length	14280 mm
Contraction Cross-Section	1400 x 2350 mm
Contraction Ratio	8.4:1
Cone Angle of the Diffuser	~3^o
Fan power at 1000 rpm	45 kW

The propeller and its supporting bar are positioned at the center of the test section. The laser beam device is located at the back of the propeller, which is sufficiently far away from the propeller. A hole is drilled at the floor of the test section so that the vertical part of the cantilever beam can to move freely and horizontally without touching any surroundings. The installation of the upper section of the propeller test apparatus into the wind tunnel is shown in Figure 3.14 and 3.15.

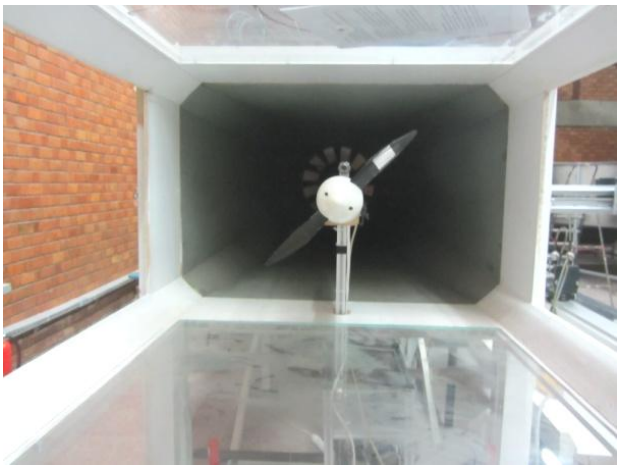

Figure 3.14 The position of the propeller in the test section of the wind tunnel

Figure 3.15 Installation of the upper section of the propeller test apparatus into the wind tunnel

The lower section of the propeller test apparatus is just placed under the test section of the wind tunnel as seen in Figure 3.16.

Figure 3.16 General view of the installation of the propeller test apparatus to the test section of the wind tunnel

The data that is necessary for evaluating the performance of propellers tested in the wind tunnel are the air velocity by adjusting the fan power according to Table 3.1, current from ammeter and wattmeter, DC voltage from voltmeter, AC voltage from electric motor and rotational speed from the tachometer. The ambient temperature and pressure data have been taken from the devices in METU laboratory. The diagram of the measurement system is shown in Figure 3.17.

3.4 Test Procedure

The data used for the performance tests of the propellers in the wind tunnel are gathered as shown in the diagram of the measurement system in Figure 3.17. The procedure for testing of each propeller includes the following steps:

a) Assemble the propeller to the propeller test apparatus.
b) Turn on the power supply.
c) Hear the special beep sound of the electric motor to be sure if it's ready.
d) Check that the power supply and servo tester are on.
e) Check if the propeller starts to turn without any problem.
f) Adjust the speed of the wind tunnel to the target speed (5 to 20 m/s)
g) Adjust the rotational speed of the propeller to the requested revolution per minute (rpm) by turning the knob on the servo tester counterclockwise very slowly until required rotational speed is reached by observing the value on the tachometer's screen.
h) Read the scale value in kg on the portable electronic scale's screen.
i) Read the current value from both analog ammeter and digital wattmeter.
j) Read the inlet voltage value from both analog voltmeter and digital wattmeter.
k) Read the AC voltage value from multimeter that is connected to the terminals of the brushless electric motor.
l) Read the rotational speed (rpm) from the tachometer.
m) Record the ambient temperature and pressure during the test.
n) Tabulate all readout values.
o) If a negative thrust value is obtained at the scale, terminate the test for the related step and go to a new test step or start a new propeller test.

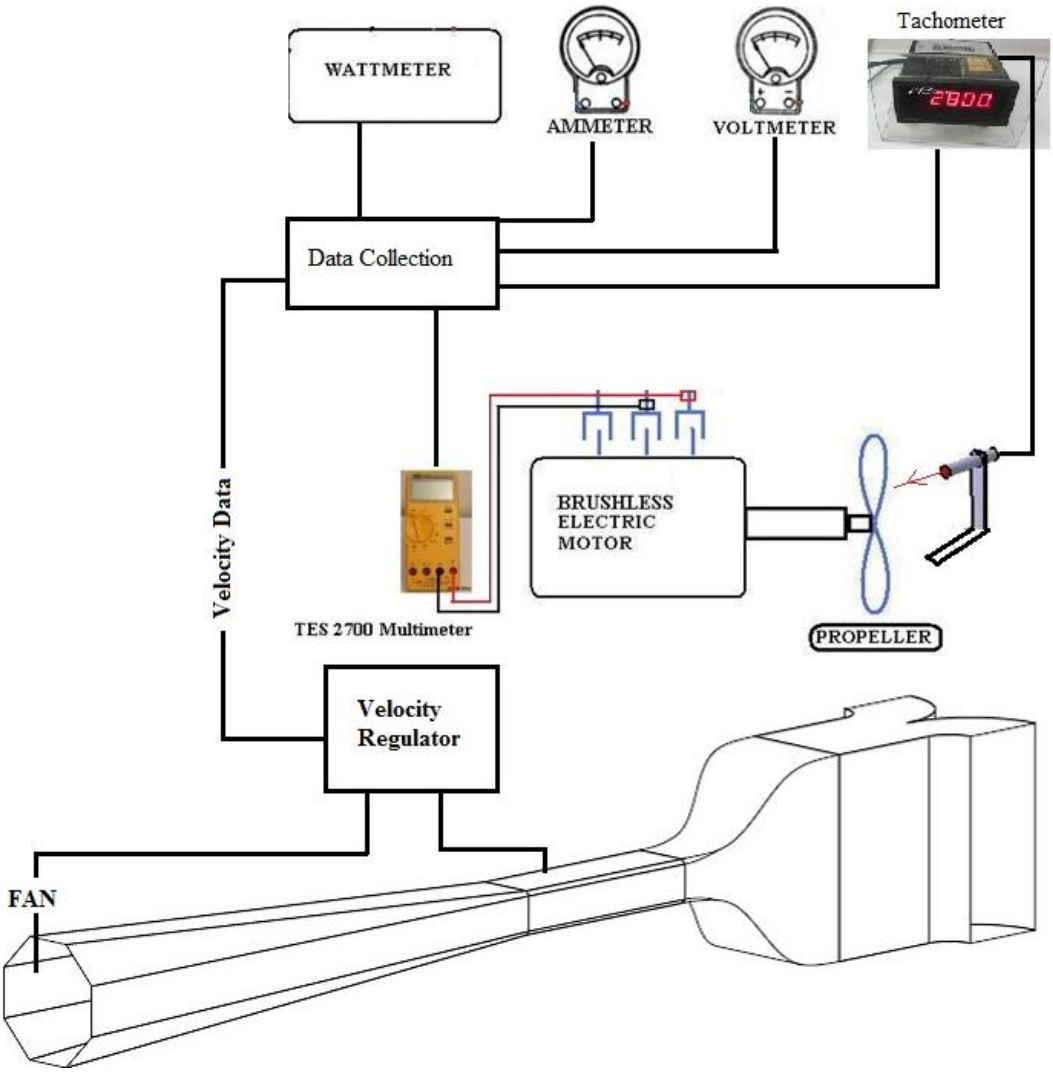

Figure 3.17 Measurement system diagram

CHAPTER 4

PROPELLER TESTING

4.1 Static Thrust Measurements

The static thrust indicates the performance of a propeller when there is no free stream velocity. In this case, the advance ratio J that is $V/(nd_p)$ becomes zero since the free stream velocity V is zero. At the same time, the propeller efficiency η also becomes zero since the efficiency is given as$C_T\, J/C_P$.

In propeller test apparatus, four different propellers have been tested statically in the propeller test apparatus and their specifications are given in Appendix C. These are:

- Prop6 propeller
- Prop1 propeller
- eProp2 propeller
- eProp1 propeller

Emax GT 2826/04 Brushless Electric Motor has been used in the static tests for all propellers. The specifications of electric motor used in static tests are presented in Appendix A.

4.1.1 Static Thrust of Prop6 Propeller

The 3D CAD model and prototype of the Turbotek Prop6 (10x7) propeller are shown in Figures 4.1 and 4.2, respectively.

Figure 4.1 3D CAD model of Turbotek Prop6 (10x7) Propeller [24]

Figure 4.2 Prototype of Turbotek Prop6 (10x7) Propeller [24]

The variation of static thrust with the rotational speed is given in Figure 4.4 and it is tabulated in Appendix B. One can observe that the thrust increases as the rotational speed increases. At the same time, the comparison with respect to the thrust values of Turbotek Prop6 Propeller in Design Document [24] is shown in the same Figure 4.4. It is seen that, the experimental results of each studies in the regions having the same rotational speeds are quite close to each other.

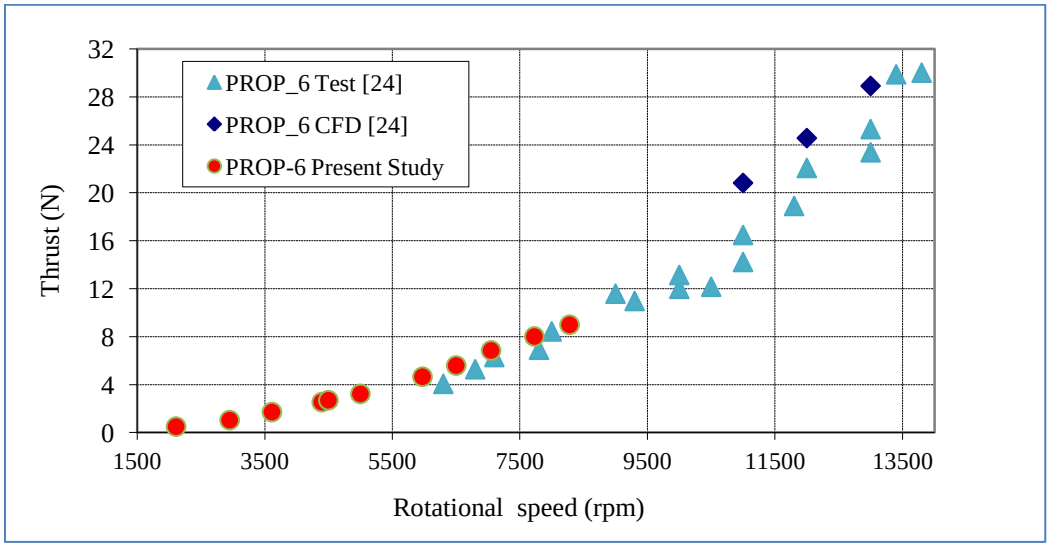

Figure 4.4 Variation of the static thrust of the Prop6 (10x7) propeller with the rotational speed [24]

4.1.2 Static Thrust of Prop1 Propeller

The 3D CAD model and prototype of the Turbotek Prop1 (10x6) propeller are shown in Figures 4.5 and 4.6, respectively.

Figure 4.5 3D CAD model of Turbotek Prop1 (10x6) Propeller [25]

Figure 4.6 Prototype of Turbotek Prop1 (10x6) Production Propeller [25]

The variation of static thrust with the rotational speed is given in Figure 4.7 and it is tabulated in Appendix B. At the same time, the comparison with respect to the thrust values of Turbotek Prop1 Propeller in Design Document [25] is shown in the same Figure 4.7. Here, it can be said that the results are compatible to each other though there are some differences.

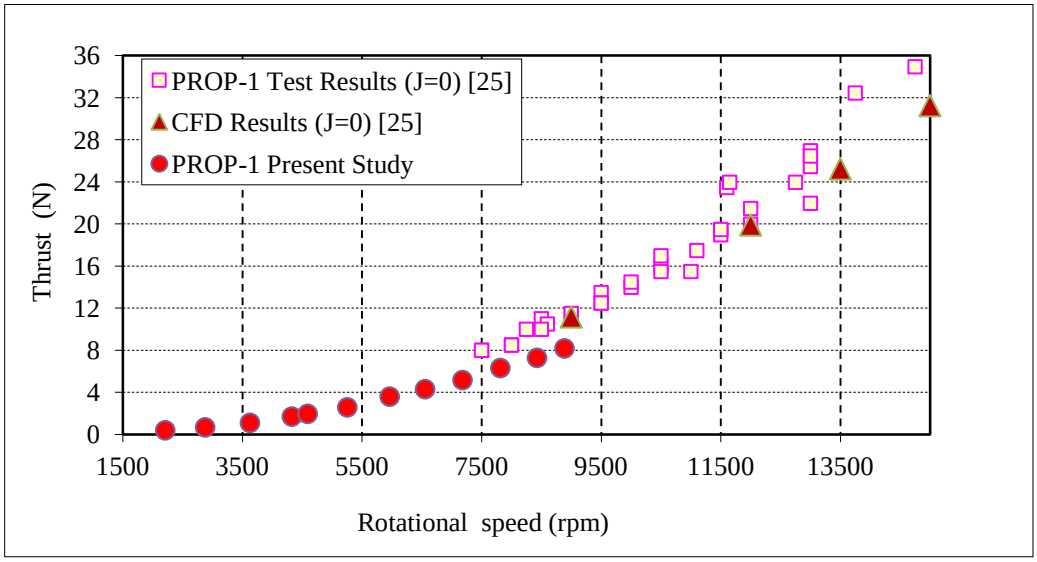

Figure 4.8 Variation of the static thrust of the Turbotek Prop1 (10x6) propeller with the rotational speed) [25]

4.1.3 Static Thrust of eProp2 Propeller

The 3D CAD model and prototype of the Turbotek eProp2 (12x7) propeller are shown in Figures 4.9 and 4.10, respectively.

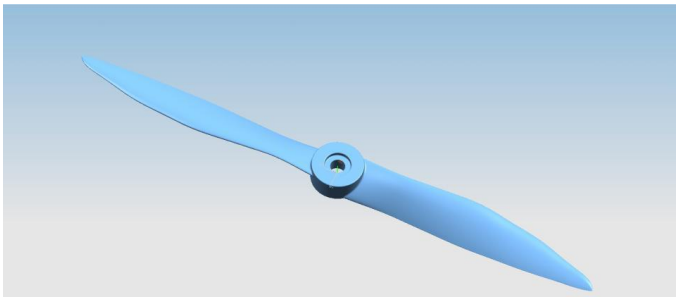

Figure 4.9 3D CAD model of Turbotek eProp2 (12x7) [26]

Figure 4.10 Prototype of Turbotek eProp2 (12x7) Propeller [26]

The variation of static thrust with the rotational speed is given in Figure 4.11 and it is tabulated in Appendix B.

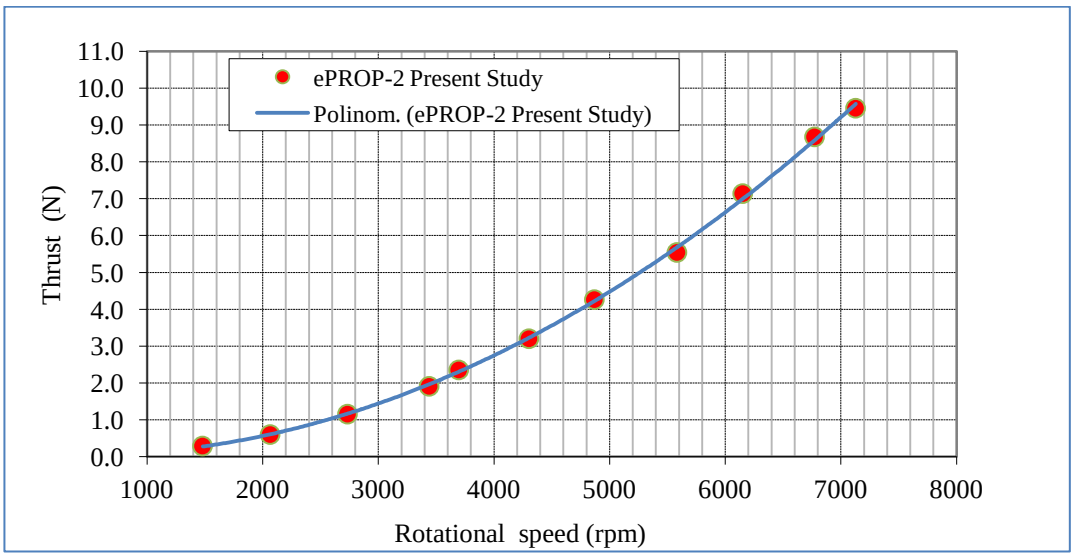

Figure 4.11 Variation of the static thrust of the Turbotek eProp2 (12x7) propeller with the rotational speed

As there is not any test or analysis result of Turbotek eProp2 Propeller in Design Document [26], a comparison of the present study with the thrust values could not be done.

4.1.4 Static Thrust of eProp1 Propeller

The 3D CAD model and prototype of the Turbotek eProp1 (10x7) propeller are shown in Figures 4.13 and 4.14, respectively.

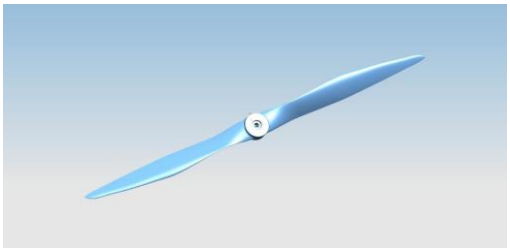

Figure 4.13 3D CAD model of Turbotek eProp1 (10x7) [27]

Figure 4.14 Prototype of Turbotek eProp1 (10x7) Propeller [27]

The variation of static thrust with the rotational speed is given in Figure 4.15 and it is tabulated in Appendix B.

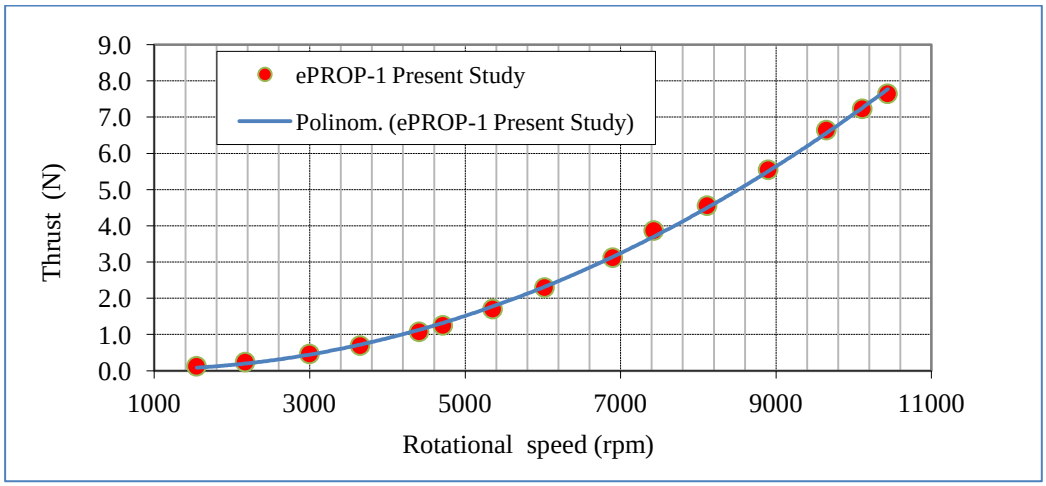

Figure 4.16 Variation of the static thrust of the Turbotek eProp1 (10x7) propeller with the rotational speed

As there is not any test or analysis result of Turbotek eProp1 Propeller in Design Document [27], a comparison of the present study with the thrust values could not be done.

4.2 Dynamic Thrust Measurements in the Wind Tunnel

Propeller tests in the wind tunnel of Fluid Mechanics Laboratory of Mechanical Engineering Department in METU have been carried out with the same 4 propellers that are used in static tests. The inlet air flow velocities have been ranging from 5 to 20 m/s, while the rotational speed of the propeller has been changed from 2,000 rpm to 10,000 rpm.

The propellers in the wind tunnel have been tested with GT2826/04 Brushless Electric Motor.

In order to see the repeatability of the wind tunnel tests, one of the propellers, Prop6, has been tested two times. It has been observed that each test results match quite well with each other so that the tests are repeatable. These test results are tabulated in Appendix C.

4.2.1 Dynamic Thrust of Prop6 Propeller

The variation of the thrust coefficient, power coefficient and efficiency with the advance ratio at 7,000 and 8,500 rpm are shown in Figures 4.17, 4.18 and 4.19, respectively. The variation of the thrust coefficient, power coefficient and efficiency with the advance ratio at 8,500 rpm is shown on a single graph in Figure 4.20.

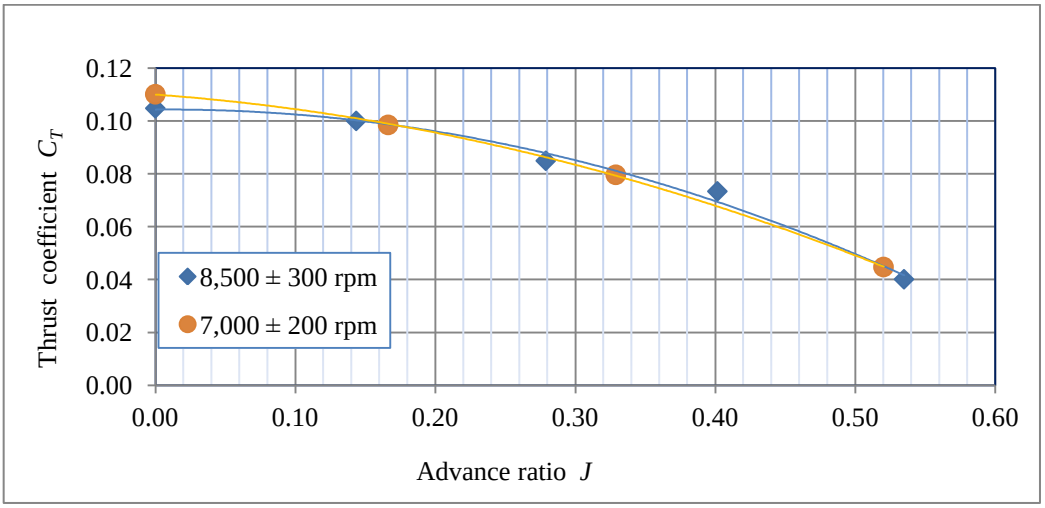

Figure 4.17 The variation of the thrust coefficient with the advance ratio for Turbotek Prop6 (10x7) propeller at 7,000 and 8,500 rpm

Since the lift coefficient of the airfoils is a very weak function of the Reynolds numbers or in the lift coefficient changes too little, thrust coefficient versus advance ratio curves for different rotational speeds almost overlap each other, as shown in Figure 4.17.

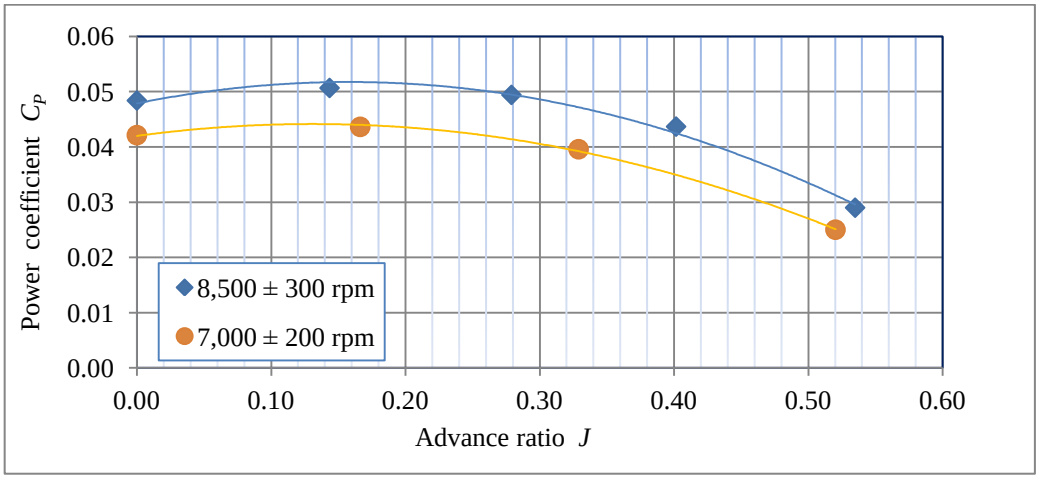

Figure 4.18 The variation of the power coefficient with the advance ratio for Turbotek Prop6 (10x7) propeller at 7,000 and 8,500 rpm

Airfoil section of Perv6 is NACA 4409. The aerodynamic data of NACA 4409 based on Reynolds number is given in Appendix C. The drag coefficient versus

angle of attack shifts down as the Reynolds number is increased. For this reason, the power coefficient versus advance ratio curve shifts up and a deviation occurs in the graphs of power coefficients as the rotational speed is increased from 7,000 rpm to 8,500 rpm, as shown in Figure 4.18.

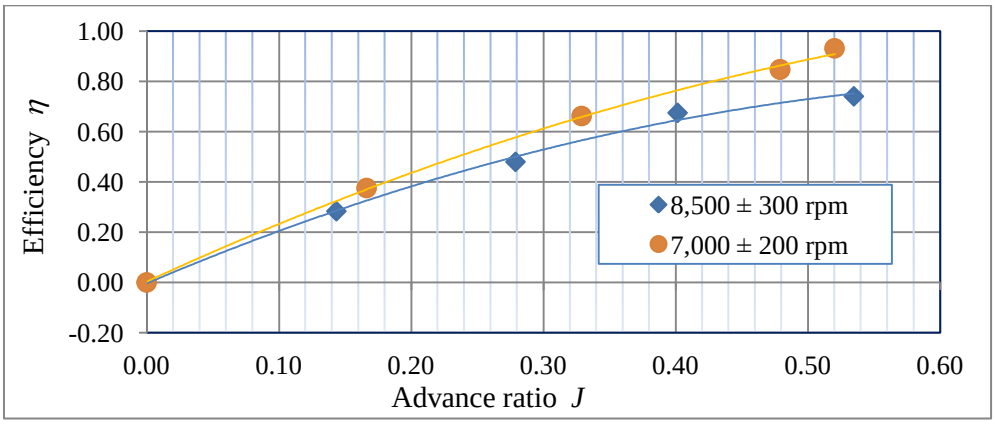

Figure 4.19 The variation of the efficiency with the advance ratio for Turbotek Prop6 (10x7) propeller at 7,000 and 8,500 rpm

As shown in Figure 4.19, though thrust coefficients at different rotational speeds include approximate values, there is a deviation in the graphs of efficiency due to the distinction of power coefficients.

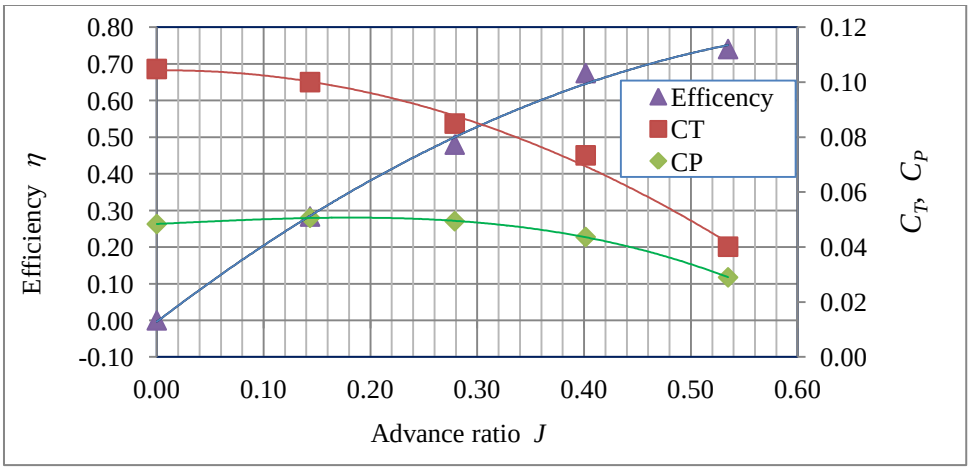

Figure 4.20 The variation of the thrust coefficient, power coefficient and efficiency with the advance ratio at 8,500 rpm

The performance of the Turbotek Prop6 (10x7) propeller is obtained by analytic analysis and Computational Fluid Dynamics (CFD) at 11,000 rpm. The variation of thrust coefficient, power coefficient and efficiency with the advance ratio, which are obtained by analytical analysis (11,000 rpm), CFD (11,000 rpm) and wind tunnel test (8,500 rpm) are compared in Figures 4.21, 4.22 and 4.23, respectively.

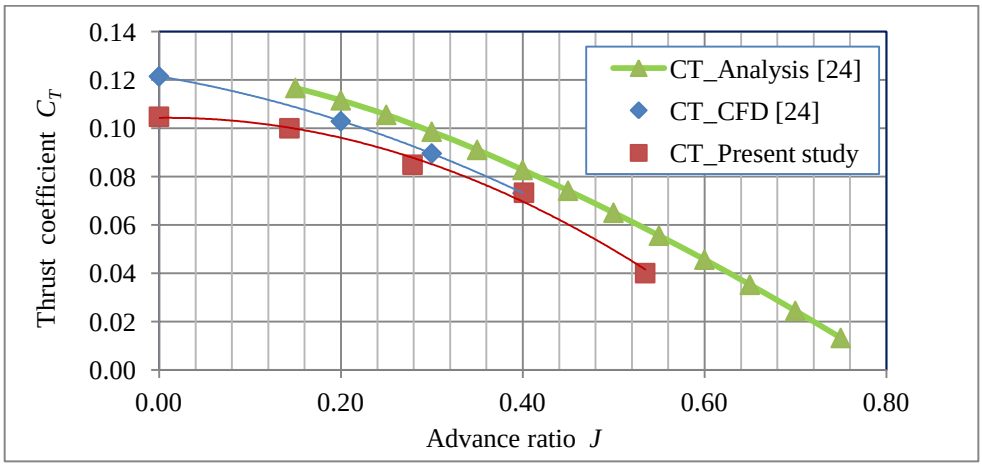

Figure 4.21 Comparison of the variation of the thrust coefficient with the advance ratio for Turbotek Prop6 (10x7) propeller at 8,500 rpm

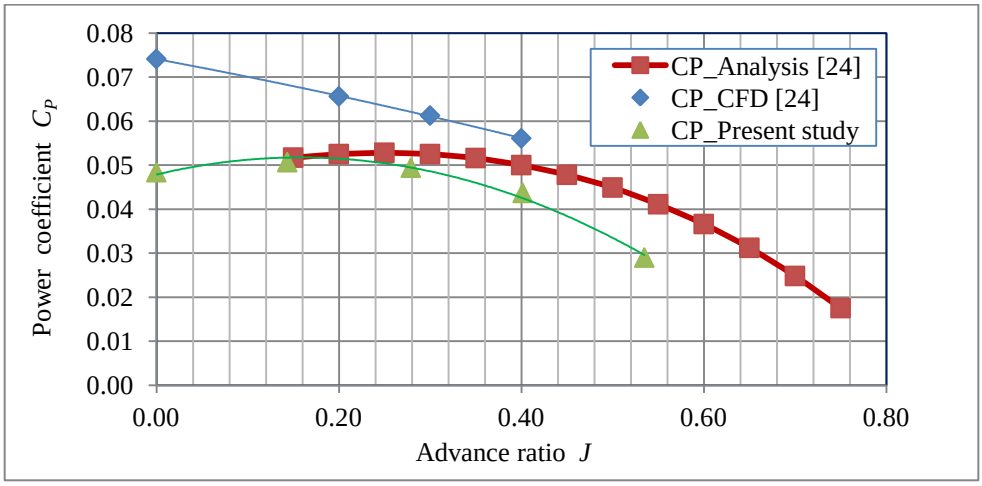

Figure 4.22 Comparison of the variation of the power coefficient with the advance ratio for Turbotek Prop6 (10x7) propeller at 8,500 rpm

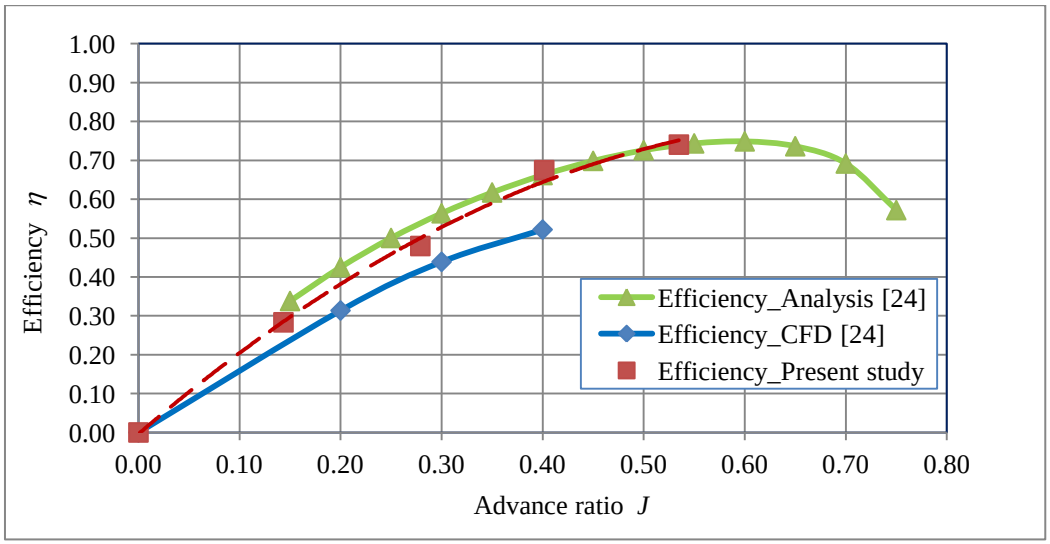

Figure 4.23 Comparison of the variation of the efficiency with the advance ratio for Turbotek Prop6 (10x7) propeller at 8,500 rpm

Although the results that are obtained at 8,500 rpm by the wind tunnel tests in present study are compared with those obtained by Turbotek [24] at 11,000 rpm, variation of thrust coefficient, power coefficient and efficiency match quite well, as shown in Figures 4.21, 4.22 and 4.23 respectively.

4.2.2 Dynamic Thrust of Prop1 Propeller

The variation of the thrust coefficient, power coefficient and efficiency with the advance ratio at 7,300 and 9,050 rpm are shown in Figures 4.24, 4.25 and 4.26, respectively. The variation of the thrust coefficient, power coefficient and efficiency with the advance ratio at 9,050 rpm is shown on a single graph in Figure 4.27.

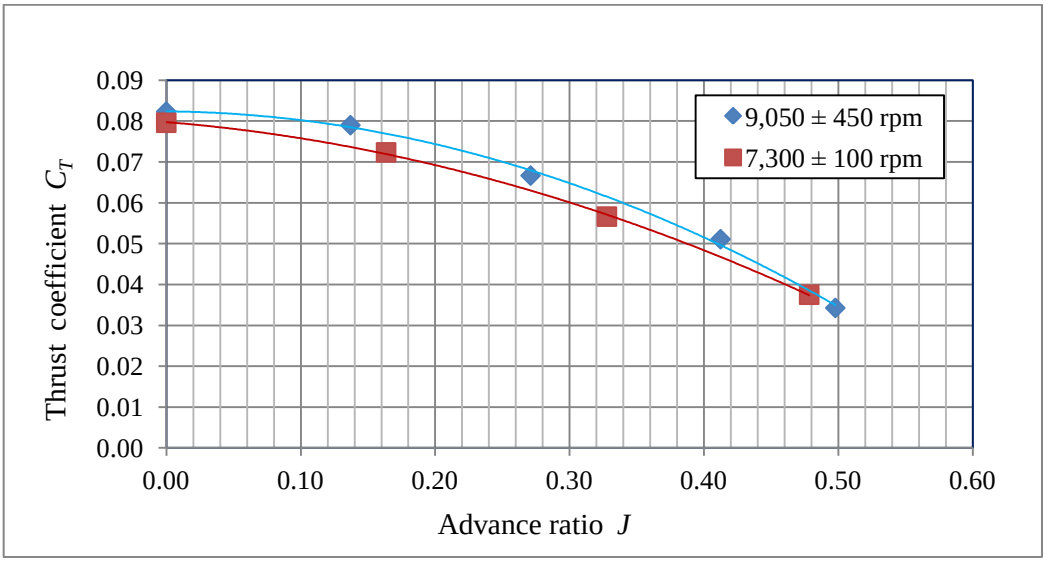

Figure 4.24 The variation of the thrust coefficient with the advance ratio for Turbotek Prop1 (10x6) propeller at 7,300 and 9,050 rpm

Since the lift coefficient of the airfoils is a very weak function of the Reynolds numbers or the lift coefficient changes too little, thrust coefficient versus advance ratio curves for different rotational speeds almost follows each other closely as shown in Figure 4.24.

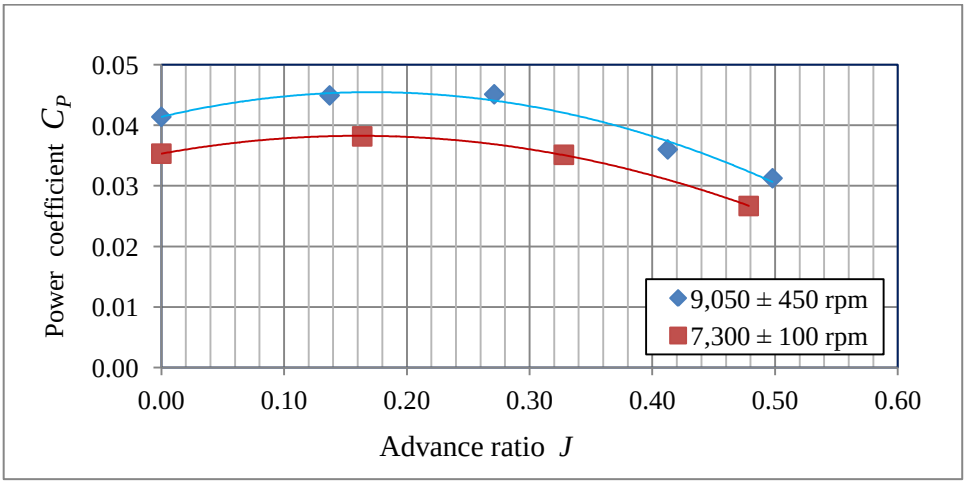

Figure 4.25 The variation of the power coefficient with the advance ratio for Turbotek Prop1 (10x6) propeller at 7,300 and 9,050 rpm

Airfoil section of Prop1 is GO 797. The aerodynamic data of GO 797 based on Reynolds number is given in Appendix C. The drag coefficient versus angle of attack shifts down as the Reynolds number is increased. For this reason, the power coefficient versus advance ratio curve shifts up and a deviation occurs in the graphs of power coefficients as the rotational speed is increased from 7,300 rpm to 9,050 rpm, as shown in Figure 4.25.

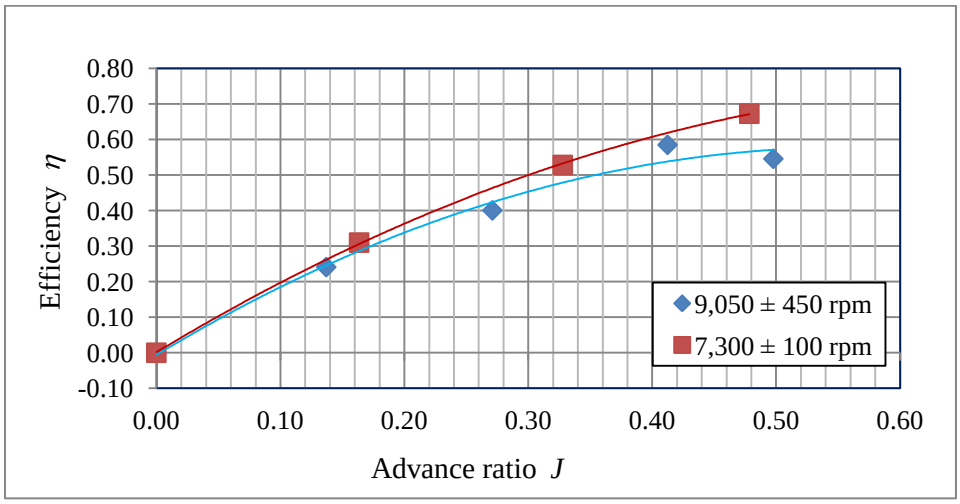

Figure 4.26 The variation of the efficiency with the advance ratio for Turbotek Prop1 (10x6) propeller at 7,300 and 9,050 rpm

As shown in Figure 4.26, thrust coefficients at different rotational speeds are similar; the graphs of efficiency have a deviation due to the distinction of power coefficients.

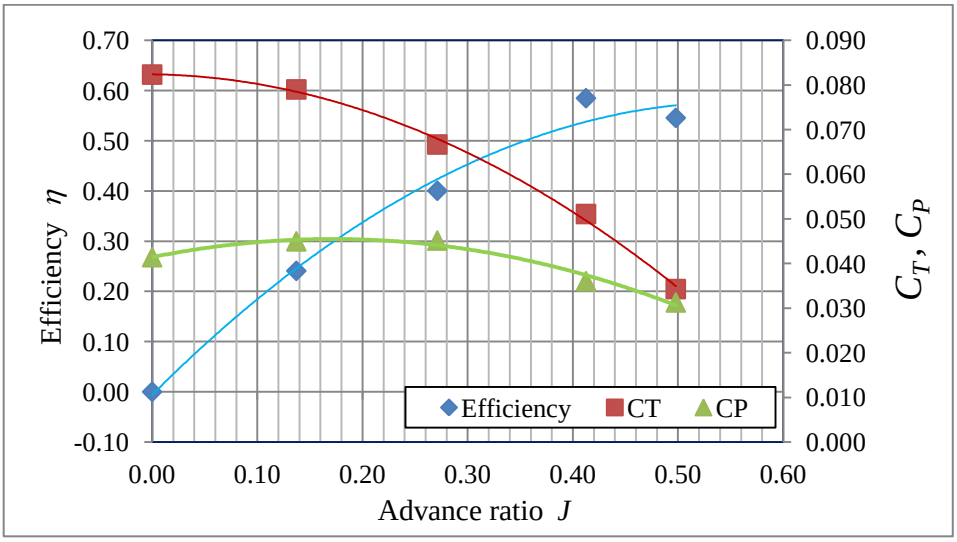

Figure 4.27 The variation of the thrust coefficient, power coefficient and efficiency with the advance ratio at 9,050 rpm

The performance of the Turbotek Prop1 (10x6) propeller is obtained by analytic analysis and Computational Fluid Dynamics (CFD) at 9,000 rpm. The variation of thrust coefficient, power coefficient and efficiency with the advance ratio, which are obtained by analytical analysis (9,000 rpm), CFD (9,000 rpm) and wind tunnel test (9,050 rpm) are compared in Figures 4.28, 4.29 and 4.30, respectively.

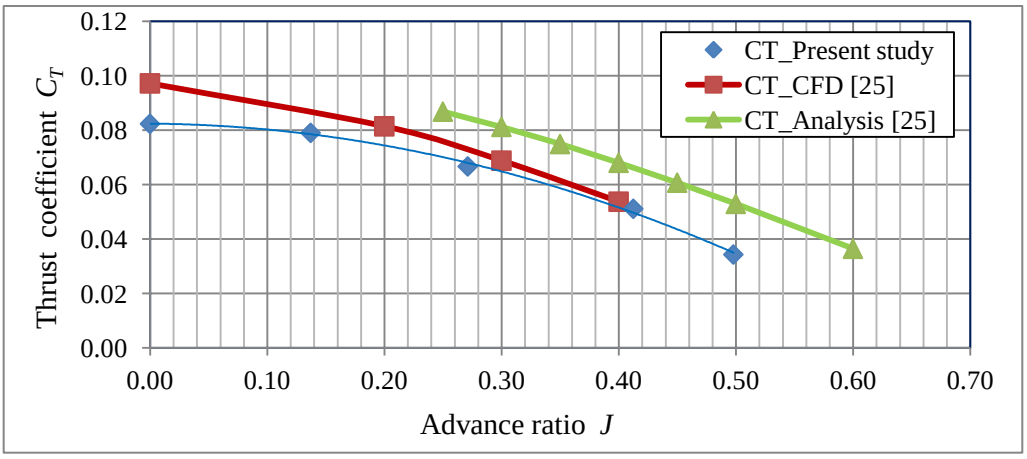

Figure 4.28 Comparison of the variation of the thrust coefficient with the advance ratio for Turbotek Prop1 (10x6) propeller at 9,050 rpm

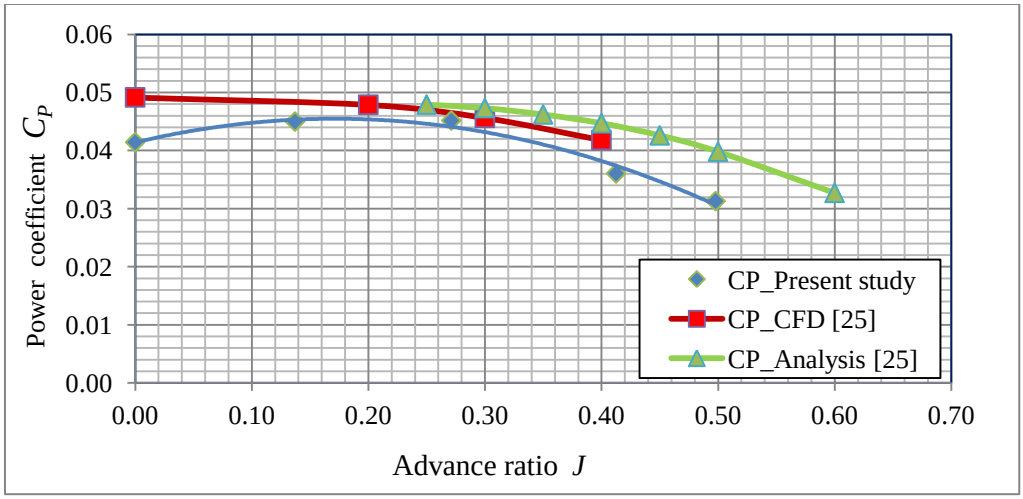

Figure 4.29 Comparison of the variation of the power coefficient with the advance ratio for Turbotek Perv1 (10x6) propeller at 9,050 rpm

Since the difference between rotational speeds of 9,050 and 9,000 rpm is less than those in the other graphs of power coefficients, there is much more accordance in Figure 4.29.

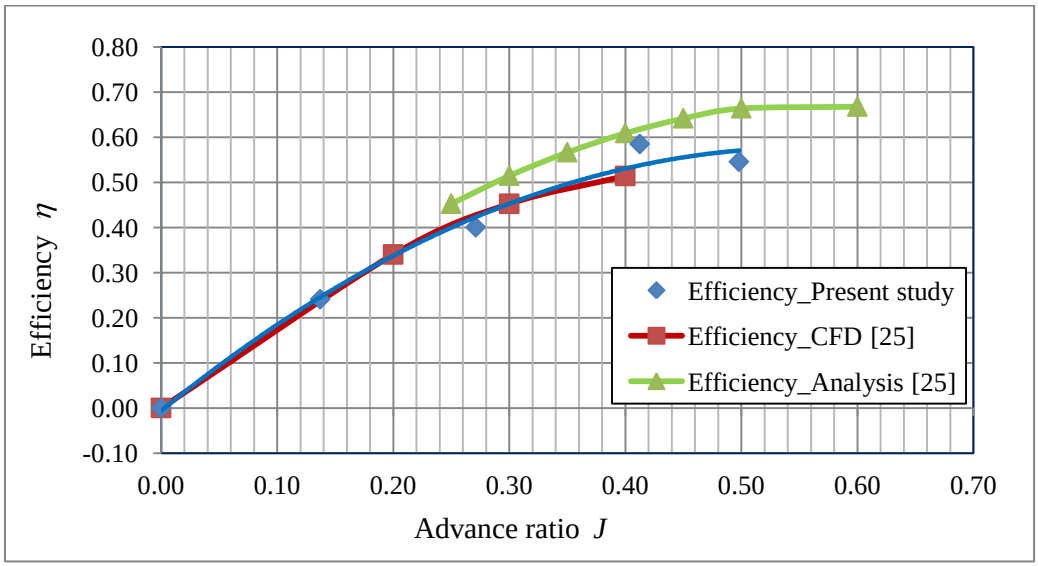

Figure 4.30 Comparison of the variation of the efficiency with the advance ratio for Turbotek Perv1 (10x6) propeller at 9,050 rpm

Although the results that are obtained at 9,050 rpm by wind tunnel tests in present study are compared with those obtained by Turbotek [25] at 9,000 rpm, variation of thrust coefficient, power coefficient and efficiency match quite well, as shown in Figures 4.28, 4.29 and 4.30 respectively.

4.2.3 Dynamic Thrust of eProp2 Propeller

The variation of the thrust coefficient, power coefficient and efficiency with the advance ratio at 5,650 and 7,250 rpm are shown in Figures 4.31, 4.32 and 4.33, respectively. The variation of the thrust coefficient, power coefficient and efficiency with the advance ratio at 7,250 rpm is shown on a single graph in Figure 4.34.

Since eProp2 propeller is a 12 inch propeller, the blockage ratio of the wind tunnel has become more than desired. The studies regarding the blockage ratio in literature are tabulated in Appendix C. In literature, the blockage ratio, which is the ratio of modal frontal-area to the test-section cross-sectional area, has been a value between 1-10% and is proposed for low speed wind tunnel testing as a maximum 7.5% [16][29]. For this reason, the deviation in the graphs of eProp2 propeller has become quite higher in Figures 4.31, 4.32 and 4.33, respectively.

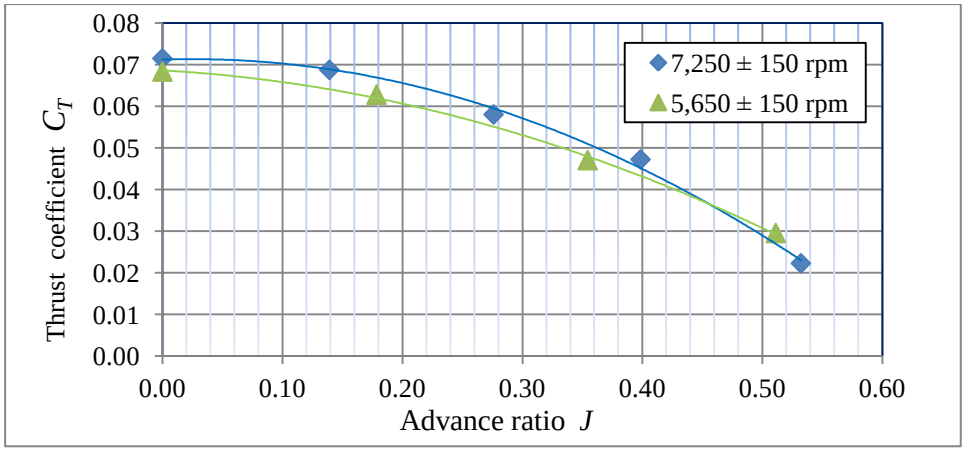

Figure 4.31 The variation of the thrust coefficient with the advance ratio for Turbotek eProp2 (12x7) propeller at 5,650 and 7,250 rpm

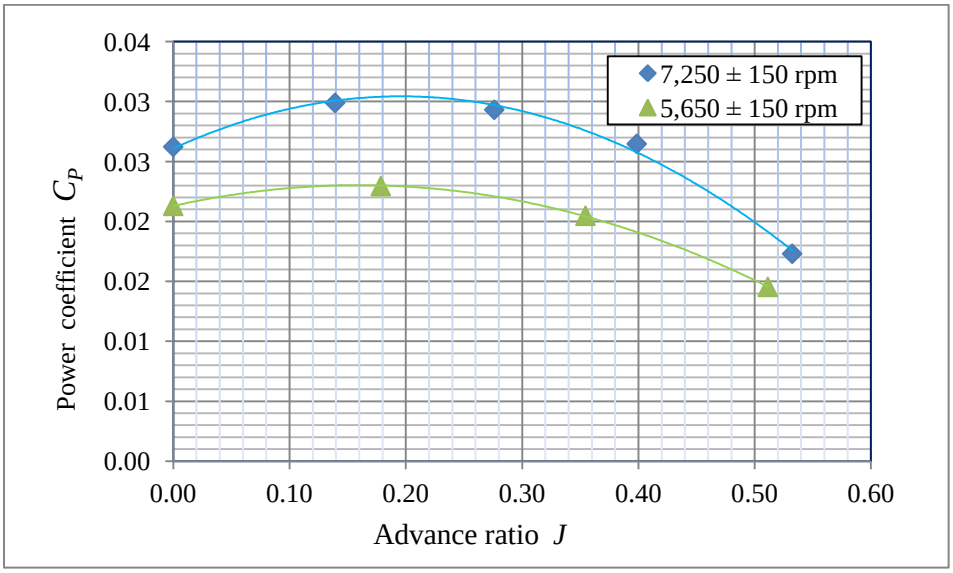

Figure 4.32 The variation of the power coefficient with the advance ratio for Turbotek eProp2 (12x7) propeller at 5,650 and 7,250 rpm

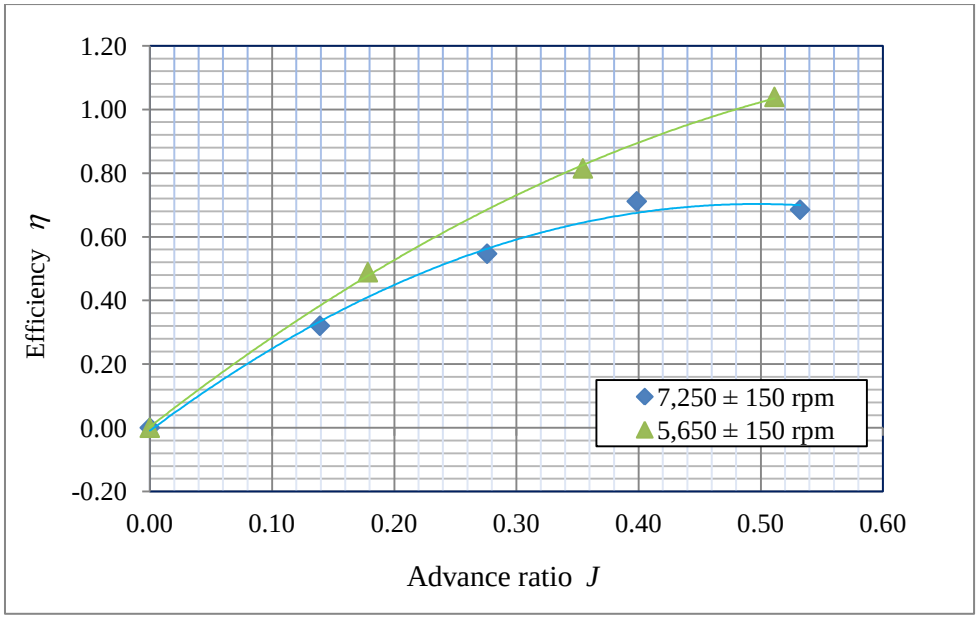

Figure 4.33 The variation of the efficiency with the advance ratio for Turbotek eProp2 propeller at 5650 and 7250 rpm

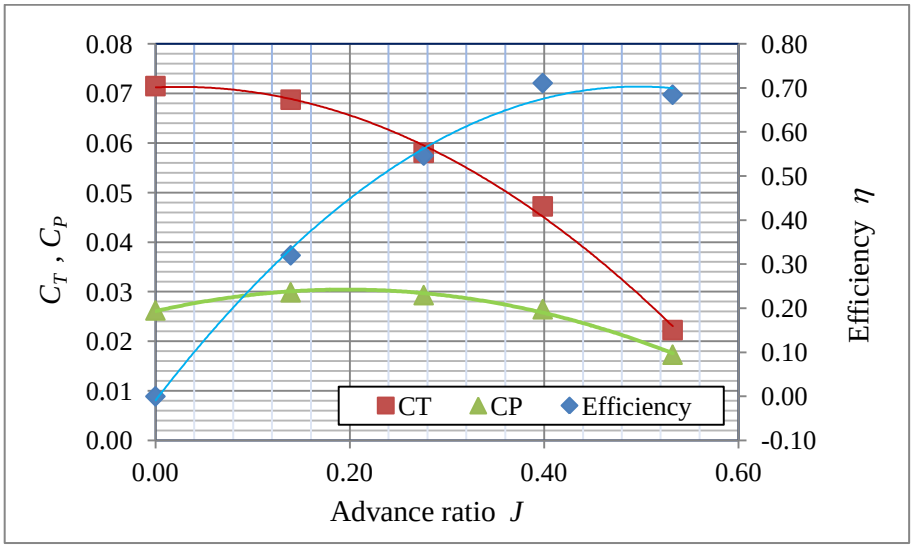

Figure 4.34 The variation of the thrust coefficient, power coefficient and efficiency with the advance ratio at 7,250 rpm

The performance of the Turbotek eProp2 (12x7**)** propeller is obtained by analytic analysis and Computational Fluid Dynamics (CFD) at 7,000 rpm. The variation of thrust coefficient, power coefficient and efficiency with the advance ratio, which are obtained by analytical analysis (7,000 rpm), CFD (7,000 rpm) and wind tunnel test (7,250 rpm) are compared in Figures 4.35, 4.36 and 4.37, respectively.

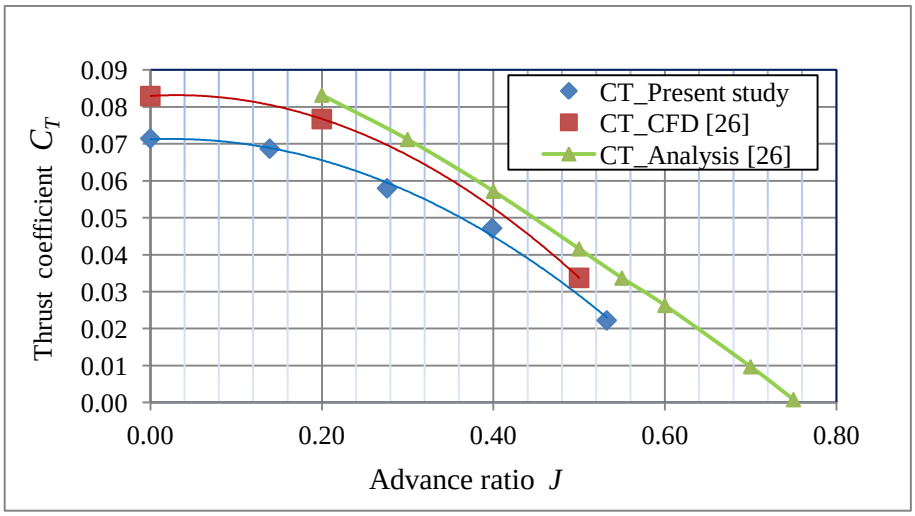

Figure 4.35 Comparison of the variation of the thrust coefficient with the advance ratio for Turbotek eProp2 (12x7) propeller at 7,250 rpm

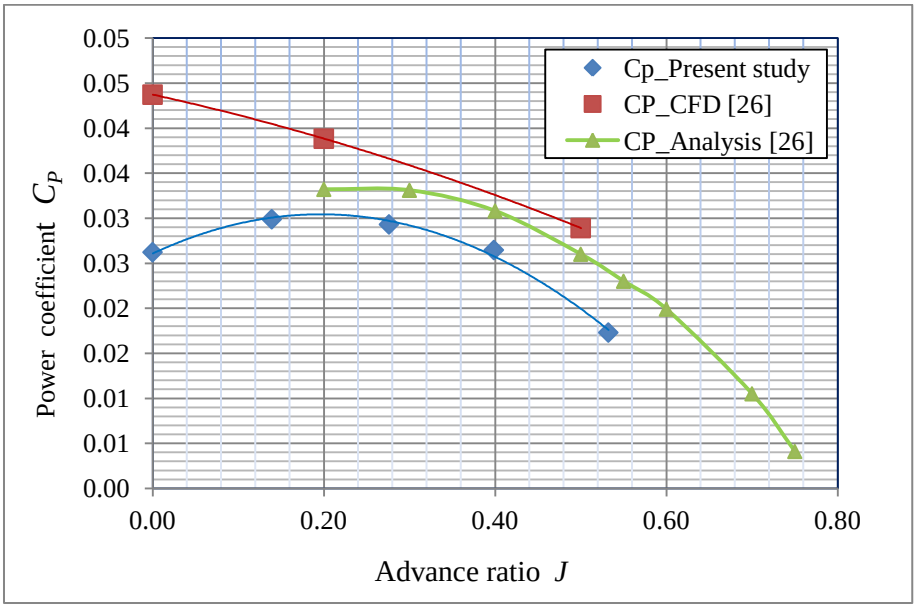

Figure 4.36 Comparison of the variation of the power coefficient with the advance ratio for Turbotek eProp2 (12x7) propeller at 7,250 rpm

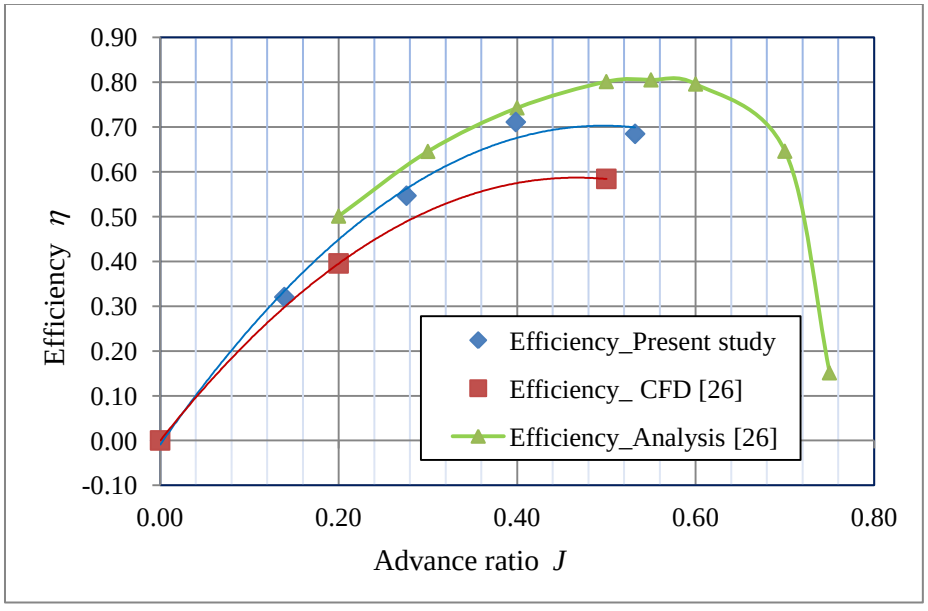

Figure 4.37 Comparison of the variation of the efficiency with the advance ratio for Turbotek eProp2 (12x7) propeller at 7,250 rpm

Although the results that are obtained at 7,250 rpm by the wind tunnel tests in present study are compared with those obtained by Turbotek [26] at 7,000 rpm, variation of thrust coefficient, power coefficient and efficiency match quite well, as shown in Figures 4.35, 4.36 and 4.37, respectively.

4.2.4 Dynamic Thrust of eProp1 Propeller

The variation of the thrust coefficient, power coefficient and efficiency with the advance ratio at 8,055 and 10,150 rpm are shown in Figures 4.38, 4.39 and 4.40, respectively. The variation of the thrust coefficient, power coefficient and efficiency with the advance ratio at 8,055 rpm is shown on a single graph in Figure 4.41.

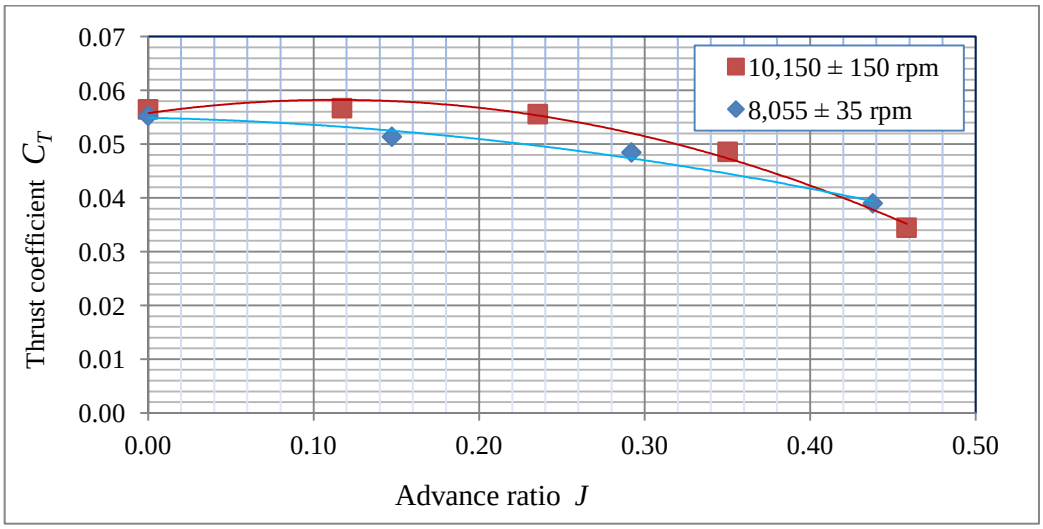

Figure 4.38 The variation of the thrust coefficient with the advance ratio for Turbotek eProp1 (10x7**)** propeller at 8,055 and 10,150 rpm

Due to its slim structure, it can be said that the manufacturing of eProp1 propeller is not good enough and it can be deformed under the loads so that it is obvious to see some amount of deviation in thrust and power coefficients at various rotational speeds as shown in Figure 4.38 and 4.39. In Figure 4.39, it can be seen that power coefficients are not stable.

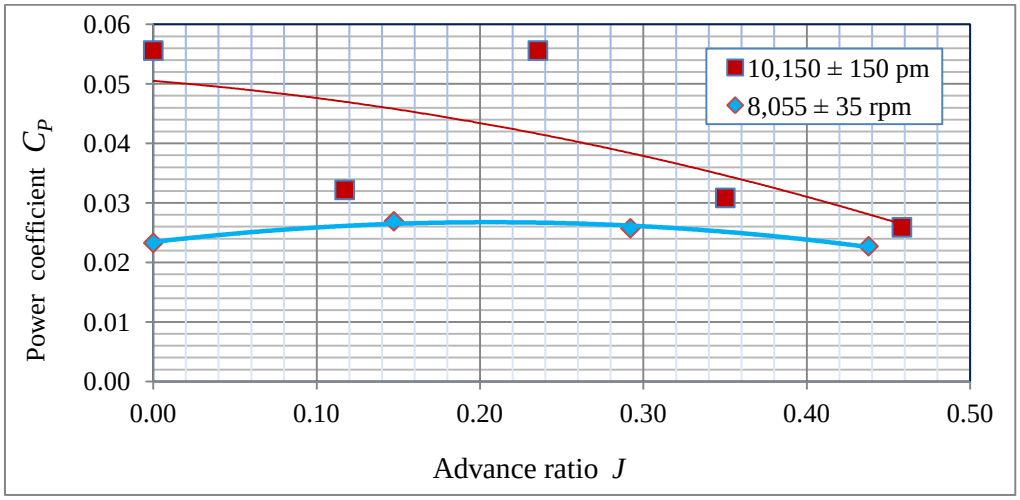

Figure 4.39 The variation of the power coefficient with the advance ratio for Turbotek eProp1 (10x7) propeller at 8,055 and 10,150 rpm

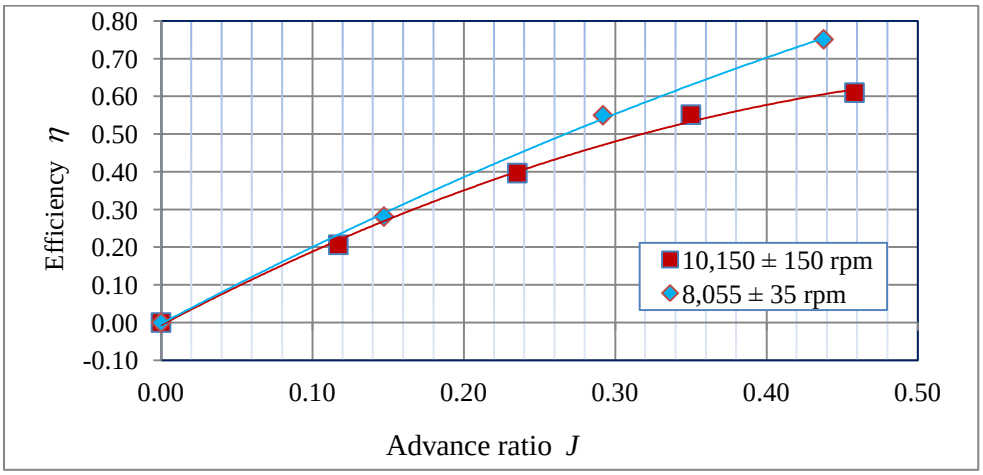

Figure 4.40 The variation of the efficiency with the advance ratio for Turbotek eProp1 (10x7) propeller at 8,055 and 10,150 rpm

As shown in Figure 4.40, though thrust coefficients at different rotational speeds include approximate values, there has been deviation in the graphs of efficiency due to the distinction of power coefficients.

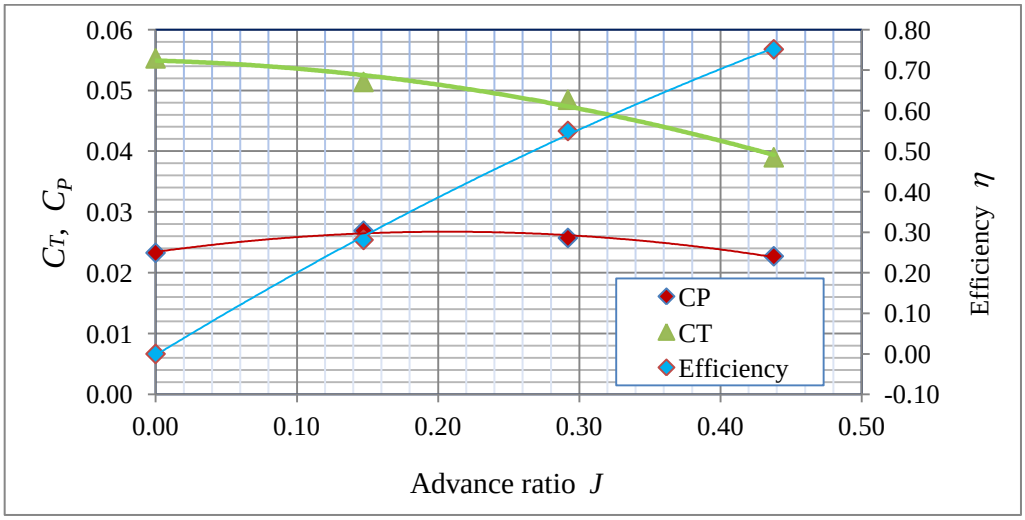

Figure 4.41 The variation of the thrust coefficient, power coefficient and efficiency with the advance ratio at 8,055 rpm

The performance of the Turbotek eProp1 (10x7) propeller is obtained by analytic analysis and Computational Fluid Dynamics (CFD) at 8,000 rpm. The variation of thrust coefficient, power coefficient and efficiency with the advance ratio, which are obtained by analytical analysis (8,000 rpm), CFD (8,000 rpm) and wind tunnel test (8,055 rpm) are compared in Figures 4.42, 4.43 and 4.44, respectively.

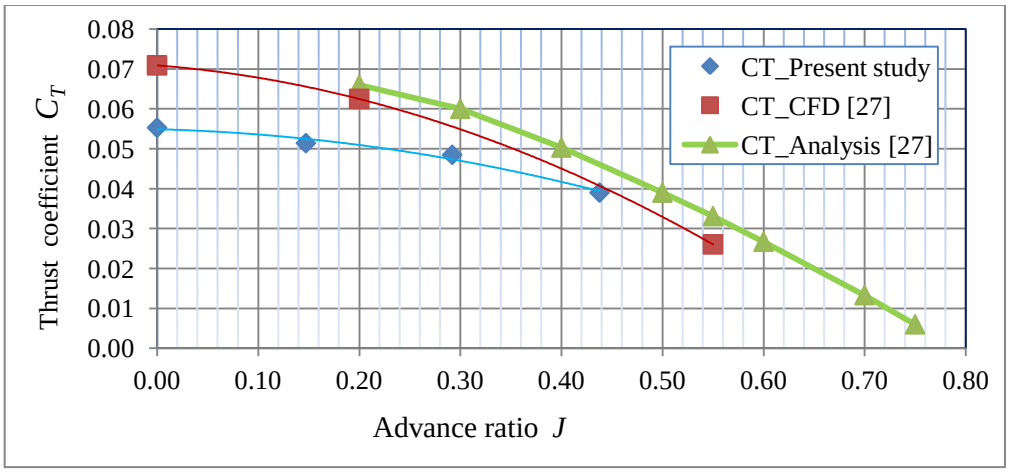

Figure 4.42 Comparison of the variation of the thrust coefficient with the advance ratio for Turbotek eProp1 (10x7) propeller at 8,055 rpm

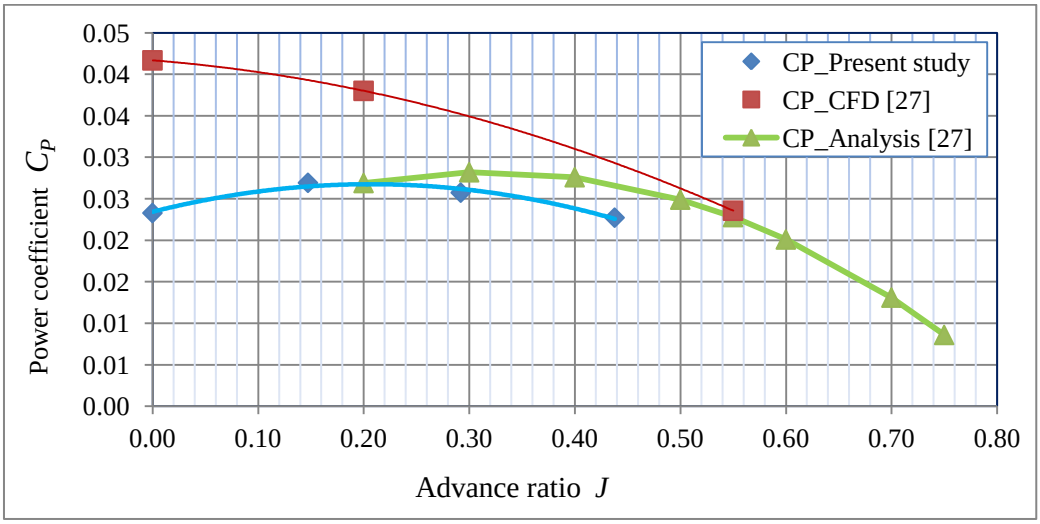

Figure 4.43 Comparison of the variation of the power coefficient with the advance ratio for Turbotek eProp1 (10x7) propeller at 8,055 rpm

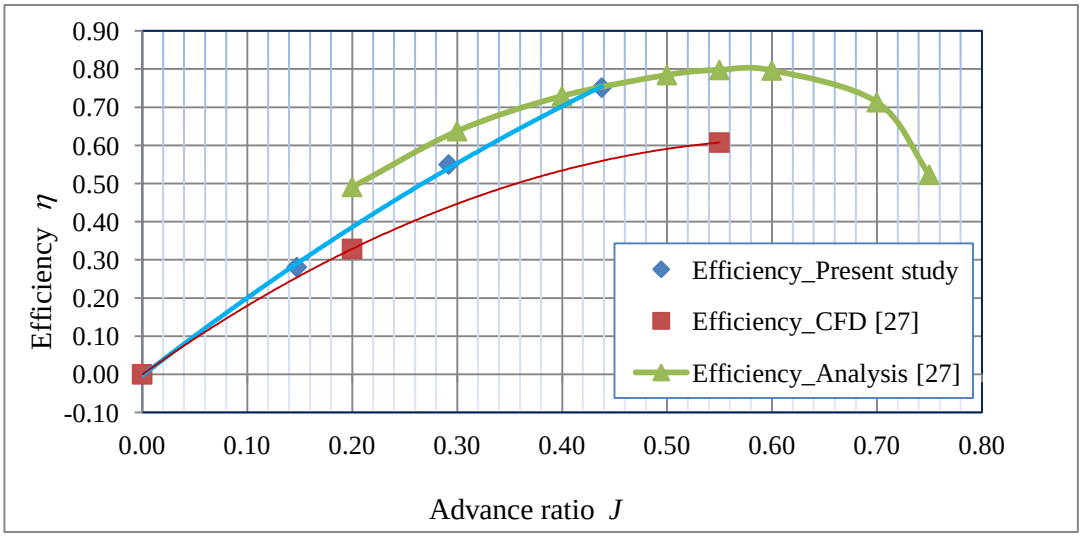

Figure 4.44 Comparison of the variation of the efficiency with the advance ratio for Turbotek eProp1 (10x7) propeller at 8,055 rpm

The results that are obtained at 8,055 rpm by the wind tunnel tests in present study are compared with those obtained by Turbotek at 8,000 rpm, variation of thrust coefficient, power coefficient and efficiency do not match very well but nevertheless it can be said by any means there is an amount of compatibility between the curves as shown in Figures 4.42, 4.43 and 4.44 respectively.

CHAPTER 5

CONCLUSIONS AND FUTURE WORK

In this thesis, the design procedures of the mini aircraft propellers are studied and performances of propellers which are designed and prototyped by Turbotek, Inc. are determined by static and dynamic tests.

For static tests, a propeller test apparatus is designed and assembled. In static tests, thrust, torque, power and efficiencies of four different Turbotek propellers are obtained as a function of the rotational speed of the propellers. The obtained data are compared with the results of the analytical calculations, CFD analysis and static tests carried out by Turbotek. The deviations in the power coefficient and efficiency depend on the airfoil used in the propeller and Reynolds numbers based on the rotational speeds of the propeller. On the other hand, thrust coefficients are quite compliant. This is due to the fact that drag force strongly depends on the Reynolds number, while the lift force is a weak function of the Reynolds number change considerably too much according to their relevant Reynolds numbers.

For dynamic tests, the same apparatus is placed in the wind tunnel of Fluid Mechanics Laboratory of Mechanical Engineering Department in METU. In the wind tunnel, propellers are tested at different rotational speeds and air inflow velocities. In dynamic tests, the variation of the thrust coefficient, power coefficient and efficiency of the same four Turbotek propellers are obtained as a function of the advance ratio. These experimental results are compared to the analytical and CFD results available in the design documents of the propellers. Turbotek and experimental results are found to be satisfactory. Although the thrust coefficients are quite compliant there is an apparent difference in the power

coefficients of the propellers. This difference may be due to the imprecise measurement of the power consumed by the electric motor. As is known, a DC motor power formulae is used for the power calculation of the tested propeller. Instead, a torque transducer had to be used in order to obtain more precise data. The other reason is due to the difference in power coefficients at different rotational speeds and incompatibility between the rotational speeds of Turbotek and METU wind tunnel tests. From a general point of view, the results of the Turbotek dynamic tests and METU wind tunnel match quite well within an acceptable limit. However, ePerv1 propeller shows a distinct deviation due to its slim structure which implies that the manufacturing of ePerv1 propeller is not sufficiently good. It should be emphasized that the equation used for the calculation of rotational speed is satisfactory, since the calculated results matches quite well with values that are read from the tachometer. Thus, the formulation regarding the rotational speed showed correct values. For this reason, it was supposed that the power formulation which is dependent on the formulation of the rotational speed would also give correct results. During the wind tunnel tests, due to the limitation of power supply which provides the rotational speeds of the propeller, the advance ratio is kept around 0.5

The shortcomings of the performance tests can be summarized as follows:

- In the wind tunnel, tests are carried out at constant air velocities of 5, 10, 15 and 20 m/s and rotational speeds ranging from 2,000 to 10,000 rpm (revolution per minute). For this reason, a limited number of data are obtained. The results can be improved by performing the tests at a wider range of axial air flow velocities.

- A simple test apparatus is preferred in order to obtain results in a shorter procurement time with a low cost due the limited resources. In future studies, more technological devices such as load cells, torque transducers and a data acquisition system can be used to provide more

data in a shorter time so that more precise results can be obtained.

- Test cannot be carried out for current requirements over 19-20 A because of the limitations of power supply. Thus higher rotational speed, power and thrust can be obtained if the capacities of the power supply and electric motor are increased.

- At higher air inflow velocities, propellers require more power to operate and withstand the strong air stream. Thus, at velocities close to 20 m/s velocities, the intensity of vibrations is increased resulting in uncertainties in the precision of electronic devices. Since there are difficulties in obtaining the thrust values in some of the tests, some tests are repeated.

- Sometimes, precise results cannot be obtained during the tests due to test set-up errors. For this reason, some tests are repeated and suspicious data are removed from the analysis in order to have more precise results. In many resources, it has been stated that the power formulation of a DC motor results in deceptive results in an AC motor.

As a future work, the following items can be considered:

- The prototyped propeller can be installed on a mini aircraft and can be tested together in a wind tunnel and effect of both propeller installed to the aircraft and the drag force created can be determined.

- Having this technical information on design of propeller of an aircraft, a study can be progressed through the studies on a wind turbine which has the similar design parameters but is a reverse system with respect to the aircraft propeller.

- In general, some more technological devices such as load cell, torque transducer and data acquisition system could be used in order to obtain more precise data.

- Designing, prototyping, manufacturing, CFD analysis and the wind tunnel test of the propellers can be done altogether.

REFERENCES

[1] Yükselen, M.A., *Bölüm 11 Pervane Teorisi/Chapter 11 Propeller Theory, Aerodynamics Lecture Notes*, Faculty of Aeronautics and Astronautics, Department of Aeronautical Engineering, Istanbul Technical University, Turkey, http://web.itu.edu.tr/~yukselen/Uck351/11-%20Pervane%20teorisi.pdf, July 2014.

[2] Aerospaceweb.org | Helicopter Theory - Early History, *Early Helicopter History*, http://www.aerospaceweb.org/design/helicopter/history.shtml, August 2014.

[3] Science & Society Picture Library, *Leonardo da Vinci Helicopter, c late 15th century*, http://www.scienceandsociety.co.uk , August 2014.

[4] Gamble, D.E., *Automated Dynamic Propeller Testing at Low Reynolds Numbers*, Master of Science Thesis, Oklahoma State University, December 2009, ProQuest LLC, UMI number: 1474037.

[5] Greatrix, D.R., *Powered Flight The Engineering of Aerospace Propulsion, Chapter 3*, Department of Aerospace Engineering, Ryerson University, Toronto, Canada Library of Congress Control Number: 2011944772, Springer-Verlag London Limited 2012.

[6] *A short History of the Propeller - Timetable: Development of the Propeller*, http://www.mh-aerotools.de/airfoils/prophist.htm, August 2014.

[7] Heinzen, S.B., *Development of a Passively Varying Pitch Propeller* Dissertation of Doctor of Philosophy, Aerospace Engineering, North Carolina State University, 2011, published by ProQuest LLC, UMI number:3538373. http://repository.lib.ncsu.edu/ir/bitstream/1840.16/8112/1/etd.pdf, August 2014.

[8] Tracy, I.P., *Propeller Design and Analysis for a Small, Autonomous UAV*, Massachusetts Institute of Technology, Bachelor of Science Thesis, June 2011.

[9] Bettinger, B., *Manufacturing, Analysis and Experimental Testing of Multi-Bladed Propellers For SUAS* Oklahoma State University, Master of Science Thesis, May 2012, ProQuest LLC, UMI number:1518080.

[10] Merchant, M.P., *Propeller Performance Measurement for Low Reynolds Number Unmanned Aerial Vehicle Applications,* Master of Science Thesis, Wichita State University, December 2005.

[11] Khalid, A., *Design, Development and Testing of Variable Pitch Propeller Thrust Measurement Apparatus-Freshmen Research Project*, Southern Polytechnic University, 2012 ASEE Southeast Section Conference, http://se.asee.org/proceedings/ASEE2012/Papers/FP2012kha112_508.PDF, August 2014.

[12] Brandt, J.B., Selig, M.S., *Propeller Performance Data at Low Reynolds Numbers* 49th AIAA Aerospace Sciences Meeting, 4-7 January 2011, Orlando, FL, AIAA 2011-1255.

[13] Whitmore, S.A., Merrill, R. S., *Nonlinear Large Angle Solution of the Blade Element Momentum Theory Propeller Equations*, Utah University, Journal of Aircraft, Vol.49, No.4, p1126, July-August 2012, http://arc.aiaa.org, DOI:10.2514/1.C 031645.

[14] Demirtaş, H., *Düşük Hızlı Uçaklarda Aerodinamik Pervane Tasarımı ve Optimizasyonu/Aerodynamic Design and Optimization of a Propeller for a Low Speed Aircraft* Master of Science Thesis, Mechanical Engineering Department, Erciyes University, Turkey, July 2006.

[15] Pamuk, B., *Pervane Modellenmesi/Propeller Modelling* Master of Science Thesis, Mechanical Engineering Department, Ondokuz Mayıs University, Turkey, 2012.

[16] Barlow, J.B., Rae, W.H. Jr., Pope, A., (1999) *Low-Speed Wind Tunnel Testing, 3rd Ed.,* John Wiley & Sons Inc., New York.

[17] Uzol, O., *Propeller Theory" AE334 SYS-I Lecture Notes,* Department of Aerospace Engineering, Middle East Technical University, Ankara, Turkey, 2009.

[18] Cavcar, M., *Blade Element Theory*, Anadolu University, School of Civil Aviation, Eskisehir, Turkey, 2004.

[19] *Aerodynamic for Students Glauert Blade Element Theory*, Analysis of Propellers Glauert Blade Element Theory, University of Sydney, 1996-2006, http://www.ewp.rpi.edu/hartford/~ernesto/F2012/EP/MaterialsforStudents/McCosker/Aerodynamics-for-Students-GlauerBEM.pdf, July 2014.

[20] Nicolai, L.M., Carichner, G.E., *Fundamentals of Aircraft and Airship Design- Propeller Propulsion Systems* Lockheed Martin Aeronautics Company, CA, USA, AIAA Education Series, Virginia Polytechnic Institute and State University, Blacksburg, Virginia Published by AIAA, Chapter 17, 2010.

[21] Howey, R.W., *Simplified Propellers for Low Speed home Built Aircraft, 4th Ed.,* Jan.1982.

[22] Ingram, G., *Wind Turbine Blade Analysis using the Blade Element Momentum Method Version 1.1*, October 18, 2011, https://community.dur.ac.uk/g.l.ingram/download/wind_turbine_design.pdf, July 2014.

[23] Weick, F. E., *Aircraft Propeller Design 1st Ed.,* Tenth Impression, McGraw-Hill Book Company, Inc., New York and London, 1930.

[24] ÇETE, A.Ruhşen, *TURBOTEK PERV6 Pervanesi Tasarım Dökümanı (TURBOTEK PERV6 Propeller Design Document),* TURBOTEK Turbomakina Teknolojileri Ltd. Şti., ODTÜ (METU) Teknokent, Ankara, Turkey, www.turbotek.com.tr, 31.12.2007.

[25] ÇETE, A.Ruhşen, *TURBOTEK PERV1 Pervanesi Tasarım Dökümanı (TURBOTEK PERV1 Propeller Design Document) Version 1.1,* TURBOTEK Turbomakina Teknolojileri Ltd. Şti., ODTÜ (METU) Teknokent, Ankara, Turkey, www.turbotek.com.tr, 31.12.2007.

[26] ÇETE, A.Ruhşen, *TURBOTEK ePERV2 Pervanesi Tasarım Dökümanı (TURBOTEK ePERV2 Propeller Design Document) Version 1.0,* TURBOTEK Turbomakina Teknolojileri Ltd. Şti., ODTÜ (METU) Teknokent, Ankara, Turkey, www.turbotek.com.tr, 31.12.2008.

[27] ÇETE, A.Ruhşen, *TURBOTEK ePERV1 Pervanesi Tasarım Dökümanı (TURBOTEK ePERV1 Propeller Design Document) Version 1.0* TURBOTEK Turbomakina Teknolojileri Ltd. Şti., ODTÜ (METU) Teknokent, Ankara/Turkey, www.turbotek.com.tr, 31.12.2008.

[28] Miley, S.C., *A Catalog of Low Reynolds Number Airfoil Data for Wind Turbine Applications*, Department of Aerospace Engineering, Texas A&M University, College Station, Texas, U.S. Department of Commerce, National Technical Information Service, DE82-021712, Feb 1982.

[29] Ross, I.J., *Wind Tunnel Blockage Corrections: An Application to Vertical-Axis Wind Turbines,* Master of Science Thesis in Aerospace Engineering, University of Dayton, May 2010.

APPENDICES

APPENDIX A

COMPONENTS USED IN PROPELLER TEST APPARATUS

A.1 Brushless Electric Motor

Emax Grand Turbo Electric Motor GT 2826/04 has been shown in Figure A.1. This electric motor is a brushless type and turns the propeller according to the inlet voltage supplied. It gives 1090 rpm per Volt. Its specification is indicated in the following table.

Table A.1 Technical specification of Emax Grand Turbo Electric Motor GT 2826/04

Motor	Kv (no load rpm per volt)	internal resistance (mOhms)	Magnetic poles	No-load Test voltage (V)	no-load current (A)	Limitation regarding Max Power (W)	Limitation regarding max. Current (A)	Motor Case Length (mm)
GT 2826/04	1090	24	14	11.1	0.1	752W	47A	28.5

Figure A.1 Emax Grand Turbo Electric Motor GT 2826/04

A.2 Electronic Speed Control (ESC)

It controls the speed of brushless electric motor. It has been chosen as 60 A UBEC type. The view of ESC is shown in Figure A.2.

Figure A.2 ESC

A.3 Portable Electronic Scale

It is an electronic type and has the accuracy of 5 g for 0 to 10 kg. It is shown in Figure A.3.

Figure A.3 Portable Electronic Scale

A.4 Power Supply

A 12 V DC power supply having max 350 W has been used for converting 220 V AC input to 12 V DC. It can be adjusted up to 14 V DC. Its view is shown in Figure A.4.

Figure A.4 Ampere Power Supply (12V DC 350W/29)

A.5 Servo Tester

G.T. Power Servo Tester has been chosen. This device is directly connected to ESC and speed control is adjusted by turning the knob at servo tester between minimum and maximum positions. It is shown in Figure A.5.

Figure A.5 G.T. Power Servo Tester

A.6 Digital Power meter (Wattmeter)

A digital Wattmeter is also used to measure current, volt and power values simultaneously. Its maximum voltage is 60 V and maximum current is 100 A. It is shown in Figure A.6.

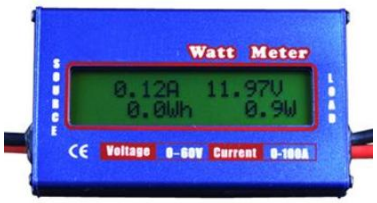

Figure A.6 Digital power meter

A.7 Analog Voltmeter

A DC analog voltmeter having maximum 30 V has been used in order to see the voltage for comparison with the wattmeter values. It is shown in Figure A.7.

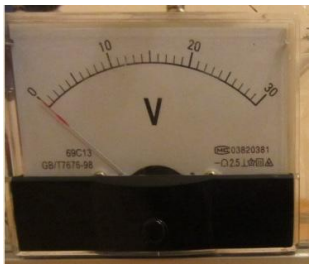

Figure A.7 Analog DC Voltmeter 30V

A.8 Analog Ammeter

A DC analog Ammeter having maximum 20 A has been used in order to see the voltage for comparison with the wattmeter values. It is shown in Figure A.8.

Figure A.8 Analog Ammeter DC (0~20A)

A.9 Digital Multimeter

Digital Multimeter (TES 2700) has the capacity for the DC currents between 0 to 20 A and for the AC currents at 40 Hz to 400 Hz/0-600 V. It has been used to measure the voltage values at the inlet of electric motor. It is shown in Figure A.9.

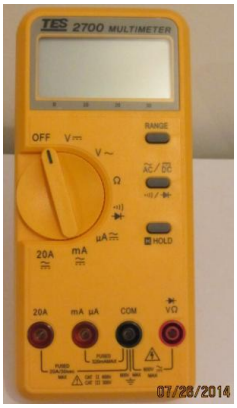

Figure A.9 Multimeter

A.10 Tachometer

The other method is to use a photo reflector laser beam device that senses each pass of the propeller blade by the help of a reflector tape sticked on the blade surface facing the laser beam and a main processor device. This device is called tachometer and is shown in Figure A.10.

(a) (b)

Figure A.10 (a) Laser Beam (b) Tachometer

APPENDIX B

STATIC TEST RESULTS OF PROPELLERS

Table B.1 Static Thrust of Turbotek Production Propeller- Prop6 (10x7)

Volt [V]	Scale Mass [kg]	Thrust [kg]	Thrust [N]	Current (Iin) [A]	N [rpm]	Pm,out [W]	Pm,in [W]	Motor Eff.
1.22	0.175	0.021	0.20	0.60	1345	0.60	0.73	0.82
1.94	0.430	0.051	0.50	0.80	2110	1.34	1.55	0.87
2.67	0.900	0.106	1.04	1.43	2950	3.50	3.81	0.92
3.24	1.485	0.175	1.71	2.14	3613	6.51	6.94	0.94
3.90	2.205	0.259	2.54	3.34	4394	12.39	13.04	0.95
4.54	2.340	0.275	2.70	3.52	4498	15.23	15.97	0.95
5.08	2.800	0.329	3.23	4.69	5000	22.78	23.80	0.96
5.90	4.040	0.475	4.66	7.29	5974	41.13	42.98	0.96
6.41	4.850	0.571	5.59	9.20	6502	56.31	58.96	0.96
7.05	5.940	0.699	6.85	11.65	7049	78.19	82.13	0.95
7.72	6.950	0.818	8.01	15.18	7728	110.86	117.13	0.95
8.34	7.800	0.918	8.99	18.53	8280	145.58	154.61	0.94

Table B.2 Static Thrust of Turbotek Production Propeller- Prop1 (10x6)

Volt [V]	Scale Mass [kg]	Thrust [kg]	Thrust [N]	Current (Iin) [A]	N [rpm]	Pm,out [W]	Pm,in [W]	Motor Eff.
1.28	0.130	0.015	0.15	0.60	1408	0.63	0.77	0.82
2.00	0.330	0.039	0.38	0.73	2209	1.25	1.46	0.86
2.59	0.570	0.067	0.66	1.22	2876	2.87	3.16	0.91
3.23	0.945	0.111	1.09	1.90	3626	5.73	6.14	0.93
3.82	1.460	0.172	1.68	2.84	4327	10.28	10.84	0.95
4.61	1.685	0.198	1.94	3.34	4591	14.69	15.41	0.95
5.14	2.220	0.261	2.56	4.59	5254	22.58	23.59	0.96
5.83	3.105	0.365	3.58	6.34	5963	35.44	36.97	0.96
6.38	3.720	0.438	4.29	8.04	6555	49.15	51.32	0.96
6.99	4.470	0.526	5.15	10.43	7181	69.57	72.86	0.95
7.70	5.460	0.642	6.30	13.20	7814	96.76	101.68	0.95
8.38	6.300	0.741	7.26	16.55	8427	131.36	138.73	0.95
8.56	7.080	0.833	8.16	19.17	8886	154.50	164.13	0.94

Table B.3 Static Thrust values of Turbotek Production Propeller- eProp2 (12x7)

Volt [V]	Scale Mass [kg]	Thrust [kg]	Thrust [N]	Current (Iin) [A]	N [rpm]	Pm,out [W]	Pm,in [W]	Motor Eff.
1.36	0.255	0.030	0.29	0.61	1481	0.69	0.83	0.83
1.91	0.525	0.062	0.61	1.05	2066	1.79	2.01	0.89
2.54	1.005	0.118	1.16	1.63	2735	3.83	4.14	0.92
3.15	1.660	0.195	1.91	2.64	3441	7.83	8.30	0.94
3.82	2.045	0.241	2.36	3.12	3697	11.32	11.93	0.95
4.55	2.780	0.327	3.21	4.53	4304	19.68	20.61	0.95
5.19	3.700	0.435	4.27	6.37	4870	31.59	33.07	0.96
5.79	4.810	0.566	5.55	8.89	5584	49.05	51.50	0.95
6.38	6.195	0.729	7.14	11.68	6153	70.67	74.55	0.95
7.00	7.530	0.886	8.68	15.20	6774	100.16	106.37	0.94
7.38	8.205	0.965	9.46	18.19	7129	125.66	134.29	0.94

Table B.4 Static Thrust values of Turbotek Production Propeller-eProp1 (10x7)

Volt [V]	Scale Mass [kg]	Thrust [kg]	Thrust [N]	Current (Iin) [A]	N [rpm]	Pm,out [W]	Pm,in [W]	Motor Eff.
1.39	0.105	0.012	0.12	0.60	1545	0.69	0.83	0.82
1.96	0.205	0.024	0.24	0.62	2171	1.01	1.22	0.83
2.66	0.400	0.047	0.46	1.17	2998	2.82	3.12	0.90
3.24	0.600	0.071	0.69	1.59	3650	4.77	5.15	0.93
3.86	0.930	0.109	1.07	2.13	4409	7.74	8.23	0.94
4.54	1.085	0.128	1.25	2.54	4714	10.92	11.52	0.95
5.06	1.475	0.174	1.70	3.30	5355	15.95	16.71	0.95
5.70	1.990	0.234	2.29	4.39	6023	24.02	25.04	0.96
6.47	2.705	0.318	3.12	5.92	6900	36.84	38.32	0.96
6.99	3.355	0.395	3.87	7.14	7428	47.97	49.88	0.96
7.65	3.950	0.465	4.55	8.97	8114	65.96	68.64	0.96
8.36	4.810	0.566	5.55	11.29	8900	90.48	94.35	0.96
9.11	5.760	0.678	6.64	14.30	9649	124.53	130.32	0.96
9.52	6.270	0.738	7.23	16.24	10111	147.41	154.66	0.95
9.77	6.630	0.780	7.64	18.20	10436	168.87	177.75	0.95

APPENDIX C

WIND TUNNEL (DYNAMIC) TEST RESULTS OF PROPELLERS

During the dynamic tests the ambient pressure and temperature in the laboratory are measured to be 919 mbar and 22.9 ^{o}C, respectively. The density of air can be calculated from the perfect gas equation of state

$$\rho = \frac{p}{RT} = \frac{91900 \text{ N/m}^2}{(287.1 \text{ J/kgK})(295.9 \text{ K})} = 1.082 \text{ kg/m}^3 \qquad \text{(C.1)}$$

Table C.1 METU Wind Tunnel (Dynamic) Test Results of Prop6 (10x7) Propeller

V [m/s]	Current [A]	AC Voltage (V)	rpm (measured)	rpm (calculated)	Scale Readout [kg]	Drag [kg]	Thrust [kg]	Thrust [N]	Advance Ratio	Thrust Coef. CT	Pin [W]	Pm, out [W]	Motor Efficiency	Puseful [W]	Power Coeff. CP	Propeller Efficiency
0			7049				0.699	6.85	0	0.11		78.19		0.00	0.04	0.00
0			8280				0.918	8.99	0	0.10		145.58		0.00	0.05	0.00
5	0.8	2.1	2372	2319	0.09	0.01	0.02	0.22	0.50	0.03	1.72	1.49	0.87	1.12	0.02	0.75
5	1.2	2.6	2918	2838	0.40	0.01	0.06	0.58	0.40	0.05	3.21	2.92	0.91	2.91	0.02	1.00
5	2.2	3.3	3680	3533	0.96	0.01	0.13	1.23	0.32	0.07	7.25	6.81	0.94	6.14	0.03	0.90
5	3.4	3.9	4392	4158	1.66	0.01	0.21	2.03	0.27	0.08	13.33	12.66	0.95	10.17	0.03	0.80
5	3.7	4.6	4494	4864	1.75	0.01	0.22	2.14	0.26	0.08	16.61	15.84	0.95	10.72	0.03	0.68
5	5.3	5.2	5209	5547	2.55	0.01	0.31	3.07	0.23	0.09	27.70	26.51	0.96	15.33	0.04	0.58
5	6.9	5.7	5766	6079	3.31	0.01	0.40	3.94	0.20	0.09	39.45	37.76	0.96	19.69	0.04	0.52
5	9.2	6.4	6401	6704	4.22	0.01	0.51	4.99	0.18	0.10	58.35	55.72	0.95	24.93	0.04	0.45
5	12.3	7.1	7101	7390	5.29	0.01	0.63	6.22	0.17	0.10	87.09	82.78	0.95	31.10	0.04	0.38
5	15.2	7.7	7651	7985	6.20	0.01	0.74	7.28	0.15	0.10	116.82	110.55	0.95	36.38	0.05	0.33

Table C.1 (continued)																
5	19.1	8.3	8231	8581	7.25	0.01	0.87	8.49	0.14	0.10	159.29	149.73	0.94	42.43	0.05	0.28
10	2.2	3.9	4426	4175	0.11	0.09	0.10	1.03	0.53	0.04	8.66	8.16	0.94	10.26	0.02	1.26
10	2.6	4.5	4614	4821	0.30	0.09	0.13	1.25	0.51	0.05	11.80	11.19	0.95	12.45	0.02	1.11
10	4.3	5.2	5360	5545	1.02	0.09	0.21	2.07	0.44	0.06	22.42	21.47	0.96	20.70	0.03	0.96
10	6.4	5.8	5934	6191	1.90	0.09	0.32	3.09	0.40	0.07	37.03	35.50	0.96	30.90	0.03	0.87
10	8.7	6.4	6533	6773	2.79	0.09	0.42	4.11	0.36	0.08	55.61	53.19	0.96	41.10	0.04	0.77
10	11.5	7.1	7181	7425	3.68	0.09	0.52	5.14	0.33	0.08	81.51	77.66	0.95	51.42	0.04	0.66
10	14.4	7.7	7727	7978	4.52	0.09	0.62	6.10	0.31	0.08	110.37	104.66	0.95	61.05	0.04	0.58
10	19.9	8.5	8468	8771	5.84	0.09	0.78	7.63	0.28	0.08	169.28	159.00	0.94	76.27	0.05	0.48
15	6.7	6.5	6811	6893	0.55	0.20	0.27	2.60	0.52	0.04	43.58	41.87	0.96	39.00	0.02	0.93
15	9.4	7.1	7397	7521	1.45	0.20	0.37	3.64	0.48	0.05	67.20	64.38	0.96	54.56	0.03	0.85
15	12.3	7.7	7943	8103	2.38	0.20	0.48	4.71	0.45	0.06	95.06	90.69	0.95	70.65	0.03	0.78
15	16.1	8.3	8441	8659	3.30	0.20	0.59	5.77	0.42	0.06	134.46	127.42	0.95	86.56	0.04	0.68
15	19.5	8.7	8824	8949	4.50	0.20	0.73	7.15	0.40	0.07	168.95	159.03	0.94	107.31	0.04	0.67
20	13.1	8.4	8833	8863	0.82	0.30	0.40	3.92	0.53	0.04	110.82	105.87	0.96	78.40	0.03	0.74
20	17.5	9.0	9366	9364	1.85	0.30	0.52	5.11	0.50	0.05	157.59	149.39	0.95	102.15	0.03	0.68
20	20.0	9.3	9620	9564	2.14	0.30	0.56	5.44	0.49	0.05	184.80	174.35	0.94	108.84	0.04	0.62

Table C.2 Geometrical data of NACA 4409 of the Turbotek Prop6 (10x7) Propeller [24]

r/R	r (m)	ϕ (°)	Chord (m)
0.35	0.0445	17.2464	0.0235
0.55	0.0699	21.9877	0.0281
0.75	0.0953	16.5543	0.0255
0.95	0.1207	13.9024	0.0131

Table C.3 CFD results of Turbotek Prop6 (10x7) Propeller [24]

rpm	Advance ratio	Total power (W)	Thrust (N)	C_T	C_P	Efficiency
11000	0	591.55	20.82	0.1214862	0.0741246	0
12000	0	750.90	24.56	0.1204197	0.0724749	0
13000	0	957.56	28.91	0.1207794	0.0726917	0
11000	0	591.55	20.82	0.1214862	0.0741246	0
11000	0.2	523.67	17.64	0.1029307	0.0656189	0.31372
11000	0.3	488.89	15.36	0.0896267	0.0612607	0.43891
11000	0.4	447.54	12.54	0.0731718	0.0560793	0.52192

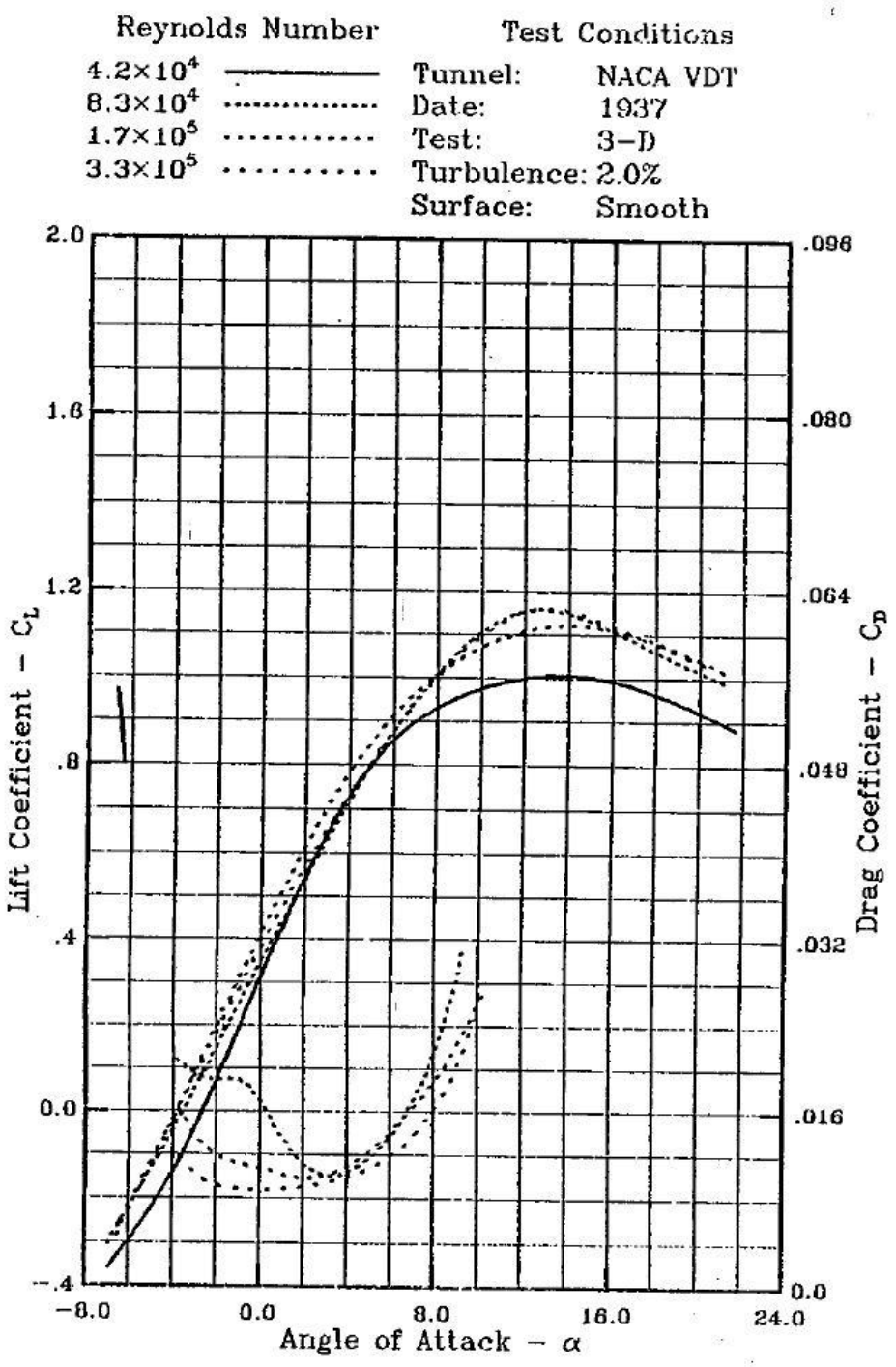

Figure C.1 Aerodynamics data of NACA 4409 airfoil used in sections of Prop6 propeller [24][28]

Table C.4 Aerodynamics data of NACA 4409 airfoil [28]

NACA 4409

Tunnel: NACA VDT / Date: 1937 / Test: 3-D / Turbulence: 2.0% / Surface: Smooth

RN	4.2×10^4		8.3×10^4		1.7×10^5		3.3×10^5			6.5×10^5		
AOA	CL	CD	CL	CD	CL	CD	CL	CD	CM	CL	CD	CM
-7.0	-	-	-	-	-	-	-	-	-	-.24	-	-
-6.0	-.30	.0486	-.22	-	-.23	-	-.22	-	-	-.16	-	-
-5.0	-.22	.0350	-.14	-	-.13	-	-.12	-	-	-.08	-	-
-4.0	-.14	.0289	-.04	-	-.02	-	-.02	-	-	-.00	-	-.09
-3.0	-.04	.0275	.05	.0227	.09	.0160	.08	.0119	-.09	.09	-	-.09
-2.0	.07	.0271	.15	.0219	.20	.0138	.18	.0105	-.09	.18	.0107	-.09
-1.0	.19	.0261	.25	.0219	.30	.0128	.28	.0101	-.09	.28	.0099	-.09
.0	.31	.0251	.34	.0196	.41	.0123	.38	.0100	-.10	.38	.0095	-.10
1.0	.43	.0243	.44	.0157	.51	.0117	.48	.0101	-.10	.48	.0095	-.10
2.0	.54	.0235	.54	.0128	.61	.0113	.57	.0103	-.10	.58	.0100	-.10
3.0	.64	.0227	.63	.0116	.70	.0115	.65	.0107	-.10	.67	.0107	-.10
4.0	.73	.0221	.72	.0118	.78	.0125	.73	.0114	-.10	.75	.0116	-.10
5.0	.80	.0218	.80	.0133	.85	.0140	.81	.0123	-.10	.83	.0127	-.10
6.0	.86	.0220	.88	.0158	.91	.0162	.88	.0137	-.11	.90	.0140	-.10
7.0	.90	.0227	.95	.0195	.97	.0187	.94	.0157	-.11	.97	.0156	-.10
8.0	.93	.0241	1.01	.0247	1.01	.0217	1.00	.0186	-.11	1.02	.0176	-.10
9.0	.96	.0261	1.06	.0327	1.04	.0255	1.05	.0230	-.11	1.07	.0201	-.10
10.0	.98	.0288	1.11	-	1.07	.0302	1.10	-	-.11	1.12	.0232	-.10
11.0	.99	.0325	1.14	-	1.09	-	1.13	-	-.11	1.15	-	-.10
12.0	1.00	.0374	1.15	-	1.11	-	1.15	-	-.11	1.17	-	-.11
13.0	1.01	-	1.16	-	1.12	-	1.16	-	-.12	1.19	-	-.11
14.0	1.01	-	1.15	-	1.12	-	1.15	-	-.13	1.19	-	-.11
15.0	1.00	-	1.13	-	1.12	-	1.14	-	-.14	1.18	-	-.12
16.0	.99	-	1.11	-	1.11	-	1.12	-	-.16	1.17	-	-.13
17.0	.98	-	1.08	-	1.10	-	1.10	-	-.17	1.15	-	-.14
18.0	.96	-	1.06	-	1.08	-	1.08	-	-	1.12	-	-.16
19.0	.94	-	1.04	-	1.06	-	1.06	-	-	1.09	-	-
20.0	.92	-	1.02	-	1.04	-	1.04	-	-	1.06	-	-
21.0	.90	-	.99	-	1.02	-	-	-	-	-	-	-

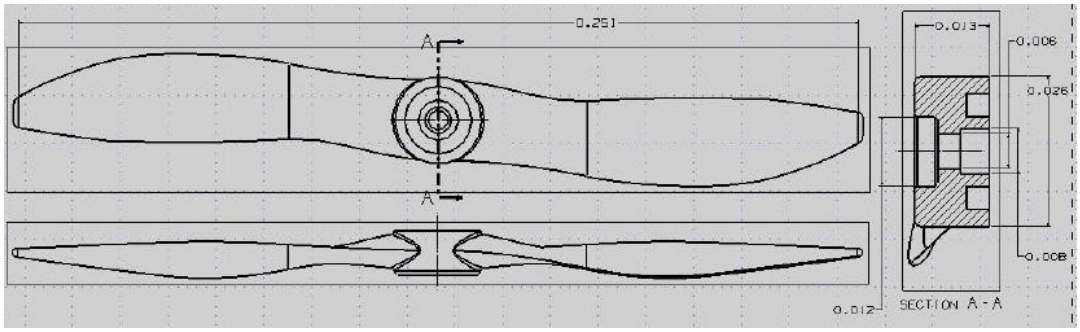

Figure C.2 Basic Dimensions of Turbotek Prop6 (10x7) Propeller [24]

Table C.5 Calculated analysis of Turbotek Prop6 (10x7) Propeller [24]

Advance ratio	rpm	Thrust (N)	Power (W)	Efficiency	C_T	C_P
0.15	11000	20.0436	413.974	0.3382	0.1167	0.0517
0.2	11000	19.1796	419.962	0.4253	0.1116	0.0525
0.25	11000	18.1437	422.117	0.5004	0.1056	0.0528
0.3	11000	16.9473	419.875	0.5639	0.0986	0.0525
0.35	11000	15.6471	413.087	0.6174	0.0911	0.0516
0.4	11000	14.2324	400.259	0.6623	0.0828	0.0500
0.45	11000	12.7549	382.513	0.6987	0.0742	0.0478
0.5	11000	11.1888	358.805	0.7261	0.0651	0.0449
0.55	11000	9.5467	328.767	0.7437	0.0556	0.0411
0.6	11000	7.8575	293.163	0.7489	0.0457	0.0366
0.65	11000	6.0715	249.602	0.7363	0.0353	0.0312
0.7	11000	4.2141	198.528	0.6919	0.0245	0.0248
0.75	11000	2.2925	139.980	0.5720	0.0133	0.0175
0.8	11000	0.1616	70.764	0.0851	0.0009	0.0088

Table C.6 METU Wind Tunnel (Dynamic) Test Results of Prop1 (10x6) Propeller

V [m/s]	Current [A]	AC Voltage [V]	rpm (measured)	rpm (calculated)	Scale Readout [kg]	Drag [kg]	Thrust [kg]	Thrust [N]	Advance Ratio	Thrust Coefficient CT	Pin [W]	Pm, out [W]	Power Coefficient CP	Propeller Efficiency
0			7181				0.526	5.15	0.00	0.080		69.57	0.035	0.00
0			8886				0.833	8.16	0.00	0.082		154.50	0.041	0.00
5	1.1	2.4	2675	2613	0.040	0.010	0.015	0.1	0.44	0.016	2.54	2.28	0.022	0.32
5	1.2	2.6	2889	2778	0.145	0.010	0.027	0.3	0.41	0.025	2.99	2.70	0.021	0.49
5	1.7	3.2	3578	3433	0.460	0.010	0.064	0.6	0.33	0.039	5.55	5.17	0.021	0.61
5	2.9	3.9	4416	4159	1.030	0.010	0.131	1.3	0.27	0.052	11.07	10.49	0.023	0.61
5	3.1	4.5	4533	4822	1.120	0.010	0.142	1.4	0.26	0.054	13.99	13.32	0.027	0.52
5	4.4	5.1	5196	5446	1.716	0.010	0.212	2.1	0.23	0.061	22.34	21.38	0.029	0.49
5	6.5	5.9	5981	6215	2.560	0.010	0.311	3.0	0.20	0.068	38.01	36.43	0.032	0.42
5	8.3	6.4	6549	6782	3.155	0.010	0.381	3.7	0.18	0.069	53.36	51.08	0.034	0.37
5	11.3	7.1	7218	7445	4.020	0.010	0.483	4.7	0.16	0.072	80.10	76.36	0.038	0.31
5	13.7	7.7	7817	8038	4.835	0.010	0.579	5.7	0.15	0.074	105.53	100.29	0.039	0.28
5	19.0	8.5	8614	8807	6.300	0.010	0.751	7.4	0.14	0.079	162.27	152.79	0.045	0.24
10	3.9	5.2	5442	5570	0.500	0.092	0.151	1.5	0.43	0.040	20.40	19.52	0.023	0.76
10	5.6	5.8	6012	6183	1.125	0.092	0.224	2.2	0.39	0.048	32.46	31.14	0.027	0.71
10	8.3	6.5	6672	6881	1.830	0.092	0.307	3.0	0.35	0.054	53.78	51.51	0.033	0.58
10	10.4	7.0	7203	7384	2.420	0.092	0.376	3.7	0.33	0.057	73.12	69.84	0.035	0.53
10	13.1	7.8	7872	8109	3.380	0.092	0.489	4.8	0.30	0.062	101.74	96.86	0.037	0.50
10	16.2	8.4	8417	8686	4.255	0.092	0.592	5.8	0.28	0.065	134.96	127.91	0.040	0.45
10	19.5	8.6	8711	8906	4.730	0.092	0.648	6.4	0.27	0.067	168.63	158.67	0.045	0.40
15	8.5	7.1	7405	7476	0.535	0.201	0.264	2.6	0.48	0.038	60.03	57.61	0.027	0.67
15	11.2	7.8	7960	8173	1.400	0.201	0.365	3.6	0.45	0.045	87.07	83.30	0.031	0.64
15	15.3	8.3	8589	8694	2.400	0.201	0.483	4.7	0.41	0.051	127.83	121.40	0.036	0.58
15	19.2	9.0	9277	9290	3.360	0.201	0.596	5.8	0.38	0.054	172.78	163.05	0.038	0.54
20	16.6	9.0	9488	9387	0.780	0.304	0.395	3.9	0.50	0.034	149.48	142.02	0.031	0.55
20	19.8	9.4	9918	9750	1.630	0.304	0.495	4.9	0.48	0.039	186.81	176.48	0.034	0.55

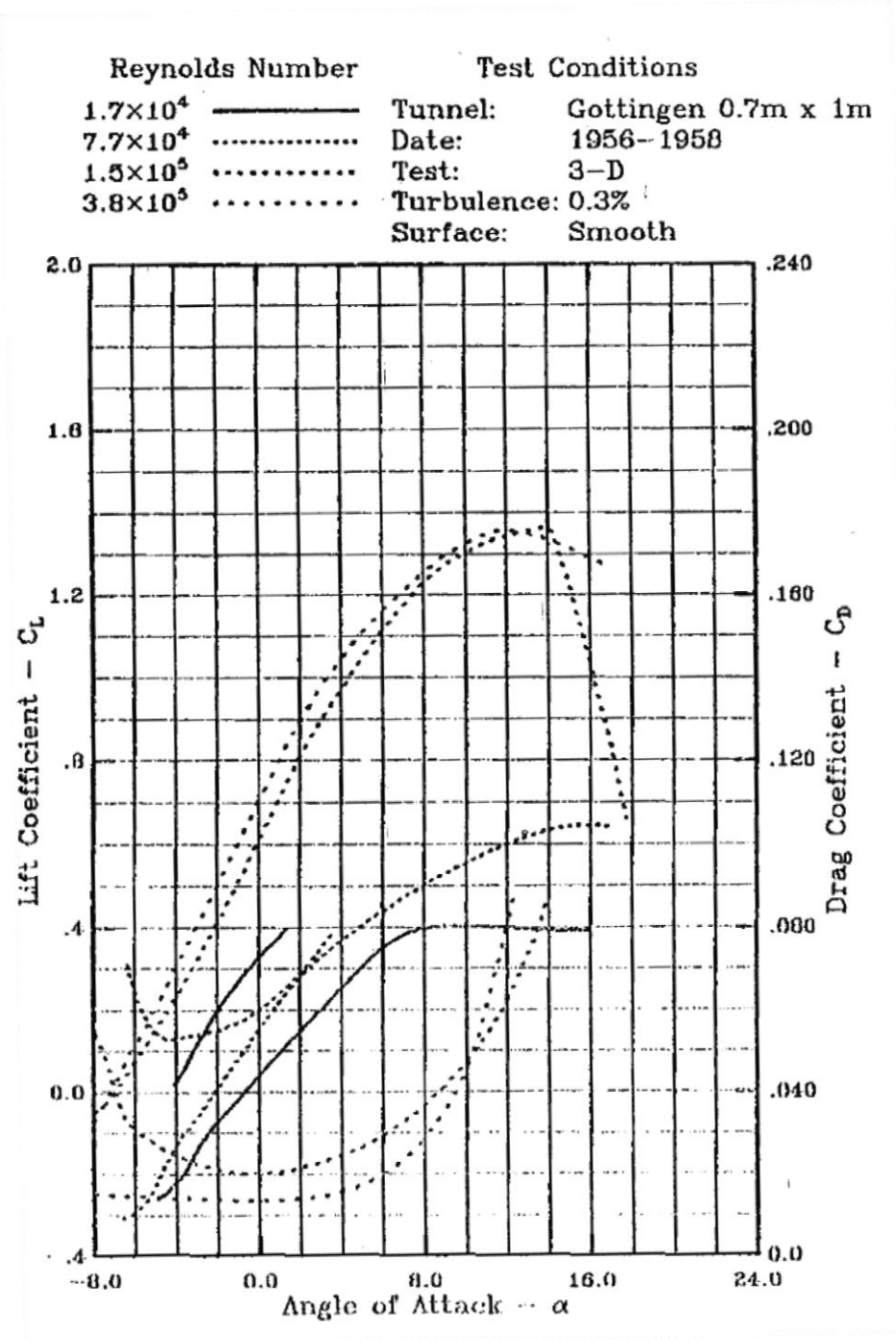

Figure C.3 Aerodynamics data of GO 797 airfoil used in sections of Prop1 propeller [25][28]

Table C.7 Aerodynamics data of GO 797 airfoil [28]

GO 797

Tunnel: Gottingen 0.7m x 1m / Date: 1956-1958 / Test: 3-D / Turbulence: 0.3% / Surface: Smooth

RN	$1.7x10^4$			$7.7x10^4$			$1.5x10^5$			$3.8x10^5$		
AOA	CL	CD	CM	CL	CD	CM	CL	CD	CM	CL	CD	CM
-8.0	--	--	-	-	-	-	-.05	.0555	-.10	-.07	.0154	-
-7.0	--	--	--	--	--	-	-.00	.0414	-.11	.02	.0150	-.11
-6.0	-	--	-	-.29	.0648	-.03	.07	.0310	-.11	.11	.0148	-.11
-5.0	--	--	-	-.23	.0546	-.05	.15	.0273	-.11	.21	.0146	-.10
-4.0	-.22	.0425	-.02	-.13	.0530	-.07	.23	.0245	-.12	.30	.0143	-.10
-3.0	-.14	.0513	-.03	-.06	.0539	-.07	.32	.0225	-.12	.40	.0141	-.10
-2.0	-.07	.0598	-.03	.01	.0551	-.07	.41	.0212	-.12	.50	.0139	-.10
-1.0	-.02	.0669	-.04	.08	.0571	-.08	.51	.0204	-.11	.60	.0138	-.10
.0	.04	.0727	-.04	.15	.0600	-.08	.61	.0202	-.11	.71	.0137	-.11
1.0	.10	.0779	-.05	.22	.0639	-.08	.71	.0206	-.11	.80	.0137	-.11
2.0	.15	.0832	-.05	.28	.0689	-.08	.81	.0215	-.11	.89	.0140	-.10
3.0	.20	.0890	-.05	.33	.0750	-.08	.90	.0229	-.11	.98	.0147	-.10
4.0	.25	.0952	-.06	.37	.0821	-.08	.97	.0246	-.10	1.05	.0158	-.09
5.0	.31	.1016	-.06	.41	.0901	-.08	1.05	.0269	-.10	1.11	.0175	-.09
6.0	.35	.1079	-.06	.44	.0994	-.08	1.11	.0296	-.10	1.16	.0200	-.08
7.0	.38	.1141	-.06	.47	.1103	-.08	1.18	.0328	-.09	1.21	.0236	-.08
8.0	.40	.1198	-.05	.50	.1226	-.08	1.23	.0369	-.09	1.25	.0286	-.08
9.0	.40	.1253	-.05	.53	.1357	-.08	1.27	.0416	-.08	1.29	.0355	-.07
10.0	.40	.1306	-.05	.56	.1502	-.09	1.31	.0471	-.08	1.33	.0459	-.07
11.0	.40	.1360	--	.58	.1681	-.10	1.33	.0541	-.07	1.35	.0615	-.07
12.0	.40	.1417	--	.60	--	-.10	1.34	.0637	-.07	1.36	.0810	-.07
13.0	.40	.1476	-	.62	--	-.10	1.36	.0738	-.06	1.35	.1015	-.08
14.0	.39	--	--	.63	--	-.11	1.37	.0855	-.06	1.34	.1199	-.08
15.0	.39	--	-	.64	--	-.10	1.33	.1305	-.07	1.32	.1366	-.08
16.0	.39	-	--	.64	--	-	1.03	--	-.08	1.29	--	-
17.0	--	--	--	--	--	-	.83	-	-.09	-	-	-

Table C.8 Geometrical data of GO 797 of the Turbotek Prop1 (10x6) Propeller [25]

r/R	r (m)	ϕ (°)	Chord (m)
0.40	0.0508	22.3531	0.0220
0.45	0.0572	21.84349	0.0222
0.50	0.0635	20.60476	0.0227
0.55	0.0699	19.04836	0.0232
0.60	0.0762	17.57802	0.0237
0.65	0.0826	16.30325	0.0239
0.70	0.0889	15.21357	0.0237
0.75	0.0953	14.2263	0.0229
0.80	0.1016	13.20378	0.0213
0.85	0.1080	11.99605	0.0187
0.90	0.1143	10.53223	0.0150
0.95	0.1207	8.514022	0.0100

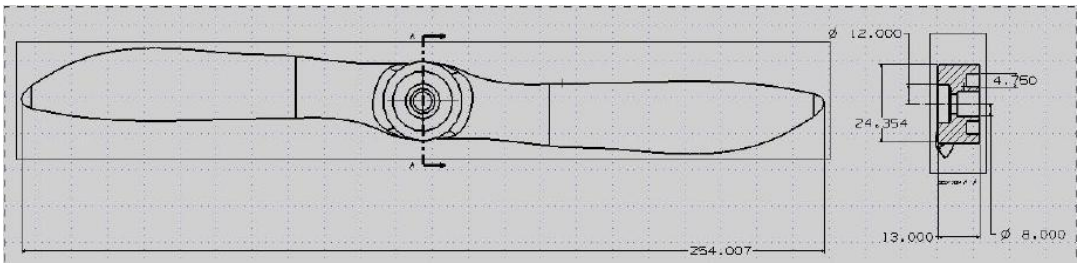

Figure C.4 Basic Dimensions of Turbotek Prop1 (10x6) Propeller [25]

Table C.9 CFD results of Turbotek Prop1 (10x6) Propeller [25]

rpm	Inlet velocity (m/s)	Advance ratio	Total power (W)	Thrust (N)	C_T	C_P	Efficiency
9000	0	0	214.79	11.15	0.09719	0.04914	0
12000	0	0	504.67	19.89	0.09752	0.04871	0
13500	0	0	716.05	25.22	0.09770	0.04854	0
15000	0	0	912.32	31.23	0.09800	0.04508	0
9000	7.62	0.2	209.25	9.34	0.08141	0.04787	0.34012
9000	11.43	0.3	199.35	7.89	0.06877	0.04561	0.45238
9000	15.24	0.4	182.63	6.16	0.05369	0.04178	0.51404

Table C.10 Calculated analysis of Turbotek Prop1 (10x6) Propeller [25]

AdvanceRatio	RPM	Thrust (N)	Power (W)	Efficiency	C_T	C_P
0.25	9000	9.9801	209.9791	0.4527	0.0868	0.0479
0.3	9000	9.3369	207.2992	0.5148	0.0812	0.0473
0.35	9000	8.6085	202.5754	0.5667	0.0749	0.0462
0.4	9000	7.8247	195.7398	0.6092	0.0680	0.0447
0.45	9000	6.9822	186.4995	0.6419	0.0607	0.0426
0.5	9000	6.0818	174.4660	0.6641	0.0529	0.0398
0.6	9000	4.1829	143.1654	0.6679	0.0364	0.0327

Table C.11 METU Wind Tunnel (Dynamic) Test Results of eProp2 (12x7) Propeller

V [m/s]	Current [A]	AC Voltage [V]	rpm (measured)	rpm (calculated)	Scale Readout [kg]	Drag [kg]	Thrust [kg]	Thrust [N]	Advance Ratio	Thrust Coefficient CT	Pm, out [W]	Power Coefficient CP	Propeller Efficiency
0			5584				0.566	5.55	0.00	0.068	49.05	0.021	0.00
0			7129				0.965	9.46	0.00	0.071	125.66	0.026	0.00
5	0.9	1.9	2126	2057	0.100	0.013	0.025	0.24	0.46	0.021	1.44	0.011	0.84
5	1.6	2.6	2851	2801	0.515	0.013	0.074	0.72	0.35	0.034	3.97	0.013	0.91
5	2.9	3.3	3578	3474	1.050	0.013	0.136	1.34	0.28	0.040	8.80	0.015	0.76
5	3.2	3.9	3703	4107	1.525	0.013	0.192	1.89	0.27	0.053	11.65	0.017	0.81
5	4.4	4.5	4190	4726	2.100	0.013	0.260	2.55	0.23	0.056	18.51	0.019	0.69
5	6.3	5.1	4786	5374	2.970	0.013	0.362	3.55	0.21	0.060	30.77	0.021	0.58
5	9.2	5.8	5514	6018	4.200	0.013	0.507	4.97	0.18	0.063	50.87	0.023	0.49
5	12.2	6.4	6071	6562	5.225	0.013	0.628	6.15	0.16	0.064	73.69	0.025	0.42
5	17.0	7.1	6745	7158	6.735	0.013	0.805	7.89	0.15	0.067	112.36	0.028	0.35
5	20.2	7.4	7071	7441	7.650	0.013	0.913	8.95	0.14	0.069	139.74	0.030	0.32
10	2.7	4.0	3992	4279	0.035	0.092	0.096	0.94	0.49	0.023	10.07	0.012	0.93
10	3.7	4.5	4412	4790	0.580	0.092	0.160	1.57	0.45	0.031	15.88	0.014	0.99
10	5.8	5.1	4953	5406	1.500	0.092	0.268	2.63	0.40	0.041	28.24	0.018	0.93
10	8.5	5.8	5553	6002	2.495	0.092	0.385	3.78	0.35	0.047	46.36	0.020	0.81
10	12.3	6.5	6193	6644	3.835	0.092	0.543	5.32	0.32	0.053	74.97	0.024	0.71
10	16.2	7.1	6760	7184	5.020	0.092	0.682	6.69	0.29	0.056	107.52	0.026	0.62
10	20.3	7.5	7130	7468	5.880	0.092	0.784	7.68	0.28	0.058	140.52	0.029	0.55
15	6.7	5.8	5775	6089	0.520	0.201	0.262	2.57	0.51	0.030	37.04	0.015	1.04
15	10.0	6.4	6391	6666	1.475	0.201	0.374	3.67	0.46	0.034	60.77	0.018	0.90
15	14.6	7.1	6902	7265	3.030	0.201	0.557	5.46	0.43	0.044	97.94	0.023	0.84
15	19.9	7.7	7408	7703	4.145	0.201	0.688	6.74	0.40	0.047	142.30	0.026	0.71
20	13.3	7.4	7397	7590	0.170	0.304	0.324	3.17	0.53	0.022	92.63	0.017	0.68
20	15.1	7.7	7674	7893	0.800	0.304	0.398	3.90	0.51	0.025	109.85	0.018	0.71
20	18.6	8.1	7941	8196	1.455	0.304	0.475	4.65	0.50	0.028	140.84	0.021	0.66

Table C.12 Geometrical data of NACA 4 series of the Turbotek Turbotek eProp2 (12x7) propeller [26]

r/R	r	ϕ (°)	chord c (m)	camber ratio p/c	camber place m/c	thickness ratio t/c
0,25	0,0381	27,35321	0,02245	4,46732	4,04767	11,97841
0,26278	0,04005	26,96735	0,02263	4,47333	4,05347	12,05752
0,30024	0,04576	25,83604	0,02316	4,49066	4,07364	12,25372
0,35983	0,05484	24,03639	0,02401	4,51743	4,1155	12,45597
0,4375	0,06667	21,69104	0,02511	4,55083	4,18802	12,51708
0,52794	0,08046	19,06716	0,02524	4,5876	4,29813	12,29946
0,625	0,09525	16,50903	0,02263	4,62453	4,44698	11,72028
0,72206	0,11004	13,95091	0,02003	4,68935	4,47996	11,19679
0,8125	0,12382	12,38856	0,01561	4,80233	4,27348	11,13131
0,89017	0,13566	11,36232	0,01106	4,93982	3,91354	11,40025
0,94976	0,14474	10,57485	0,00757	5,07069	3,52293	11,81034
0,98722	0,15045	10,07983	0,00193	5,16423	3,22652	12,15869
1	0,1524	9,91099	0	5,19812	3,11644	12,29349

Table C.13 CFD results of Turbotek eProp2 (12x7) propeller [26]

Advance ratio	Flow velocity (m/s)	Lifiting Coeff. C_L	CFD Thrust (N)	Moment Coeff. C_M	Moment (Nm)	CFD Power (W)	CFD CT	CFD CP	CFD Efficiency
0	0,0	10.455	11.89	0.2484	0.304	222.8436	0.0830	0.0437	0
0.2	67.733	9.2175	11	0.2264	0.270	197.9203	0.0768	0.0388	0.3953
0.5	186.267	4.0151	4.84	0.1631	0.201	147.3407	0.0338	0.0289	0.5841

Table C.14 Calculated analysis of Turbotek eProp2 (12x7) propeller [26]

Advance ratio	rpm	Thrust (N)	Power (W)	Efficiency	CT	CP
0.2	7000	12.003	170.44	0.5009	0.0832	0.0332
0.3	7000	10.269	169.76	0.6453	0.0712	0.0331
0.4	7000	8.2465	157.958	0.7426	0.0572	0.0308
0.5	7000	6.0016	133.193	0.8012	0.0416	0.0260
0.55	7000	4.8620	118.128	0.8050	0.0337	0.0230
0.6	7000	3.8006	101.895	0.7958	0.0263	0.0199
0.7	7000	1.3970	53.8507	0.6458	0.0097	0.0105
0.75	7000	0.1202	21.256	0.1509	0.0008	0.0041

Table C.15 METU Wind Tunnel (Dynamic) Test Results of eProp1 (10x7) Propeller

V [m/s]	Current [A]	AC Voltage [V]	rpm (measured)	rpm (calculated)	Scale Readout [kg]	System Drag [kg]	Thrust [kg]	Thrust [N]	Advance Ratio	Thrust Coefficient CT	Pm,in [W]	Pm, out [W]	Motor Efficiency	Puseful [W]	Power Coefficient CP	Propeller Efficiency
0			8114				0.465	4.55	0.00	0.055		65.96		0.00	0.023	0.00
0			10111				0.738	7.23	0.00	0.056		147.41		0.00	0.027	0.00
5	1.2	2.8	3104	2973	0.075	0.013	0.022	0.21	0.38	0.018	3.25	2.95	0.91	1.07	0.019	0.36
5	1.5	3.2	3636	3495	0.285	0.013	0.046	0.46	0.32	0.028	4.90	4.52	0.92	2.28	0.018	0.50
5	2.2	3.9	4427	4162	0.615	0.013	0.085	0.84	0.27	0.034	8.52	8.02	0.94	4.18	0.017	0.52
5	2.5	4.6	4705	4893	0.765	0.013	0.103	1.01	0.25	0.036	11.56	10.95	0.95	5.04	0.020	0.46
5	3.6	5.2	5425	5537	1.185	0.013	0.152	1.49	0.22	0.041	18.34	17.53	0.96	7.47	0.021	0.43
5	4.8	5.8	6060	6147	1.680	0.013	0.211	2.06	0.19	0.045	27.68	26.56	0.96	10.32	0.023	0.39
5	6.1	6.4	6720	6785	2.205	0.013	0.272	2.67	0.18	0.047	38.67	37.16	0.96	13.35	0.023	0.36
5	8.1	7.0	7395	7472	2.810	0.013	0.344	3.37	0.16	0.049	57.17	54.91	0.96	16.83	0.026	0.31
5	10.0	7.7	8019	8121	3.480	0.013	0.422	4.14	0.15	0.051	76.75	73.61	0.96	20.70	0.027	0.28
5	12.4	8.3	8759	8714	4.390	0.013	0.529	5.19	0.13	0.054	103.16	98.65	0.96	25.94	0.028	0.26
5	15.9	9.0	9377	9365	5.195	0.013	0.624	6.12	0.13	0.056	142.30	135.40	0.95	30.58	0.031	0.23
5	19.2	9.6	10081	9976	6.150	0.013	0.736	7.22	0.12	0.057	184.66	174.89	0.95	36.09	0.032	0.21
10	2.5	4.8	5063	5133	0.100	0.092	0.104	1.01	0.47	0.032	11.73	11.11	0.95	10.15	0.016	0.91
10	3.1	5.1	5450	5507	0.320	0.092	0.129	1.27	0.43	0.034	15.94	15.21	0.95	12.68	0.018	0.83
10	4.3	5.8	6173	6201	0.815	0.092	0.188	1.84	0.38	0.039	25.14	24.12	0.96	18.39	0.019	0.76
10	5.9	6.4	6795	6831	1.285	0.092	0.243	2.38	0.35	0.041	37.75	36.29	0.96	23.81	0.022	0.66
10	8.0	7.1	7487	7532	1.950	0.092	0.321	3.15	0.32	0.045	56.52	54.31	0.96	31.48	0.024	0.58
10	9.7	7.7	8089	8184	2.665	0.092	0.405	3.97	0.29	0.048	75.25	72.23	0.96	39.72	0.026	0.55
10	12.4	8.4	8790	8799	3.330	0.092	0.484	4.74	0.27	0.049	103.53	99.05	0.96	47.39	0.028	0.48
10	16.1	9.0	9442	9358	4.335	0.092	0.602	5.90	0.25	0.053	144.63	137.53	0.95	58.97	0.031	0.43
10	19.4	9.6	10033	9970	5.300	0.092	0.715	7.01	0.24	0.056	186.78	176.80	0.95	70.10	0.033	0.40

Table C.15 (continued)

V [m/s]	Current [A]	AC Voltage [V]	rpm (measured)	rpm (calculated)	Scale Readout [kg]	System Drag [kg]	Thrust [kg]	Thrust [N]	Advance Ratio	Thrust Coefficient CT	Pm,in [W]	Pm, out [W]	Motor Efficiency	Puseful [W]	Power Coefficient CP	Propeller Efficiency
15	6.2	6.8	7350	7298	0.300	0.201	0.236	2.31	0.48	0.034	42.44	40.84	0.96	34.67	0.019	0.85
15	7.0	7.1	7600	7544	0.500	0.201	0.259	2.54	0.47	0.035	49.26	47.41	0.96	38.13	0.020	0.80
15	8.7	7.7	8093	8142	1.070	0.201	0.326	3.20	0.44	0.039	66.41	63.87	0.96	47.99	0.023	0.75
15	11.3	8.3	8824	8786	1.750	0.201	0.406	3.98	0.40	0.041	94.06	90.19	0.96	59.75	0.025	0.66
15	15.2	9.0	9501	9453	2.700	0.201	0.518	5.08	0.37	0.045	137.08	130.69	0.95	76.18	0.029	0.58
15	18.6	9.6	10120	9992	3.700	0.201	0.636	6.23	0.35	0.049	178.70	169.49	0.95	93.47	0.031	0.55
15	19.9	9.8	10196	10153	4.030	0.201	0.675	6.61	0.35	0.051	194.97	184.52	0.95	99.18	0.033	0.54
20	12.8	9.1	9650	9542	0.625	0.304	0.377	3.70	0.49	0.032	116.17	111.35	0.96	73.90	0.023	0.66
20	16.3	9.7	10310	10107	1.400	0.304	0.468	4.59	0.46	0.034	157.82	150.49	0.95	91.77	0.026	0.61
20	19.9	10.2	10850	10600	2.320	0.304	0.576	5.65	0.44	0.038	203.03	192.55	0.95	112.99	0.028	0.59

Table C.16 Geometrical data of NACA 4 series of the Turbotek eProp1 (10x7) propeller [27]

r/R	*r*	*ϕ (°)*	*chord c (m)*	*camber ratio p/c*	*camber place m/c*	*thickness ratio t/c*
0,25	0,03175	30,96767	0,01251	2,89595	4,02	8,60499
0,26278	0,03337	30,38719	0,01268	3,15077	4,04428	8,90324
0,30024	0,03813	28,68533	0,01317	3,81167	4,09989	9,70541
0,35983	0,0457	25,97806	0,01396	4,59804	4,14046	10,75945
0,4375	0,05556	22,44987	0,01498	5,13454	4,10506	11,72387
0,52794	0,06705	19,41923	0,01526	5,06284	3,93794	12,26333
0,625	0,07937	18,7545	0,01336	4,15227	3,60792	12,14365
0,72206	0,0917	18,08977	0,01146	3,2801	3,25279	11,54672
0,8125	0,10319	16,15913	0,00906	3,3133	3,0171	10,78229
0,89017	0,11305	13,99785	0,00677	3,9931	2,88802	9,96558
0,94976	0,12062	12,33944	0,005	4,92278	2,83492	9,23848
0,98722	0,12538	11,29693	0,00128	5,68857	2,82195	8,73677
1	0,127	10,94134	0	5,9818	2,82113	8,55776

Table C.17 CFD results of Turbotek eProp1 (10x7) propeller [27]

Advance ratio	Flow velocity (m/s)	Lifiting Coeff. C_L	CFD Thrust (N)	Moment Coeff. C_M	Moment (Nm)	CFD Power (W)	CFD C_T	CFD C_P
0	0.0	10.46	6.40	0.25	0.15	127.42	0.0709	0.0417
0.2	67.73	9.22	5.64	0.23	0.14	116.20	0.0625	0.0380
0.55	186.27	4.02	2.35	0.14	0.09	72.05	0.0260	0.0236

Table C.18 Calculated analysis of Turbotek eProp1 (10x7) propeller [27]

Advance ratio	rpm	Thrust (N)	Power (W)	Efficiency	C_T	C_P
0.2	8000	6.0002	82.7452	0.4912	0.0660	0.0269
0.3	8000	5.4518	86.8998	0.6374	0.0600	0.0282
0.4	8000	4.5732	84.9595	0.7292	0.0503	0.0276
0.5	8000	3.5459	76.5574	0.7843	0.0390	0.0249
0.55	8000	3.0035	70.1334	0.7977	0.0331	0.0228
0.6	8000	2.4241	61.8624	0.7963	0.0267	0.0201
0.7	8000	1.2093	40.1961	0.7132	0.0133	0.0131
0.75	8000	0.5460	26.5169	0.5230	0.0060	0.0086

Table C.19 Blockage ratios of various wind tunnels for the test of propellers

	Test Section			Propellers			Blockage Ratio
Wind Tunnel	Width (m)	Height (m)	Area (m^2)	Brand	Diameter (m)	Area (m^2)	
University of Illinois at Urbana-Champaign (UIUC) Subsonic Wind Tunnel [12]	0.8530	1.2190	1.0398	APC 11x8	0.2794	0.0613	0.06
				Graupner CAM Slim 10x8 (True diameter:9.9 in)	0.2515	0.0497	0.05
				GWS Slow Flyer 11x4.7	0.2794	0.0613	0.06
				Master Airscrew G/F 11x4	0.2794	0.0613	0.06
North Carolina State University (NCSU) Subsonic Wind Tunnel, 43x33 in [7]	1.0922	0.8382	0.9155	APC 18x8	0.4572	0.1641	0.18
				8012 F2P (trimmed diameter:18 in)	0.4572	0.1641	0.18
Wichita State University (WSU) Low Speed Wind Tunnel, 3x4 ft [10]	0.9144	1.2192	1.1148	Zinger 14x4	0.3556	0.0993	0.09
				Zinger 14x6	0.3556	0.0993	0.09
				Zinger 16x6	0.4064	0.1297	0.12
				Master Airscrew 16x8, (3-Blade)	0.4064	0.1297	0.12
				APC 12x12E	0.3048	0.0729	0.07
				APC 16x12E	0.4064	0.1297	0.12
				APC 8.8x7.5	0.2235	0.0392	0.04
				Rew-up 12x8	0.3048	0.0729	0.07
				Zinger 22x8	0.5588	0.2451	0.22
Oklahoma State University (OSU) Wind Tunnel, 3x3 ft [4]	0.9144	0.9144	0.8361	APC 18x12	0.4572	0.1641	0.20
				APC 18x8	0.4572	0.1641	0.20
				APC 14x12	0.3556	0.0993	0.12
METU Wind Tunnel	0.7500	0.5020	0.3765	Turbotek Prop6 (10x7) [24]	0.2540	0.0506	0.13
				Turbotek Prop1 (10x6) [25]	0.2540	0.0506	0.13
				Turbotek eProp2 (12x7) [26]	0.3048	0.0729	0.19
				Turbotek eProp1 (10x7) [27]	0.2540	0.0506	0.13

Table C.20 Repeatability of METU Wind Tunnel (Dynamic) Test Results of Prop6 (10x7) Propeller

Velocity (m/s)	**Velocity (m/s) (repetition)**	Current [A]	**Current [A] (repetition)**	AC Voltage (V)	**AC Voltage (V) (repetition)**	rpm (measured)	**rpm (measured) (repetition)**	rpm (calculated)	**rpm (calculated) (repetition)**	Scale Readout [kg]	**Scale Readout [kg] (repetition)**	Drag (kg)	Thrust [N]	**Thrust [N] (repetition)**	Advance Ratio	**Advance Ratio (repetition)**	Thrust Coef. CT	**Thrust Coef. CT (repetition)**	Pm, out [W]	**Pm, out [W] (repetition)**	Power Coeff. CP	**Power Coeff. CP (repetition)**	Propeller Efficiency	**Propeller Efficiency (repetition)**
5	**5.0**	0.80	**1.06**	2.15	**2.29**	2372	**2527**	2319	**2473**	0.085	**0.165**	0.013	0.225	**0.317**	0.50	**0.47**	0.032	**0.040**	2.92	**2.90**	0.041	**0.034**	0.39	**0.55**
5	**5.0**	1.22	**1.22**	2.63	**2.61**	2918	**2911**	2838	**2818**	0.395	**0.385**	0.013	0.582	**0.571**	0.40	**0.41**	0.055	**0.054**	6.81	**6.59**	0.052	**0.050**	0.43	**0.43**
5	**5.0**	2.20	**2.15**	3.29	**3.27**	3680	**3651**	3533	**3506**	0.955	**0.920**	0.013	1.228	**1.188**	0.32	**0.32**	0.072	**0.071**	12.66	**12.71**	0.048	**0.049**	0.48	**0.47**
5	**5.0**	3.42	**3.42**	3.90	**3.91**	4392	**4391**	4158	**4172**	1.655	**1.620**	0.013	2.035	**1.995**	0.27	**0.27**	0.084	**0.083**	15.84	**15.84**	0.035	**0.035**	0.64	**0.63**
5	**5.0**	3.65	**3.66**	4.55	**4.54**	4494	**4481**	4864	**4850**	1.750	**1.745**	0.013	2.144	**2.139**	0.26	**0.26**	0.085	**0.085**	26.51	**24.83**	0.055	**0.052**	0.40	**0.43**
5	**5.0**	5.31	**5.06**	5.22	**5.13**	5209	**5098**	5547	**5456**	2.550	**2.435**	0.013	3.067	**2.934**	0.23	**0.23**	0.090	**0.090**	37.76	**38.19**	0.050	**0.054**	0.41	**0.38**
5	**5.0**	6.87	**6.95**	5.74	**5.74**	5766	**5752**	6079	**6077**	3.305	**3.245**	0.013	3.937	**3.868**	0.20	**0.21**	0.095	**0.093**	55.72	**57.74**	0.055	**0.057**	0.35	**0.33**
5	**5.0**	9.16	**9.40**	6.37	**6.43**	6401	**6451**	6704	**6767**	4.215	**4.300**	0.013	4.986	**5.084**	0.18	**0.18**	0.097	**0.098**	82.78	**82.78**	0.060	**0.058**	0.30	**0.31**
5	**5.0**	12.31	**12.31**	7.08	**7.08**	7101	**7098**	7390	**7390**	5.285	**5.300**	0.013	6.220	**6.237**	0.17	**0.17**	0.099	**0.099**	110.55	**111.80**	0.058	**0.059**	0.28	**0.28**
5	**5.0**	15.19	**15.37**	7.69	**7.69**	7651	**7643**	7985	**7980**	6.200	**6.220**	0.013	7.275	**7.298**	0.15	**0.15**	0.099	**0.100**	149.73	**147.13**	0.063	**0.062**	0.24	**0.25**
10	**10.0**	2.23	**2.23**	3.88	**3.85**	4426	**4383**	4175	**4133**	0.110	**0.080**	0.092	1.026	**0.992**	0.53	**0.54**	0.042	**0.041**	11.19	**11.21**	0.024	**0.025**	0.92	**0.88**
10	**10.0**	2.63	**2.65**	4.49	**4.46**	4614	**4630**	4821	**4792**	0.300	**0.270**	0.092	1.245	**1.211**	0.51	**0.51**	0.047	**0.045**	21.47	**21.27**	0.041	**0.040**	0.58	**0.57**
10	**10.0**	4.32	**4.29**	5.19	**5.18**	5360	**5277**	5545	**5532**	1.015	**1.120**	0.092	2.070	**2.191**	0.44	**0.45**	0.058	**0.063**	35.50	**34.54**	0.044	**0.044**	0.58	**0.63**
10	**10.0**	6.35	**6.22**	5.83	**5.79**	5934	**5936**	6191	**6152**	1.900	**1.820**	0.092	3.090	**2.998**	0.40	**0.40**	0.070	**0.068**	53.19	**55.23**	0.048	**0.050**	0.58	**0.54**
10	**10.0**	8.66	**9.00**	6.42	**6.42**	6533	**6574**	6773	**6764**	2.785	**2.830**	0.092	4.110	**4.162**	0.36	**0.36**	0.077	**0.077**	77.66	**76.63**	0.053	**0.051**	0.53	**0.54**

Table C.20 (continued)

Velocity (m/s)	**Velocity (m/s) (repetition)**	Current [A]	**Current [A] (repetition)**	AC Voltage (V)	**AC Voltage (V) (repetition)**	rpm (measured)	**rpm (measured) (repetition)**	rpm (calculated)	**rpm (calculated) (repetition)**	Scale Readout [kg]	**Scale Readout [kg] (repetition)**	Drag (kg)	Thrust [N]	**Thrust [N] (repetition)**	Advance Ratio	**Advance Ratio (repetition)**	Thrust Coef. CT	**Thrust Coef. CT (repetition)**	Pm, out [W]	**Pm, out [W] (repetition)**	Power Coeff. CP	**Power Coeff. CP (repetition)**	Propeller Efficiency	**Propeller Efficiency (repetition)**
10	**10.0**	11.50	**11.41**	7.09	**7.05**	7181	**7146**	7425	**7385**	3.680	**3.630**	0.092	5.142	**5.084**	0.33	**0.33**	0.080	**0.080**	104.66	**107.66**	0.053	**0.056**	0.49	**0.47**
10	**10.0**	14.40	**14.75**	7.66	**7.70**	7727	**7729**	7978	**8011**	4.515	**4.610**	0.092	6.105	**6.214**	0.31	**0.31**	0.082	**0.083**	143.34	**145.42**	0.059	**0.059**	0.43	**0.43**
10	**10.0**	18.23	**18.54**	8.34	**8.33**	8304	**8283**	8618	**8596**	5.610	**5.670**	0.092	7.367	**7.436**	0.28	**0.29**	0.085	**0.087**	159.00	**156.18**	0.052	**0.052**	0.46	**0.48**
15	**15**	4.19	**5.11**	5.77	**6.02**	6192	**6405**	6177	**6433**	0.440	**0.060**	0.201	2.473	**2.035**	0.57	**0.55**	0.052	**0.040**	41.87	**41.06**	0.033	**0.030**	0.89	**0.74**
15	**15**	6.72	**6.63**	6.49	**6.45**	6811	**6812**	6893	**6854**	0.550	**0.620**	0.201	2.600	**2.681**	0.52	**0.52**	0.045	**0.046**	64.38	**62.04**	0.038	**0.037**	0.61	**0.65**
15	**15**	9.43	**9.15**	7.13	**7.08**	7397	**7327**	7521	**7472**	1.450	**1.520**	0.201	3.638	**3.718**	0.48	**0.48**	0.053	**0.055**	90.69	**92.03**	0.042	**0.044**	0.60	**0.61**
15	**15**	12.30	**12.51**	7.73	**7.72**	7943	**7943**	8103	**8083**	2.380	**2.430**	0.201	4.710	**4.767**	0.45	**0.45**	0.060	**0.060**	127.42	**123.33**	0.048	**0.046**	0.55	**0.58**
15	**15**	16.14	**15.60**	8.33	**8.33**	8441	**8406**	8659	**8673**	3.300	**3.270**	0.201	5.770	**5.736**	0.42	**0.42**	0.065	**0.065**	159.03	**159.98**	0.050	**0.051**	0.54	**0.54**
20	**20**	8.46	**10.24**	7.63	**8.02**	8088	**8392**	8091	**8478**	0.605	**0.160**	0.304	3.672	**3.159**	0.58	**0.56**	0.045	**0.036**	105.87	**101.90**	0.038	**0.033**	0.69	**0.62**
20	**20**	13.12	**12.80**	8.45	**8.33**	8833	**8764**	8863	**8746**	0.820	**0.980**	0.304	3.920	**4.104**	0.53	**0.54**	0.040	**0.043**	149.39	**154.21**	0.041	**0.043**	0.52	**0.53**